PERFORMANCE EVALUATION OF GEOPOLYMER CONCRETE DEVELOPED USING SILLIMANITE SAND

A thesis submitted in the partial fulfillment of the requirements for the award of the degree of

MASTER OF ENGINEERING

IN

STRUCTURAL ENGINEERING

Submitted By

DIPANSHU JAIN

801724009

UNDER THE SUPERVISION OF

Dr. Prem Pal Bansal
Associate Professor and Head
Civil Engineering Department

Mr. Raju Sharma
Lecturer
Civil Engineering Department

CIVIL ENGINEERING DEPARTMENT
THAPAR INSTITUTE OF ENGINEERING & TECHNOLOGY
(A DEEMED TO BE UNIVERSITY), PATIALA, PUNJAB
JULY, 2019

DECLARATION

I, Dipanshu Jain hereby declare that the work presented in this thesis entitled "**Performance Evaluation of Geopolymer Concrete Developed using Sillimanite Sand**" in fulfillment of the requirement for the award of degree of **Master of Engineering** in **Structural Engineering** submitted at Civil Engineering Department, Thapar Institute of Engineering & Technology (Deemed to be University), Patiala is an authentic record of work carried out under supervision of **Dr. Prem Pal Bansal, Associate Professor and Head, Civil Engineering Department** and **Mr. Raju Sharma, Lecturer, Civil Engineering Department, Thapar Institute of Engineering & Technology (Deemed to be University), Patiala** from August 2018 to July 2019. The matter presented in this has not been submitted either in part or full to any other university or institute for the award of any other degree.

Date: 13-08-2019

Dipanshu

(Dipanshu Jain)

(801724009)

CERTIFICATE

This is to certify that the above declaration made by the student concerned is correct according to the best of my knowledge and belief.

Date: - 13-08-2019

Dr. Prem Pal Bansal
Associate Professor and Head
Civil Engineering Department
Thapar Institute of Engineering &
Technology (A Deemed to be University),
Patiala, Punjab

Date: - 13-08-2019

Mr. Raju Sharma
Lecturer
Civil Engineering Department
Thapar Institute of Engineering &
Technology (A Deemed to be University),
Patiala, Punjab

ACKNOWLEDGMENT

This acknowledgment is meant to be credited to all those individuals who were directly or indirectly engaged in my dissertation work.

First of all, I want to convey my gratitude and indebtedness to my Supervisor, Dr. Prem Pal Bansal, Associate Professor and Head, Civil Engineering Department and Mr. Raju Sharma, Lecturer, Civil Engineering Department, Thapar Institute of Engineering & Technology (Deemed to be University), Patiala for their profound participation, invaluable and ongoing encouragement throughout this work. I am very grateful to them for always being there whenever I need them.

I prob will not discover enough words to convey my sentiment of gratitude to the entire professors and staff of the Civil Engineering Department of Thapar Institute of Engineering & Technology (Deemed to be University), Patiala for their assistance, encouragement and personal support that helped me to complete my thesis successfully.

The cheerful support of my friend and colleagues is sincerely appreciated. Unique words of appreciation go to Mr. Hitesh Bhardwaj, Mr. Manreet Sidhu, and other laboratory staff, who helped me in my experimental work.

I also acknowledge the support of SAI Lab, TIET, Patiala and NPL Lab, New Delhi, for Microstructural testing.

Finally, I would like to dedicate this project work to my family members who have always been an excellent source of inspiration and help, particularly in all my academic efforts.

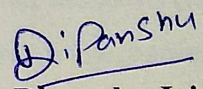

Dipanshu Jain

801724009

ABSTRACT

As the infrastructure industry continues to expand, the demand for cement is destined to rise. Cement producing industries are classified as extremally polluting industries. The primary pollutant that cement companies emit is carbon dioxide (CO_2). The production of cement causes severe greenhouse gas emission into the earth atmosphere. This issue causes the researchers to develop a new type of concrete which is different from conventional concrete and is termed as Geopolymer Concrete. Geopolymer concrete not only lowers the dependency of conventional concrete but also lowers the amount of global warming without compromising the mechanical and durability properties. Geopolymer does not form Calcium Silicate Hydrates (C-S-H) for matrix formation, unlike ordinary portland cement. Rather it forms Sodium Alumina Silicate Hydrate (N-A-S-H) gel.

The present dissertation work is performed to assess the impact by replacing natural sand with sillimanite sand in geopolymer concrete. Sillimanite sand contains high alumina and silica content and is used as a high-temperature refractory material. In geopolymer concrete, river sand has been replaced with sillimanite sand at 0, 25, 50, 75 and 100% replacement levels. Furthermore, the impact of molarities (8M and 16M) and curing type (ambient curing and steam curing) on the mechanical, durability, and microstructural characteristics of geopolymer concrete, are also evaluated.

Based on trial and error, geopolymer concrete mix design is prepared by reviewing previous literature and existing observations as standard code for geopolymer concrete is not available. Tests were conducted at the age of 28 days according to the provision of Indian Standard (IS) and American Society of Testing and Materials (ASTM) guidelines. The various mechanical test results revealed that the steam curing sample has higher strength compared to the ambient curing samples. In addition to it, GP16 (16M) mix has excellent mechanical and durability properties compared to the GP08 (8M) mix. The 25 to 50 % replacement level indicates optimum replacement level leading to higher mechanical and durability characteristics in the context of percentage replacement. An increase in percentage replacement beyond 50% indicates a reduction in the effectiveness of both mechanical and durability properties, whereas control mix demonstrates minimal durability as compared to sillimanite contained mix. The SEM, EDS, and XRD analysis also indicate dense interconnection between the gel networks due to the presence of sillimanite sand.

TABLE OF CONTENTS

LIST OF FIGURES

LIST OF TABLES

CHAPTER 1

INTRODUCTION

1.1 General

Cement is the most critical & significant component in the production of concrete. The demand for cement is growing day by day in the construction and infrastructure sectors. India is the 2nd largest cement producer with nearly 455 million tons (MT) of cement production capacity. The cement-producing industries were classified by the Central Pollution Control Board (CPCB) as extremely polluting industries. Cement industries are emitting primary pollutants, which include, carbon dioxide (CO_2), Nitrogen Dioxide (NO_2), Sulfur Dioxide (SO_2) and particulate matter, etc. Carbon dioxide is emitted when calcium carbonate is heated. The contribution of CO_2 emissions from cement manufacturing is approximately 6% because Portland cement production generates approximately one ton of CO_2 (Davidovits 1994b; Mccaffrey 2002). It is dangerous in the present-day scenario, due to the emission of greenhouse gases which traps sun's radiant energy in the environment; consequently, the temperature rises and causes global warming. The production of greenhouse gas emissions to the earth's atmosphere is estimated to be 1.35 billion tons per year (Mccaffrey 2002). Another scenario is the cost of cement, which grows every day due to of the cyclical nature of demand.

One of the alternatives to reduce greenhouse gas emissions is to reduce cement consumption while producing concrete. By replacing cement quantity with waste material such as fly ash, the objective can be achieved. The availability and abundance of fly ash create an opportunity to utilize it in concrete production. Alternatively, production of concrete can be eco-friendly or green concrete. In this context, the geopolymer concrete is now becoming prevalent as the best solution to decrease cement consumption and also reduce the 80% greenhouse gas emission into the atmosphere caused by cement and aggregate (Wallah 2010). Fly ash is one of the geopolymer concrete source materials. In the year 2017-18, 196 million tons of fly ash is generated by coal-burning in India (Authority 2018) whereas the price of fly ash is meager as compared to the cost of cement. Apart from its use in reducing carbon footprint, Geopolymer concrete has extensive properties such as high strength and durability compared to cement concrete.

When catastrophic fires occurred in France between 1970 to 1973, which involved standard organic plastic, in the aftermath of it, a French scientist, Davidovits founded a company

‘CORDI-GEOPOLYMER’ in 1972. He aimed to develop nonflammable and noncombustible plastic material.

In 1978 he proposed that an aluminum and silicone compound of most likely geological origin could react to the polymerization process by an alkaline solution and in 1979 the binder produced was named ' geopolymer.’ (Davidovits 1999). Geopolymer does not form calcium-silicate hydrates (C-S-H) for matrix formation, unlike ordinary portland cement. (Duxson et al. 2007).

1.2 Geopolymer Solids

Geopolymers can be used to describe amorphous alkali aluminosilicate, which is also commonly referred to as ‘alkali-activated cement,' ‘geocements,’ 'inorganic polymers,’ ‘hydroceramics’ etc. Geopolymer concrete can be generated through activation by using an alkaline solution to polymerize aluminosilicates such as fly ash, GGBS, metakaolin, rice husk, silica fume, and high calcium wood ash. (Duxson et al. 2007).

The term poly(sialate) was a chemical geopolymer designation. For Silicon-Oxo-Aluminate, sialate was shortened. In IV-Fold arrangement, the chain and ring of Si^{4+} and Al^{3+} were called polysilanes. These three kinds of amorphous to semi-crystalline silicon-alumina are illustrated below:

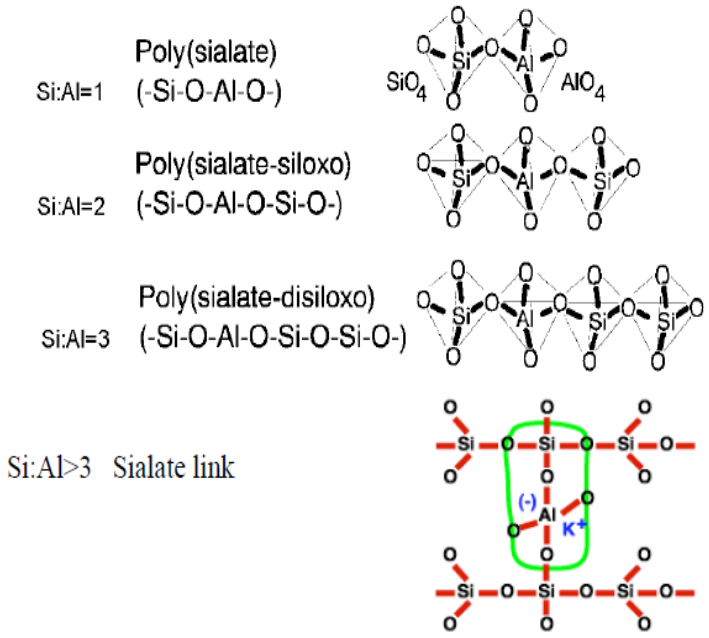

Fig 1.1: Three-Dimensional Silico Aluminate Structure Terminology *(Davidovits 2002)*

The polymerization process involves a substantially rapid chemical reaction under the alkaline Si-Al mineral atmosphere, leading in a three-dimensional polymer chain and a ring structure consisting of Si-O-Al-O bonds.

$$Mn\ [-(SiO_2)\ z\text{-}AlO_2]\ n.wH_2O \qquad (1.1)$$

Where M is monovalent cation like sodium, or potassium, z is 1 to 32, n is the rate of polymerization (Davidovits 1994a).

The schematic formation of geopolymers material is given in equations (Davidovits 1999; Van Jaarsveld, Van Deventer, and Lorenzen 1997)

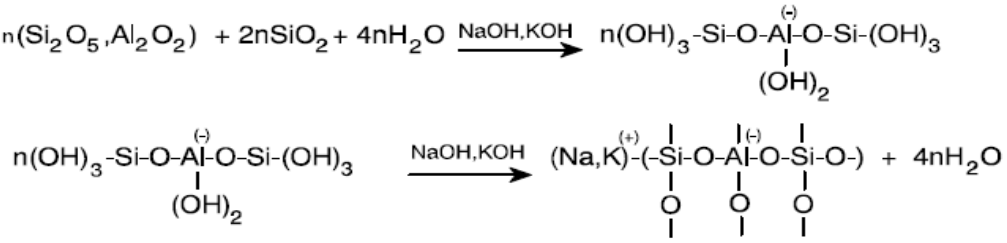

(1.2)

Also

Si-Al materials + activators (NaOH, Na_2SiO_3, KOH) + water ↓

Geopolymer binder + water (1.3)

The result of the equation is that when this water is expelled from the geopolymer concrete, it leaves the pores in the concrete behind it. Also, Water expelled during reaction from the geopolymer gives the mixture workability during handling. This mechanism contrasts with the chemical reaction of water in the Portland concrete mixture during the hydration stage (Singh et al. 2015). The reaction mechanism of geopolymer consists of three stages:

1st stage- Dissolution in which the source is broken down by the alkaline solution

2nd stage- Is polymerization when the individual monomers of alumina are polymerized to form N-A-S-H (Similar to the Portland cement CSH formation)

Final stage - is to rearrange the gel further and crystallize it into a strong material (Jansen and Christiansen 2015).

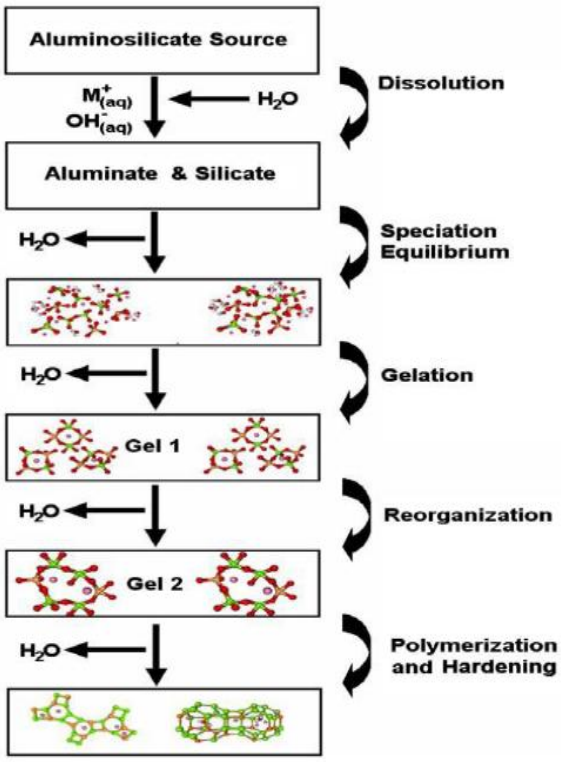

Fig 1.2: Conceptual Mechanism of Polymerization *(Duxson et al. 2007)*

The liquid alkaline activator and The source material are two primary geopolymer components. Source material can be any high Al-Si material generally byproducts such as fly ash, rice husk, slag, silica Which are high in Al-Si material is used. These material selections also depend upon cost, availability, and application.

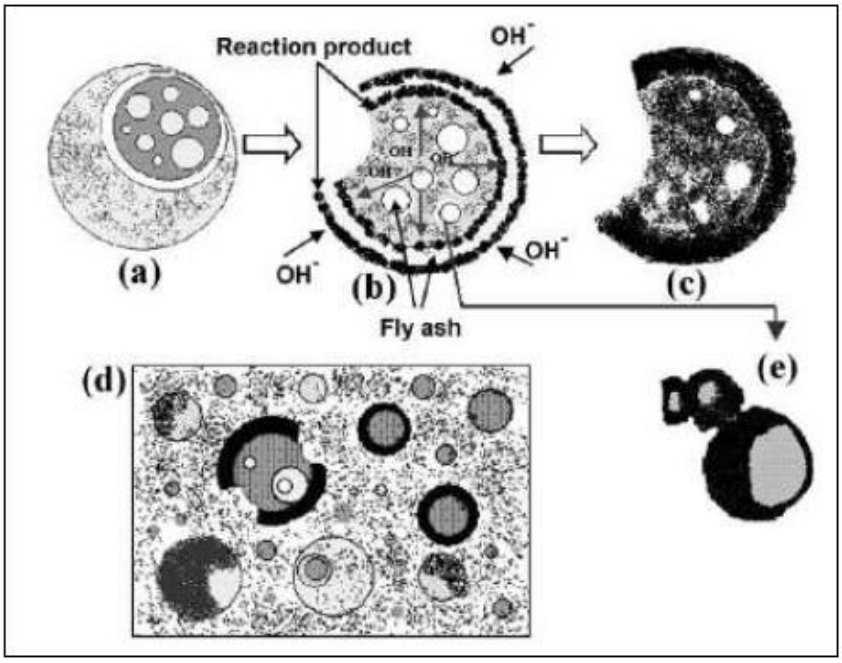

Fig 1.3: Model Describes The Alkali Fly ash Activation *(Fernández-Jiménez et al. 2005)*

The liquids commonly used for an alkaline activation are a combination of sodium flakes and the solution of sodium silicate. These chemical solution attack the flyash particle (Fernández-Jiménez et al. 2005). Which result in complete dissolution of the flyash particle from outside to inside fig 1.3(a-c). This reaction product fills up the interior space forming a dense matrix fig 1.3(b) Due to the substantial precipitation of reaction products, sections of more significant solids are covered with crust providing products that block interactions between alkaline solutions. Fig 1.3(e) this result in undissolved flyash particle. As a result, several morphologies can coexist in a single paste such as unreacted particles, unresponsive particle, reacted particle, etc.

1.3 Applications of Geopolymer Concrete

1.3.1 Application's Based on Si to Al Atomic Ratio

Davidovits suggested the possible implementation of Si to Al atomic ratio geopolymer concrete *(Davidovits, 1994b)*:

Table 1.1: Application of Geopolymer Concrete *(Davidovits, 1994b)*

Si: Al ratio	Applications
1	- Fire protection - Bricks - Ceramics
2	- Radioactive and toxic waste encapsulation - Low CO2 cements an concretes
3	- Tooling for aeronautics titanium process - Foundry equipment - Fire protection fiberglass composite - Heat resistant composites, 200^{o}C to 1000^{o}C
>3	- Tooling for aeronautics SPF aluminum - Sealants for industry, 200^{o}C to 600^{o}C
20-35	- heat resistant fiber composites and Fire resistant

1.3.2 Structural and Industrial Applications

1) *Cast in situ concrete application:* Geopolymer concrete is used in application like the construction of pavements, rapid road repairs, installation of water tanks, retaining walls, etc. Recently, Australian geopolymer cement and concrete producer have used geopolymer in pavement and water tank construction as shown in fig

Fig 1.4: Placing of Pavement Using Geopolymer Concrete *(Aldred and Day 2012)*

Fig 1.5: In Situ Water Tanks, Cast with Geopolymer Concrete (Right) and Cast with Cement Concrete (Left) *(Aldred and Day 2012)*

2) Structural application - architectural building, airport, etc. Are also constructed with the help of geopolymer concrete. The Global Change Institute of the University of Queensland is recently the first building in the globe to be constructed using Geopolymer concrete.

Fig. 1.6: The University of Queensland's Global Change Institute *(Aldred and Day 2012)*

3) Precast concrete application - Geopolymer concrete is also used in the precast application such as used in the construction of GPC panels, railway sleepers, ceramic tiles, sewer pipes, Bridge decks, electrical power poles, etc.

4) Marine application - Geopolymer concrete is used in marine structure due to its Higher Resistance against Chemical attacks and corrosive environment. It has less porous as compared to conventional concrete

5) Repairing & retrofitting application - Geopolymer concrete is used to repair and retrofitting of aging building and infrastructure with the use of either fiber composites or sheets.

6) Different application - Geopolymer concrete is also used in fire protection application for aeronautic industries and industrial building due to its higher thermal stability, in the storage of radioactive and toxic wastes, high tech mold and tooling construction, etc.

1.4 Limitations of the Geopolymer Concrete

These are the limitations of Geopolymer concrete:

1. The cost of the alkaline solution is high.
2. Base material such as flyash is not everywhere accessible.
3. Risk of safety associated with a high alkaline solution.
4. GPC needs a higher temperature curing; the ambient temperature has low strength, so there are difficulties associated with achieving it.
5. As there is not any standard design mix code for geopolymer concrete, mixes are prepared on trial and error basis.

1.5 Gaps in the Research Area

Geopolymer concrete is the best and most prominent option in the construction industry to decrease the use of OPC-based cement. However, limited studies in the area of geopolymer concrete have been carried out. Some studies indicate that with high concentrations of the alkaline solution and at high temperatures, high strength can be attained. However, this property has limited utilization in large scale field applications. So, the researcher is more consistent with developing high strength concrete with the use of another material to optimize the cost of construction. Moreover, research has also been investigated the effect of replacing fly ash content with another additive such as supplementary cementitious material, glass powder, OPC, etc. However, there have been limited studies to study the effect of sand replacement. A more concentrated strategy has been made in this research to demonstrate the

impact of replacing river sand with sillimanite sand. Sillimanite sand is used as a high-temperature refractory material with high alumina and silica content. Till date, no study has been reported to show the impact of sillimanite sand on geopolymer concrete properties. This research also aims to fill the knowledge gap and to study the impact on mechanical, durability and microstructural characteristics of geopolymer concrete of different replacements containing sillimanite sand along with different parameters such as molarity and curing conditions.

1.6 Objective of the Dissertation

The study aims to explore the strength and durability of geopolymer concrete as a partial replacement of river sand with sillimanite sand by taking into account the gap in the research area. Following are the objective of the present dissertation:

- To evaluate the influence of sillimanite sand on geopolymer concrete at different percentages such as 0%, 25%, 50%, 75% and 100% on properties such as compressive strength, split tensile strength, sorptivity, rapid chloride permeability, density-absorption, and void tests.
- To determine the influence of various molarities such as 8 M and 16 M on the mechanical and durability properties of geopolymer concrete that incorporates sillimanite sand.
- To assess the impact of various curing processes such as ambient curing and steam curing on the mechanical characteristics of geopolymer concrete containing sillimanite sand.
- To analyze the microstructural property of geopolymer concrete incorporating sillimanite sand using SEM, EDS, and XRD analysis.

1.7 Scope of the Study

Despite the numerous advantage and superior property of geopolymer concrete than conventional concrete, the geopolymer concrete has not gained much importance and acceptance in developing countries like India. In developed countries like Australia, the majority of the work on geopolymer concrete has been done. The lack of exploration of the use of alternative material which is available in India is also one of the factors that affect geopolymer concrete commercial use. Thereby, In the present research work, the application of beach mineral, i.e., sillimanite is explored for the development of geopolymer concrete. Also, the scope of the study includes the effect of molarity and curing type on the mechanical, durability, and microstructural properties of geopolymer concrete.

CHAPTER 2

LITERATURE REVIEW

2.1 General

The present section addresses the earlier geopolymer concrete studies. The section is divided into the various segment to investigate the impact of various parameters on characteristics such as split tensile strength test, compressive strength test, sorptivity, RCPT, density-absorption & void test conducted in previous research along with SEM, EDS & XRD of geopolymer concrete are discussed in detail below

2.2 Compressive Strength

2.2.1 The Effect due to Various Replacements

Sethi et al. (2016) explored the significance of glass powder (GP) and GGBS incorporation on geopolymer concrete's compressive strength. In mixture 30% of fly ash is replaced by 5% glass powder and 25% GGBS, 15% glass powder and 15% GGBS and 10% glass powder and 20% GGBS at different molarity of 4, 8 and 12M. A control mix was also cast for the comparison, the designation and result of each combination are specified in Table 2.1

Table 2.1: Compressive Strength Result in Geopolymer Concrete *(Sethi et al. 2016)*

Designation	**Compressive Strength (MPa)**	
	7 days	**28 days**
S0–G0–M12	7.37	15.11
S25–G5–M4	20.44	26.64
S25–G5–M8	14.93	23.33
S25–G5–M12	12.53	20.66
S20–G10–M4	17.28	23.91
S20–G10–M8	12.05	20.35
S20–G10–M12	15.64	23.06
S15–G15–M4	15.33	21.95
S15–G15–M8	11.11	18.13
S15–G15–M12	10.40	17.42

From the test result given in Table 2.1, it was observed that mix S25-G5-M4 exhibit high compressive strength, but with an increase in molar concentration from 4M to 10M,

compressive strength starts to decrease, this is due to GGBS has the property of being gaining strength at early age while glass powder gain's strength at later age. The percentage rise in strength at seven days is higher than that of 28 days strength of S15-G15, but it was lesser as compared to S25-G5. This resulted in a reduction in intensity owing to higher GP content due to GP being less reactive and stable.

Mehta and Siddique (2017) studied the influence on compressive strength by inclusion of OPC as partially replaced with fly ash in geopolymer concrete. Fly ash was swapped at 0, 10, 20, and 30% replacement level by OPC and testing was performed at the age of 3,7, 28 and 90 days. Figure 2.1 depicts the outcomes of the test data results.

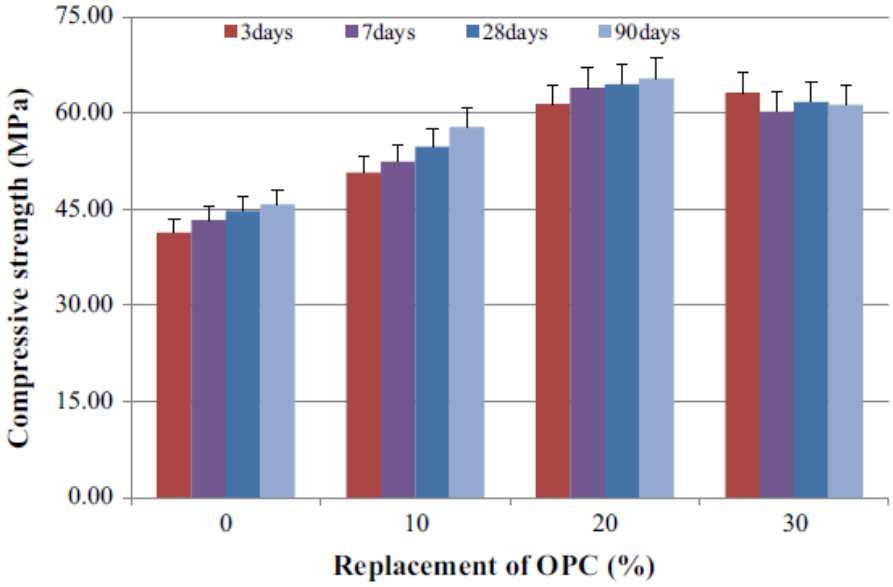

Fig 2.1: Result of Compressive Strength for Varying OPC Replacement Level

(Mehta and Siddique 2017)

The analysis of test data revealed that with up to 20% of cement substitution, there was an increase in strength, which further decrease to 30 % OPC at 28 days. However, three days strength was more than 92% of its 28 days strength. The high strength at an early age was due to the inclusion of OPC, which generate calcium silicate hydrate gel in addition to CASH and NASH. The strength was decreased at 30% replacement owing to the addition of OPC, which decreases the fly ash content result in a reduction of NASH and CASH in the system.

Muttashar et al. (2018) determined the effect of spent garnets on compressive strength by partially replacing it with sand on geopolymer concrete. The river sand is replaced by spent garnet at five different percentages from 0% to 100% at the constant liquid to binder ratio of 0.4; molarity was taken at 8M. The control specimen was designated as TR0 whereas, spent garnet sample was selected as TR1, TR2, TR3, and TR4 for four different percentage level.

Table 2.2: - Compressive Strength Result of Different Replacement Level of Spent Garnet *(Muttashar et al. 2018)*

Designation	Compressive strength (MPa)		
	3 days	7 days	28 days
TR0	70.24	73.29	79.84
TR1	71.63	73.13	78.21
TR2	67.50	70.42	76.32
TR3	65.91	69.18	75.45
TR4	61.42	66.23	70.32

Table 2.2 illustrates the compressive strength results. The outcome demonstrates that garnet concrete exhibit lower strength than control specimen and the value were dropped by -2.04%, -4.41%, -5.50% and -11.52% for TR1, TR2, TR3, and TR4 specimen correspondingly, this is due to spent garnet has finer particle, and there was no appropriate gradient and shapes of spent garnet to fill the pore volume which tends to decrease the strength.

Nguyen et al. (2018) evaluated the compressive strength property of geopolymer concrete based on the sea sand. The mix proportion was developed utilizing class F fly ash. The concentration of the sodium hydroxide solution was fixed at 12M. The test was performed by changing three different parameters. The alkaline liquid to fly ash ratio was wide-ranging from 0.35 to 0.65, aggregate to fly ash ratio was varied from 3.5 to 5.0, and Si/Al was modified from 1.2 to 1.7 by the inclusion of micro silica. The results are depicted in the figure.

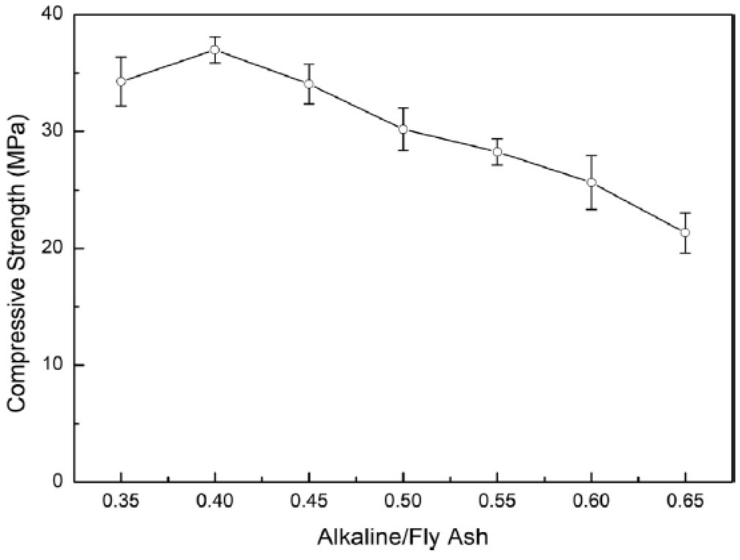

Fig 2.2: Compressive Strength for Alkaline/Flyash Ratio *(Nguyen et al., 2018)*

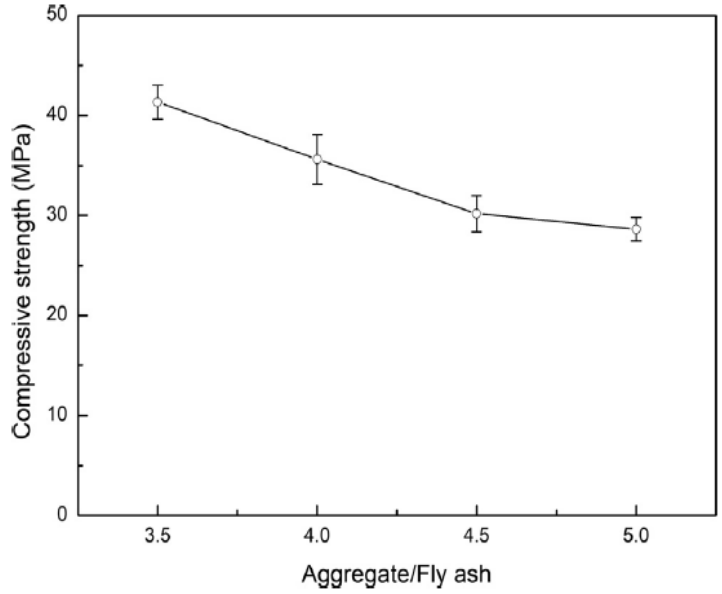

Fig 2.3: Compressive Strength for Aggregate/Flyash Ratio *(Nguyen et al. 2018)*

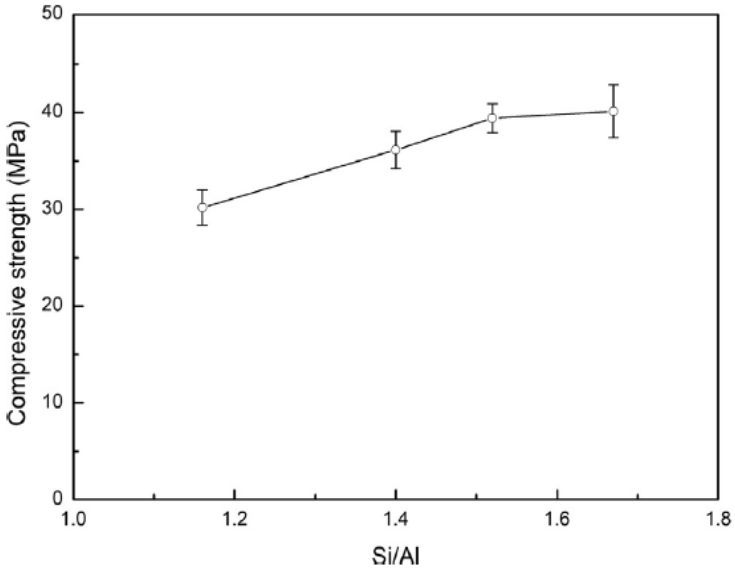

Fig 2.4: Compressive Strength for Si/Al Ratio *(Nguyen et al. 2018)*

The compressive strength value was higher at alkaline to fly ash of 0.35 to 0.45, like normal GPC and influence of aggregate to fly ash ratio was identical to aggregate to cement ratio in cement concrete. The performance reduces as aggregate content increases; this is due to geopolymer paste fill the voids inside concrete specimen results in an improvement in strength at less ratio whereas compressive strength value increases from 1.16 to 1.52 in the case of the Si/Al ratio and slightly went up when Si/Al risen from 1.52 to 1.67. The cause for the growth in strength was due to microparticle threads inside the micro silica, which reduce voids in the specimen and leads to increases in the compressive strength.

2.2.2 The Effect due to the Curing Duration and Curing Temperature

Al Bakria et al. (2011) examined the impact of curing temperature on geopolymer concrete's compressive strength. Geopolymer sample was prepared for different curing temperatures ranging from room temperature to 80^0C. The ratio of fly ash and alkaline activator was set at 2 and the ratio between sodium silicate and hydroxide was fixed at 2.5. Figure 2.5 shows the outcome at the age of 7 days.

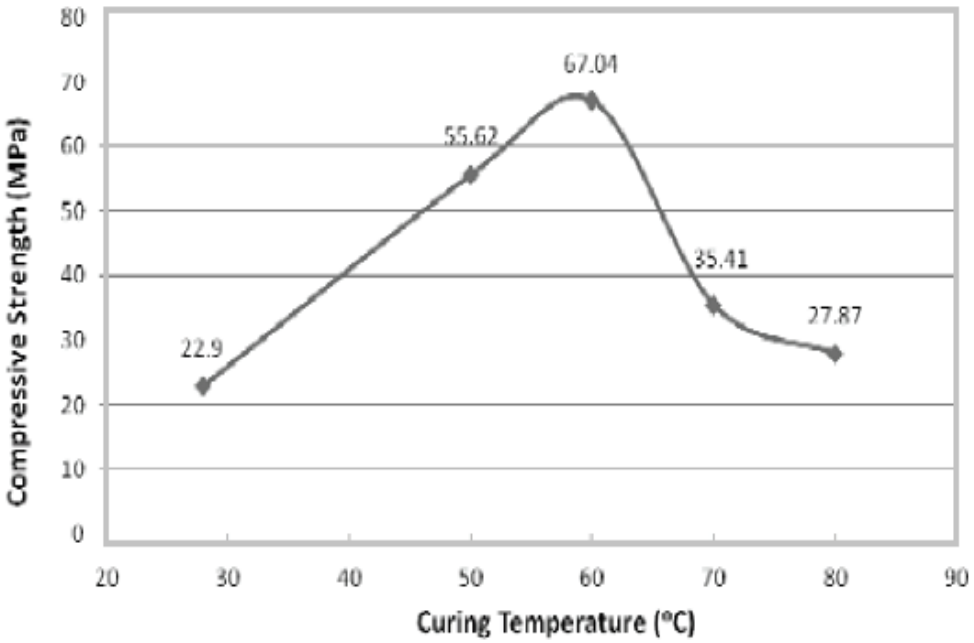

Fig 2.5: Result of Compressive Strength for Distinct Temperatures of Curing *(Al Bakria et al. 2011)*

The sample cured at 60^0C showed the maximum compressive strength, i.e., 67.04 MPa contrasted with others. At room temperature, compressive strength was lowest, i.e., 22.9MPa. The findings indicated that the curing temperature above 60^0C did not boost the compressive strength. Moreover, due to high heat, there was a substantial loss of moisture to develop better strength, and this causes the sample to crack.

Adam and Horianto (2014) observed the impact of duration and temperature of curing on the compressive strength of geopolymer mortar, which was based on fly ash. Geopolymer mortar was prepared and subjected to oven curing at 80^0C, 100^0C and 120^0C for 4, 6and 24 hours. One batch of the sample was air-cured. Test results at the age of 3,7,14 and 28 days of 80^0C, 100^0C, and 120^0C are revealed in Figure 2.6 - 2.8.

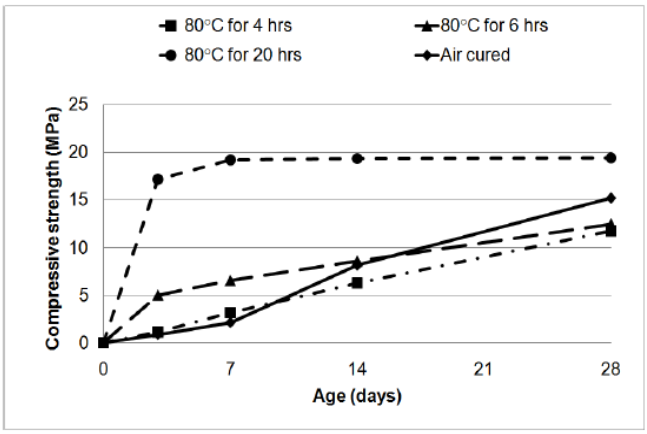

Fig 2.6: Compressive Strength for Curing at 80^0C *(Adam and Horianto 2014)*

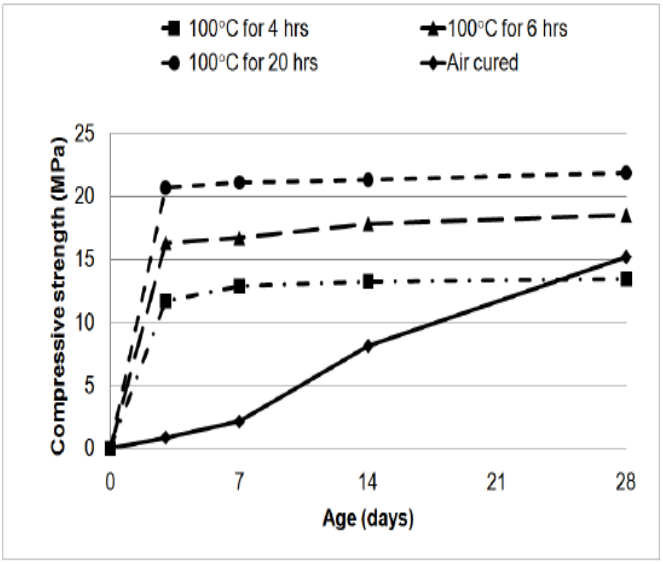

Fig 2.7: Compressive Strength for Curing at 100^0C *(Adam and Horianto 2014)*

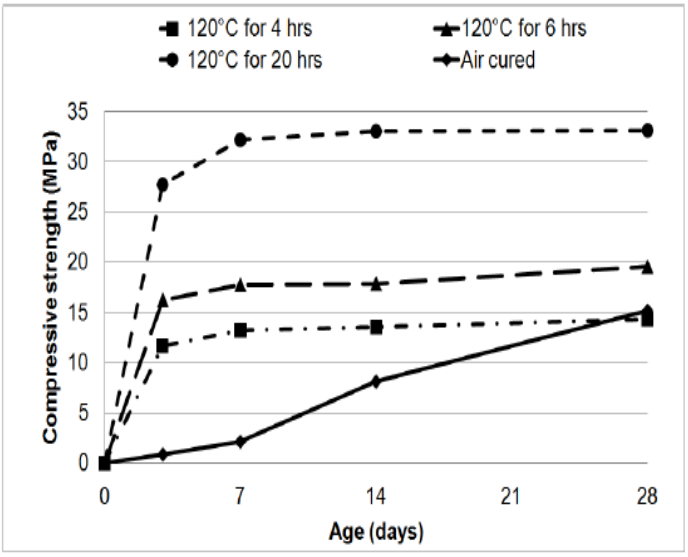

Fig 2.8: Compressive Strength for Curing at 120^0C *(Adam and Horianto 2014)*

The specimen cured at 80^0C for 4 and 6 hours (11.75 and 12.50 MPa) show less compressive strength as compared to 20 hours (19.40 MPa) at the age of 28 days. However, 4 and 6 hours specimen at 80^0C behave similarly to the air-cured specimen at the age of 28 days. This conduct indicates a slower rate of polymerization at a later age whereas specimen cured at 100^0C and 120^0 C have their peak strength attained at the period of 3 days, and constant strength was observed beyond this point. The duration and temperature of curing increased the polymerization process and boosted the strength of geopolymer.

İlkentapar et al. (2017) investigated the effect of heat curing duration and additional rest period after heat curing on compressive strength of alkali-activated class C fly ash-based geopolymer mortar. The mixture ratio of sand, fly ash, water, and sodium hydroxide were determined as 3,1,0.29 and 0.1, respectively. The sample was cured for 4 hours, 1,2,3 and seven days at 75^0C, and this samples were designated as K 1, K2, K3, and K5 respectively and tested without an extra rest period. Some of the equivalent samples were tested with an additional rest period and designated as K6, K7, K8, K9 and K10 for heat curing duration of 4hours 1,2,3, and seven days respectively as displayed in Table 2.3.

Table 2.3: Compressive Strength Result for Different Heat Curing *(İlkentapar et al. 2017)*

Mixture No	Heat Curing Duration	Extra Rest Period	Compressive Strength
K1	4 h	+0	4.41
K2	1 day	+0	33.84
K3	2 day	+0	50.50
K4	3 days	+0	63.32
K5	7 days	+0	73.57
K6	4 h	+28 days	11.82
K7	1 day	+27 days	45.30
K8	2 days	+26 days	64.78
K9	3 days	+25 days	70.03
K10	7 days	+21 days	75.69

From the result presented in Table 2.3, It has been noted that the rise in heat curing duration from 4 hours to 7 days, there has been an increase compressive strength from 4.42 MPa to 73.57 MPa of mixture no. K1, K2, K3 and K4 and K5. Whereas improvement was observed for the sample K6, K7, K9, and K10 with extra rest period but the rate of rising in

compressive strength was decreased from 168% to 34% and subsequently 28 %, 11% and 3% concerning compressive strength without an extra rest period. A possible reason for that consumable component in geopolymer reaction decreases with increase in curing time result in a reduction in the rate of growth in compressive strength.

2.2.3 The Effect due to the Sodium Hydroxide's Molarity

Reddy et al. (2010) studied the compressive strength of low lime-fly ash-based geopolymer concrete by varying molarity of NaOH solution at 10M, 12M, 14M, and 16M on different mix proportion. The sample was cured at 60^0C for 24hours, and the result was examined at 7, 14, 2, and 28 days.

Table 2.4: Compressive Strength at 60^0C *(Reddy et al. 2010)*

Conc. of NaOH	**Compressive strength (MPa)**			
	7 d	**14 d**	**21 d**	**28 d**
10 M	25.22	25.63	26.19	27.02
12 M	27.38	28.11	28.90	29.33
14 M	28.18	28.86	28.97	31.00
16 M	29.80	29.82	30.70	32.20

From Table 2.4, it was clear that with the increase in molarity, the compressive strength increases. Increase in strength is due to NaOH content improved the rigidity of the material and hardened the concrete paste result in high strength.

Malkawi et al. (2016) studied the influence of the alkaline solution on high calcium fly ash-based geopolymer mortars. The mortar was prepared by varying Na_2SiO_3/NaOH ratio between 1 and 2.5 at three different NaOH concentrations (8,10 and 12 M) the. The sample was cast at the age of 3,7 and 28 days. The findings of the experiment are depicted in Table 2.5. The test result of compressive strength was ranged between 49 to 75 MPa for the first three days. All the geopolymer mixes have gained more than 75% of their 28 days strength within three days — the application of heat curing yields in the increase in the reactivity of the aluminosilicate compound. Moreover, by increasing the Si/Al ratio by 10%, Compressive strength was increased up to 20 to 40% due to increase in the content of soluble silicate, which enhances the reaction at an early age and improves the polymerization process.

Table 2.5: Results of Geopolymer Mortar Compressive Strength *(Malkawi et al. 2016)*

Sample	Na_2SiO_3/NaOH	NaOH Concentration (M)	Compressive strength (MPa)		
			3days	7days	28days
N1	1:1	8	49.7	53.3	61.2
N2	1.5:1	8	57.7	65.3	74.1
N3	2:1	8	69.5	78.0	74.4
N4	2.5:1	8	71.2	76.1	78.2
N5	1:1	10	59.7	64.3	71.1
N6	1.5:1	10	65.3	71.0	79.9
N7	2:1	10	69.1	75.1	75.9
N8	2.5:1	10	75.1	79.3	84.3
N9	1:1	12	65.2	68.1	70.2
N10	1.5:1	12	69.3	75.1	77.2
N11	2:1	12	71.6	73.6	77.9
N12	2.5:1	12	77.2	79.0	79.1

2.3 Split Tensile Strength

2.3.1 The Effect due to Various Replacements

Sethi et al. (2016) studied the influence of the inclusion of glass powder and GGBS on the split tensile strength of geopolymer concrete with the replacement of 5,10 and 15 % of glass powder, in addition to it 15,20 and 25% replacement with GGBS has been done by varying molarity of NaOH from 4M to 8M and 12M. The testing took place at 7 and 28 days of age. The outcomes of the tests are depicted in Table 2.6. The split tensile strength of control mix was lowest (1.70MPa). From the conclusion, it was clear that as sodium hydroxide concentration increases from 4 to 12M, split tensile strength decreases. S15G15M4, S20G10M4, and S25G5M4 exhibit gain of strength at a rate of 75.29%, 96.47%, and 128.82% over control mix at the age of 28 days.

Table 2.6: Result of Geopolymer Concrete Splitting Tensile Strength *(Sethi et al. 2016)*

Designation	28 Days Strength (MPa)
S0–G0–M12	1.70
S25–G5–M4	3.89
S25–G5–M8	3.06
S25–G5–M12	2.43
S20–G10–M4	3.34
S20–G10–M8	2.60
S20–G10–M12	3.03
S15–G15–M4	2.98
S15–G15–M8	2.34
S15–G15–M12	2.14

The reason for the gain in strength with the addition of GGBS is credited to the higher content of calcium and alumina existing in GGBS, which increases the bondage between particles and hence split tensile strength increases.

Mehta and Siddique (2017) examine the influence on split tensile strength by inclusion of OPC with moderately swapped it with fly ash. The mixture was prepared by replacing OPC from 0 to 30% and were tested at 3, 7, 28, and 90 days. The results are depicted in Figure 2.9.

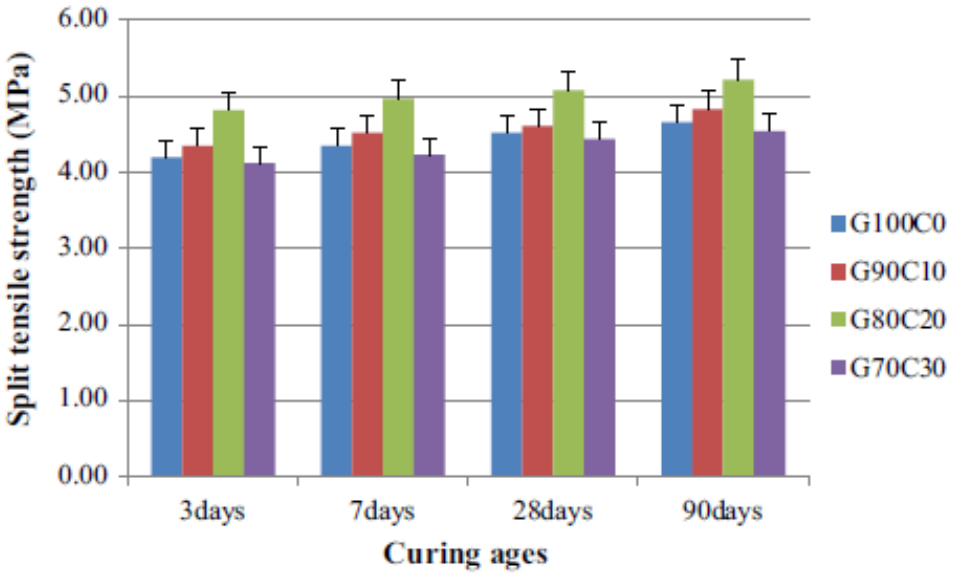

Fig 2.9: Result of Split tensile strength for varying OPC replacement level

(Mehta and Siddique 2017)

Test outcomes showed that with a rise in OPC content, the value of the split tensile strength increased to 20%, and it started to decline afterward, G80C20 has a higher value (5.28 MPa). The rise in value was due to the development of CASH and NASH, whereas the lower value of split tensile strength was due to the nonexistence of water curing needed by OPC.

Muttashar et al. (2018) evaluated the influence of Spent Garnet by partially replacing it with sand on split tensile strength of geopolymer concrete. The mixture was prepared by swapping river sand by spent garnet at varying content from 0% to100% at constant NaOH concentration 8M, whereas liquid to binder proportion was fixed at 0.4.

Table 2.7: Split Tensile Strength Result of Different Replacement Level of Spent Garnet *(Muttashar et al. 2018)*

Mixes	Split Tensile Strength (MPa)	
	7 Days	28 Days
TR0	10.1	12.95
TR1	9.92	11.2
TR2	8.76	10.01
TR3	8.1	9.91
TR4	7.54	8.77

Sample mixes were denoted as TR 0, TR 1, TR 2, TR3, and TR4; the result of the samples was shown in table 2.7. As the proportion of spent garnet was elevated, the split tensile strength of GPC was decreased. The values were dropped by 13.51%, -22.78%, -23.47% and -32.28% of sample TR 1, TR2 and TR3 and TR4 respectively. Owing to the weak bond between the spent garnet and the binder paste, the tensile strength reduced.

2.3.2 The Effect due to the Curing Duration and Curing Temperature

İlkentapar et al. (2017) noted the effect on alkaline-activated Class F geopolymer mortar by varying the extent of heat curing and extra rest period after heat curing. The sample was prepared 4, 2, 3 and 7 days and tested with and without extra rest period.

Table 2.8: Split Tensile Strength Result for Different Heat Curing *(İlkentapar et al. 2017)*

Mixture No	Heat Curing Duration	Extra Rest Period	Split tensile strength
K1	4 h	+0	0.42
K2	1 days	+0	2.59
K3	2 days	+0	3.64
K4	3 days	+0	4.91
K5	7 days	+0	5.67
K6	4 h	+28 days	1.63
K7	1 days	+27 days	4.25
K8	2 days	+26 days	5.63
K9	3 days	+25 days	5.72
K10	7 days	+21 days	6.06

Table 2.8 shows the outcomes of the split tensile strength. The rise in heat curing duration leads to the increase in split tensile strength of geopolymer mortar mixture. Table 2.8 shows that increase in heat curing duration from 4 hours to 7 days improve split tensile strength. Heat curing amplifies the process of polymerization, leading to increased strength.

Ekaputri and Priyanka (2017) studied the influence of temperature curing on the split tensile strength of geopolymer concrete. The mix proportion was prepared with fly ash to alkaline activator ratio of 65:35, the ratio of Na2SiO3/NaOH were varied from 1.5, 2, and 2.5. Steam curing was conducted at 40^0C,60^0C, and 80^0C for 24hours. The control specimen was treated at normal moist curing.

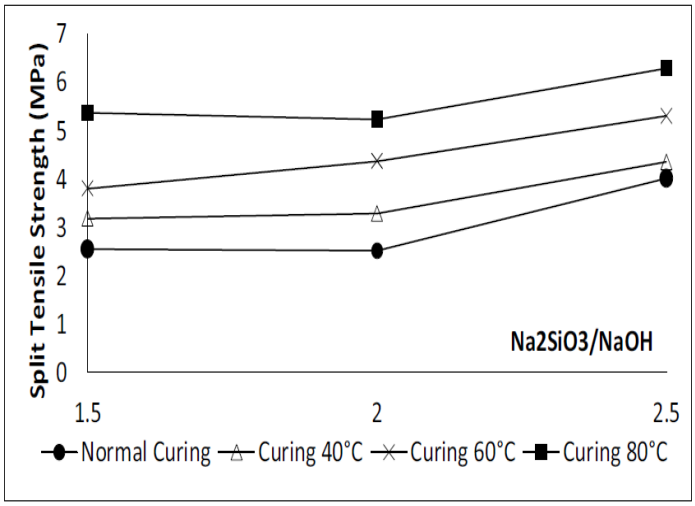

Fig 2.10: Split Tensile Strength Result for Different Curing Temperature *(Ekaputri and Priyanka 2017)*

Figure 2.10 shows the test outcomes at the age of 28 days. As temperature curing rises, the split tensile strength also increases. The highest peak was achieved at a temperature of 80^0. This is due to curing temperature increases the polymerization process, which results in increases in strength.

2.3.3 The Effect due to the Sodium Hydroxide's Molarity

Girawale (2015) determined the influence of the alkaline solution on the split tensile strength of geopolymer concrete. The mixture was prepared by varying different parameters. Na_2SiO_3/NaOH ratio was taken at 2.5,3 and 3.5 along with ranging molarity of NaOH at 12M, 14M, and 16M. Samples were tested at 28 days of age. The result showed that as the molarity of the solution increased there was an increase in split tensile strength, a comparable trend was observed in case of Na_2SiO_3/NaOH ratio. Molarity makes concrete stiffer by increasing the reliable content in it, which makes concrete harden to break, whereas Na_2SiO_3 solution enhances the geopolymeric reaction and improves the polymerization process.

Table 2.9: Split Tensile Strength Result at Various Molarity *(Girawale 2015)*

S. No.	Na_2SiO_3/NaOH Ratio	Split Tensile Strength (MPa)		
		12M	14M	16M
1.	2.5	2.456	3.448	3.916
2.	3.0	2.703	3.279	4.459
3.	3.5	2.840	3.371	4.503

Ahmed et al. (2017) investigated the impact of alkaline activator on geopolymer concrete split tensile strength. Six different mixture was prepared for carrying out the test and was made at each Na_2SiO_3 /NaOH binder ratio of 0.4 and 2.5 at 10,12 and 14 M. M40 Grade OPC was also prepared for comparison. The results of the tests are depicted in Table 2.10 at 7 and 28 days of age. The test results show that there was a rise in strength from 1.63 to 1.7 MPa and 1.85 to 2.13 MPa as molarity increases from 10M to 14M at the age of 7 and 28 days, correspondingly. This result was due to molarity makes matrix denser tend to increase the strength, whereas binder content increases the polymerization process

Table 2.10: Split Tensile Strength Result at Various Molarity *(Ahmed et al. 2017)*

Designation	Split Tensile Strength (MPa)	
	7 Day	28 Day
0M0	2.3	4.1
10M0.4	1.63	1.85
12M0.4	1.67	1.94
14M0.4	1.7	2.13
10M2.5	3.13	3.56
12M2.5	3.65	3.94
14M2.5	3.9	4.4

2.4 Sorptivity Test

Shaikh (2014) determines sorptivity due to the effect of alkali solution on geopolymer concrete. Seven mix proportion were prepared for testing. One with using cement and designated as OPC and other six were prepared using three different Na_2SiO_3/NaOH ratios of 2.5, 3 and 3.5 at two different molarities of 14M and 16M labeled as GP-14-2.5, GP-14-3, and GP-14-3.5 using 14M molarity and GP-16-2.5, GP-16-3, and GP-16-3.5 using 16M molarity.

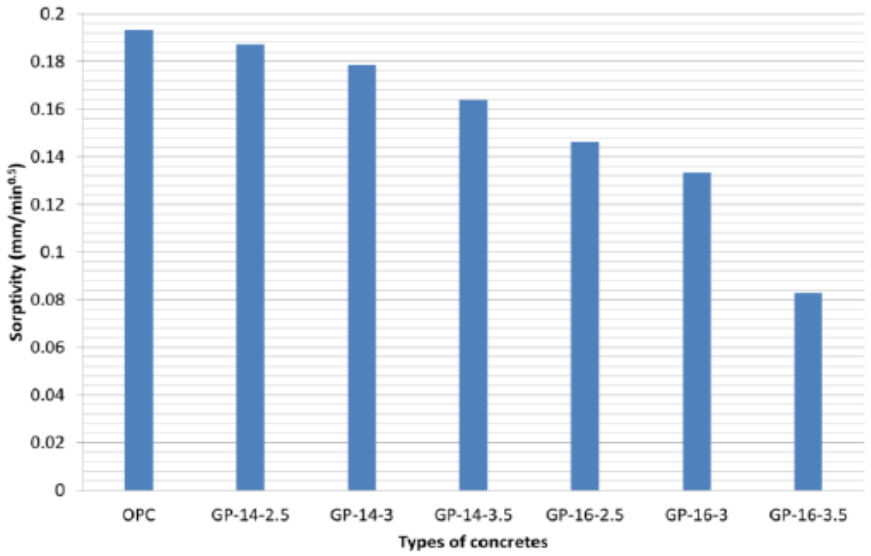

Fig 2.11: Sorptivity Test Results *(Shaikh 2014)*

It is evident from the test outcome that Sorptivity of GPC is lower than that of OPC. Sorptivity decrease with increase in Na_2SiO_3 content and concentration of NaOH. This attribute to the increasing amount of the dense- alumina silicate gel in the matrix due to more dissolution of alumina silicate component with an increase in molarity.

Ganesan et al. (2015) evaluted influence of geopolymer concrete containing steel fiber on Sorptivity. For purpose of experiment steel fiber is used in a geopolymer concrete sample with 0%, 0.25%, 0.50%, 0.75% and 1% replacement and designated as GPC, SFRGPC1, SFRGPC2, SFRGPC3 and SFRGPC4 respectively. Whereas cement concrete with 0% and 0.5% replacement of steel fibers designated as CC and SFRC2 respectively were used for comparison.

Table 2.11: Sorptivity Results *(Ganesan et al. 2015)*

Mix	**The Cumulative Volume of Water Penetrated (cm)**				**Sorptivity (cm/min$^{1/2}$)**
	30 min	**60 min**	**90 min**	**120 min**	**×10^{-3}**
GPC	0.04	0.057	0.060	0.067	2.85
SFRGPC1	0.024	0.030	0.040	0.05	2.74
SFRGPC2	0.024	0.030	0.040	0.045	2.21
SFRGPC3	0.019	0.020	0.029	0.040	2.21
SFRGPC4	0.013	0.026	0.029	0.033	2.11
CC	0.090	0.107	0.147	0.163	7.69
SFRC2	0.085	0.097	0.127	0.149	6.75

The sorptivity result was shown in Table 2.11. From observation, it was clear that Sorptivity value of GPC was inferior with that of CC. Addition of fibers improves the durability of GPC and CC. this is due to fiber bridge across microcrack lower the amount of void, which results in the denser structure and improves Sorptivity.

İlkentapar et al. (2017) illustrated the effect on alkaline-activated Class F geopolymer mortar on sorptivity by varying the extent of heat curing and extra rest period after heat curing. The sample was prepared 4, 2, 3 and 7 days and tested with and without extra rest period. The result was shown in table 2.12

Table 2.12: Sorptivity Results at Various Heat Curing Duration *(İlkentapar et al. 2017)*

Mixture No	Heat Curing Duration	Extra Rest Period	Initial Sorptivity ($mm/s^{1/2}$)
K1	4 h	+0	0.00016
K2	1 day	+0	0.00038
K3	2 days	+0	0.00047
K4	3 days	+0	0.00050
K5	7 days	+0	0.00057
K6	4 h	+28 days	0.00041
K7	1 day	+27 days	0.00043
K8	2 days	+26 days	0.00079
K9	3 days	+25 days	0.00081
K10	7 days	+21 days	0.00083

The outcome indicates that in both instances with and without an additional rest period, the rise in heat curing length increases sorptivity. Additional rest period has a higher sorptivity value than without extra rest period. The rise in sorptivity was due to the duration of heat cure, which resulted in a further drying of water, thus increasing the pore size of morter, enhancing the capillary activity of mortar in order to absorb more water.

2.5 Rapid Chloride Permeability Test

Ganesan et al. (2015) performed the rapid chloride permeability test of steel fiber reinforced geopolymer concrete. Geopolymer concrete mix design of grade M30 was made by varying fiber content, water, and superplasticizer. Designation GPC, SFRGPC1, SFRGPC2, SFRGPC3, SFRGPC4, CC, SFRC2 were given according to geopolymer concrete with 0% replacement, 0.25% replacement, 0.5% replacement, 0.75% replacement, 1.0% replacement, cement concrete with 0% replacement and 0.5% replacement of steel fiber.

Table 2.13: Rapid Chloride Permeability Test Results *(Ganesan et al. 2015)*

Mix	Charged Passed (C)	Chloride ion permeability
GPC	1321	Low
SFRGPC1	1445	Low
SFRGPC2	1392	Low
SFRGPC3	1566	Low
SFRGPC4	1762	Low
CC	1764	Low
SFRC2	1423	Low

From Table 2.13, it can be concluded that the chloride permeability of both smooth and fiber-reinforced GPC and CC was of low grade. This trend indicates that the addition of fiber did not influence the chloride resistance of GPC and CC.

Venkatesan and Pazhani (2016) determine the influence of geopolymer concrete made with black rice husk ash and ground granulated blast furnace slag on rapid chloride permeability of mix. GGBS is replaced with 0%, 10%, 20% and 30% black rice husk ash and designated as GP, GPR1, GPR2, GPR2, and GPR3 respectively.

Table 2.14: Rapid Chloride Permeability Test Results *(Venkatesan and Pazhani 2016)*

Mix	Charged Passed (C)	Chloride ion permeability
GP	1813.2	Low
GPR1	1597.5	Low
GPR2	2977.5	Moderate
GPR3	5675.1	High

Table 2.14 gives the result of the total charged passed in the sample. The reduction was noted at GPR1 with 10% BRHA as compare to control specimen. Then it increases with increase in percentage replacement. BRHA replacement reduces permeability due to micro filler property of BRHA particle. However, more addition results in appropriate SiO_2/Al_2O_3 ratio. This leads to incomplete alumina silicate geopolymer matrix, which results in increases in permeability.

Mehta and Siddique (2017) investigated the effect of rapid chloride permeability on geopolymer concrete based on low calcium fly ash by merging OPC as partial replacement of fly ash. Fly ash was swapped at 0, 10, 20 and 30 %. Testing was performed at 28, 90, and 365 days, according to ASTM C 1202. There was a significant improvement in the result of the

specimen with 20% OPC, but there was less difference between 20% and 30% OPC at 28 days. As age was increased, there was a decrease in the value of total charge passed; this is due to improvement in the microstructure. Adding calcium to high content outcomes in a compact and thick microstructure, which cause less pore volume and permeability decreases.

Table 2.15: Sorptivity results for different replacement level of OPC

(Mehta and Siddique 2017)

Designation	**Rapid Chloride Permeability: Total Charge Passed (in Coulombs)**		
	28 Days	**90 Days**	**365 Days**
G100C0	2899	2456	2156
G90C10	977	992	851
G80C20	404	186	165
G70C30	669	526	466

2.6 Density, Absorption, and Voids Test

Marín-López et al. (2009) studied the synthesis and characteristics of concrete based on metakaolin based geopolymer by conducting density, absorption, and void test. Geopolymer concrete mix was prepared by keeping constant various parameters such as H_2O/K_2O = 13.0, K_2O/Al_2O_3 = 1.03, K_2O/SiO_2 = 0.34, and SiO_2/Al_2O_3 = 2.97. For comparison, a concrete based on Portland cement was also prepared. Testing was done at different stages.

Table 2.16: Absorption, Bulk Density, Apparent Density, Volume of Permeable Voids

(Marín-López et al. 2009)

Concrete Type	**Test age Day**	**Absorption, %**	**Bulk density, g/cm^3**	**Apparent density, g/cm^3**	**Volume of permeable voids, %**
Geopolymer	4	9.48	2.10	2.60	20.76
Concrete	7	10.17	2.12	2.58	22.03
	14	10.44	2.13	2.57	22.42
	28	10.82	2.14	2.55	22.89
Portland Cement	4	10.30	2.25	2.85	22.50
Concrete	7	10.32	2.22	2.83	22.53
	14	10.34	2.21	2.79	22.56
	28	10.59	2.15	2.78	22.56

Table 2.16 gives the test result of absorption %, bulk density g/cm^3, apparent density g/cm^{3,} and volume of permeable voids %. It was observed that as setting time increases, the development of the C-S-H phase increases. Which result in increases in absorption percentage and percent of the permeable void, but density decreases. Whereas in metakaolin-

based geopolymer, density increases as setting time increases. However, the absorption percentage and volume of permeable void shows some changes due to the change in the geopolymeric reaction.

Phoo-ngernkham et al. (2013) Investigated the impact on porosity or volume of permeable pore space and water absorption of high calcium fly ash ash-based geopolymer paste with portland cement. The various mix proportion is prepared by replacing 0%, 5%, 10% and 15% OPC by mass of binder and designated as control, FA5PC, FA10PC, and FA15PC pastes respectively. The ratio of alkaline to binder by mass and Na_2SiO_3 to NaOH by mass were 0.60 and 2.0 respectively.

Table 2.17: Porosity (%) and Water Absorption (%) Results *(Phoo-ngernkham et al. 2013)*

Mixes	**Porosity (%)**				**Water absorption**
	1D	**7D**	**28D**	**90D**	**(7D) (%)**
Control	18.5	15.2	14.6	14.3	10.2
FA5PC	17.9	14.6	13.3	12.5	9.5
FA10PC	15.5	12.9	12.4	12.0	8.7
FA15PC	13.4	12.6	12.0	11.1	8.5

The outcome indicates a decrease in porosity with a rise in the proportion of OPC substitution and cure time. In the case of water absorption, the same trend was also observed. Increase in OPC content increases the dense matrix, and porosity decreases, which result due to pore structure refinement in the matrix.

2.7 Scanning Electron Microscopy (SEM), X-Ray Diffractometer (XRD) and Electron Diffraction Spectroscopy (EDS) Analysis of Geopolymer Concrete:

Xu and Van Deventer (2002) analyzed the XRD of geopolymers synthesized from kaolinite/stibite mixtures. The analysis was carried out to investigate the relative reactivity and to characterized the materials having both crystalline and amorphous phase in the gel. For analysis, geopolymers were prepared using 3 different kaolinite to stilbite ratio of 6.5,0.5 and 1 and designated as G1, G2, and G3, respectively.

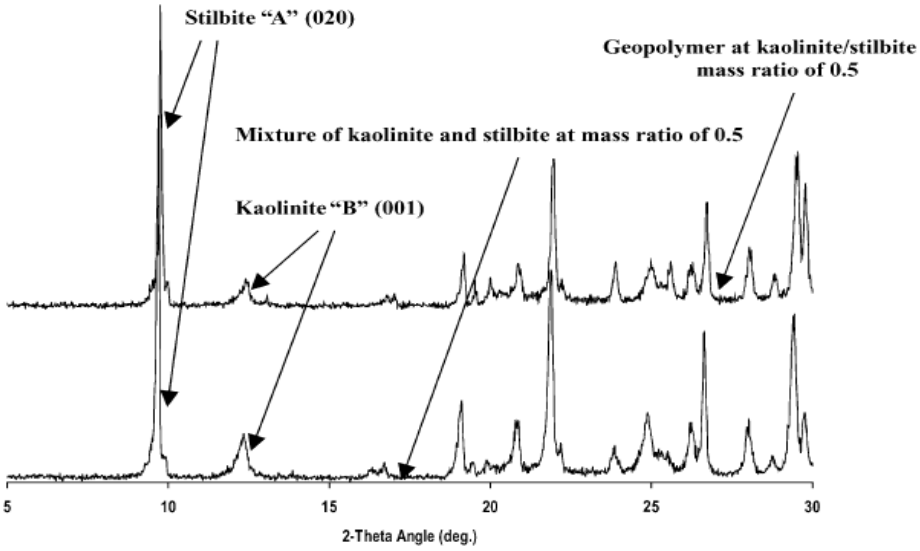

Fig 2.12: Geopolymer and Powder Mixture of Stilbite and Kaolinite at 0.5 Mass Ratio *(Xu and Van Deventer 2002)*

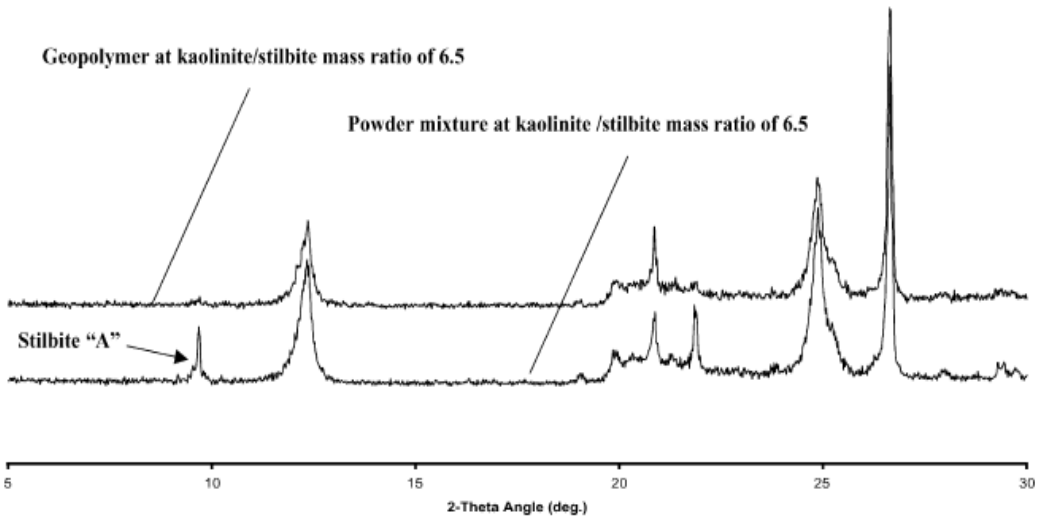

Fig 2.13: Geopolymer and Powder mixture of Stilbite and Kaolinite at 6.5 Mass Ratio *(Xu and Van Deventer 2002)*

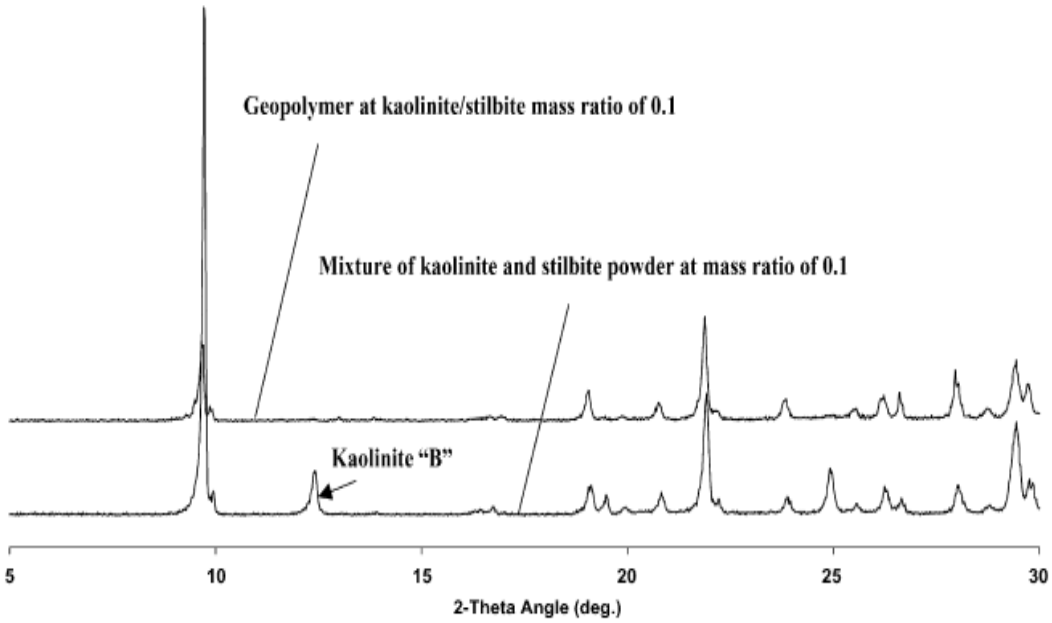

Fig 2.14: Geopolymer and Powder mixture of Stilbite and Kaolinite at 0.1 Mass Ratio *(Xu and Van Deventer 2002)*

XRD patterns are shown in Figures 2.12-2.14. The scanning pattern was noted from 5^0 to 70^0 (2θ). However, kaolinite and stilbite peaks ranged from the 5^0 to 30^0 (2θ). Figure (2.12-2.14) shows the powder mixtures and geopolymer of kaolinite to stilbite ratio of 0.5,6.5 and 0.1, respectively. For the mass ratio of 0.5 in Figure 2.12, both peaks stilbite (A) and Kaolinite (B) are detectable. It is also analyzed from Figure 2.12 that it contains amorphous to the semi-crystalline gel phase. In Figure 2.13, no peak (A) are detectable in geopolymer. It indicates that the complete transformation of crystalline to amorphous gel phase in the polymerization of G1. Kaolinite/stilbite mass ratio 0.1 from Figure 2.14 indicate only stilbite peak (B) in mixture indicate complete disappearance of kalinite due to the dissolution of kalinite during polymerization. G1, G2, and G3 indicate there is no new crystalline formation for the period of polymerization.

Kupwade-Patil and Allouche (2012) used SEM and XRD methodology to evaluate the effect of alkali-silica on fly ash-based geopolymer concrete. The mixture was made using one class C and two class F fly ash powder from different regions. Class C fly ash was acquired from Monticello, Texas. Moreover, class F fly ash was acquired from Dolet hills and Ohio region. One OPC based concrete was also prepared. Activator solution was of 14M concentration and sodium silicate to sodium hydroxide ratio was 1:1.

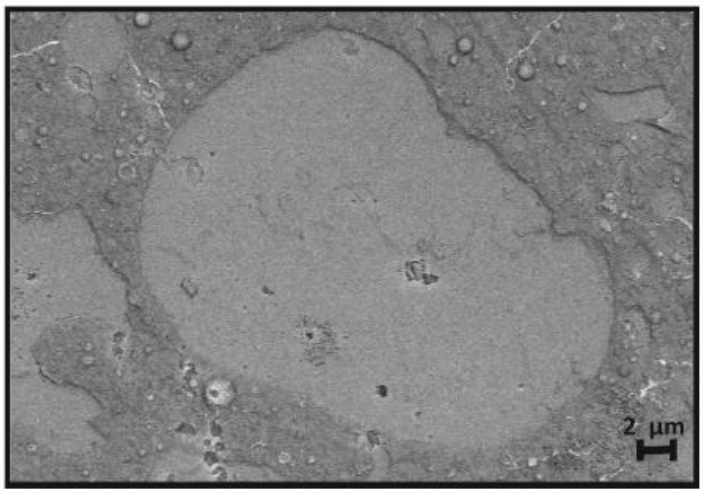

Fig 2.15: Sem Image of GPC using Ohio Fly ash (Aggregate- Matrix Interface)
(Kupwade-Patil and Allouche 2012)

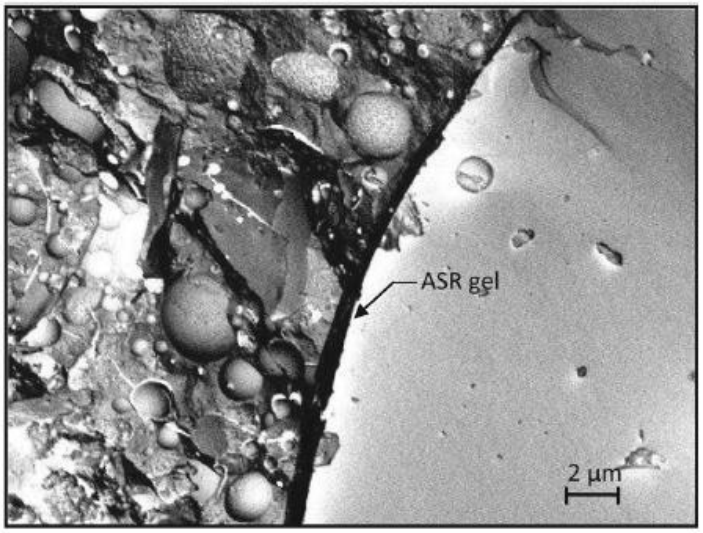

Fig 2.16: SEM Image of GPC using Monticello Fly ash (Aggregate- Matrix Interface)
(Kupwade-Patil and Allouche 2012)

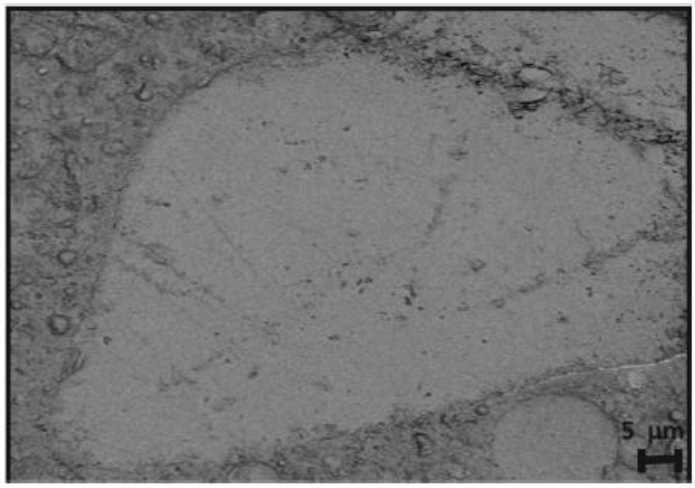

Fig 2.17: SEM Image of GPC using Dollet Hills Fly ash (Aggregate- Matrix Interface)
(Kupwade-Patil and Allouche 2012)

From SEM Figure 2.16, Gel formation was seen in the GPC-Monticello. This is because of the existence of calcium in Class C fly ash, which was observed in aggregate Paste (Ca=22%) interference. High calcium content leads to an increase in ASR (Alkali-Silica reaction) gel. Whereas in GPC sample made with class F fly ash Figure 2.15 and 2.16 indicate no ASR gel formation because of the lack of calcium in fly ash.

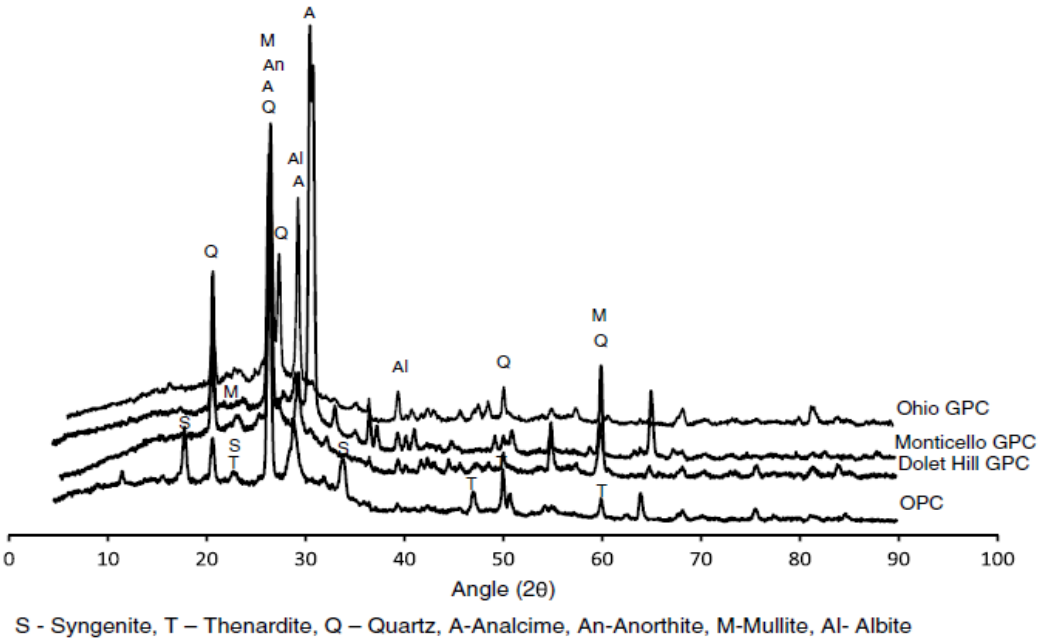

Fig 2.18: XRD Analysis of GPC and OPC *(Kupwade-Patil and Allouche 2012)*

From Figure 2.18, XRD analysis indicates the existence of Quartz, analcime, mullite, anorthite, and albite in GPC specimens. Albite is responsible for the strengthening of the matrix. Analcime is produced during mixing of NaOH with fly ash, whereas the mullite phase was involved in the zeolitizing process. In the case of OPC, it shows syngenite formation, which forms when OPC was immersed in NaOH solution.

Sethi et al. (2016) analyze the influence of the addition of GGBS and glass powder on the characteristics of geopolymer concrete using SEM and EDS analysis. Mix proportion was prepared using the substitution of 15%, 20% and 25% of fly ash with GGBS and 5%, 10% and 15% of glass powder. The effect of different molar concentration in the mixture was also analyzed and designated accordingly with ‘S’ refers to GGBS, ‘G’ refers to glass powder, whereas ‘M’ refers to molarity.

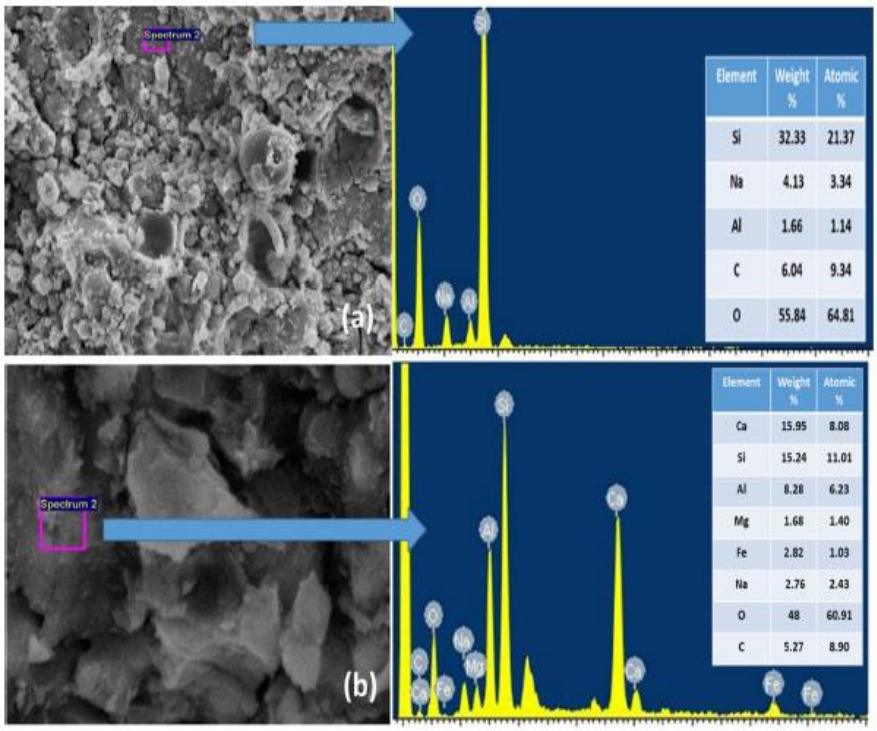

Fig 2.19: EDS Analysis of S0-G0-M12 (a) S25-G5-M4 (b) *(Sethi et al. 2016)*

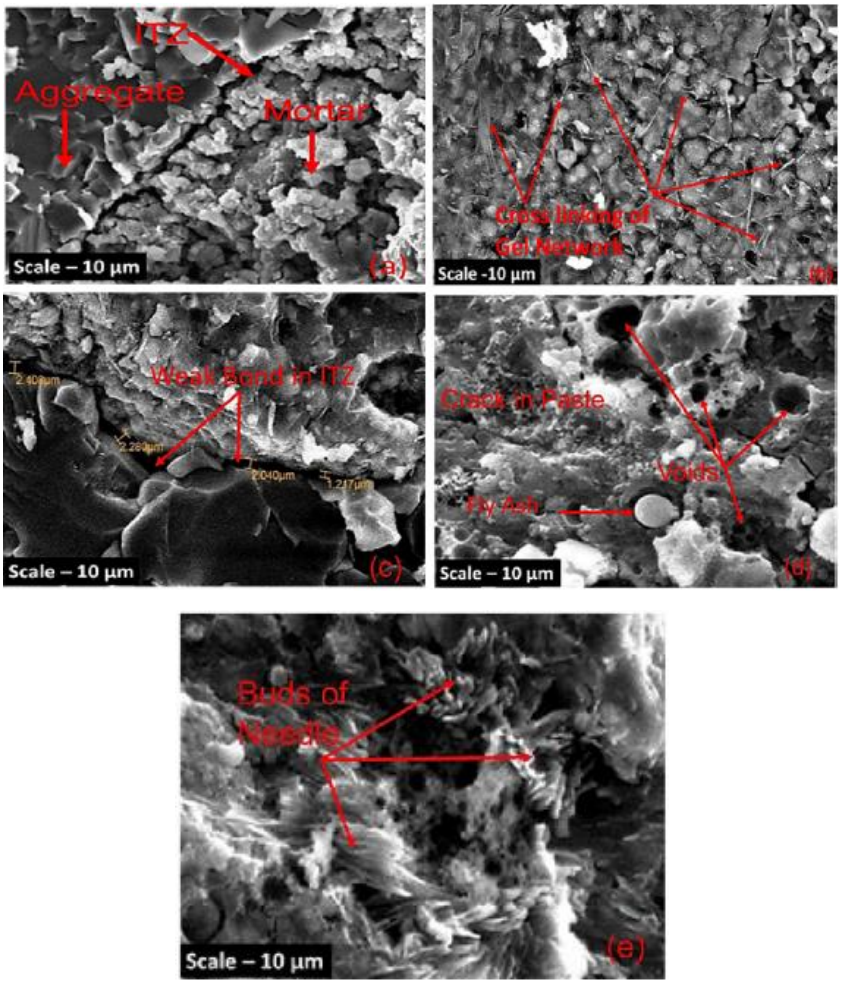

Fig 2.20: SEM Images of S0–G0–M12 (a), S25–G5–M4 (b), S20–G10–M8 (c), S25–G5–M12 (d) and S20–G10–M12 (e) *(Sethi et al. 2016)*

EDS study from Figure 2.19 demonstrates that the existence of silica, sodium, and alumina was accountable for geopolymer strengthening. The higher calcium oxide concentration yielded in increase of compressive strength of S25-G5-M4 mix. It was observed in figure 2.20 (b) that sample S25-G5-M4 have higher cross-linking of the gel network and have a higher amount of gel formation, which results in higher compressive strength. Whereas control sample using 12M NaOH Fig 2.20 (a) have lots of dispersed cracks which result in lower strength. Figure 2.20 (e) S20-G10-M12 mix shows dense matrix and the buds of the needle which enhance the strength of geopolymer mix.

Abdullah et al. (2012) analyzed the fly ash-based geopolymer lightweight concrete using a foaming agent by SEM analysis. The mixture was prepared using lightweight aggregate, class C fly ash and alkaline activator solution cured at room temperature and 60^0 C temperature designated as LW1 and LW2.

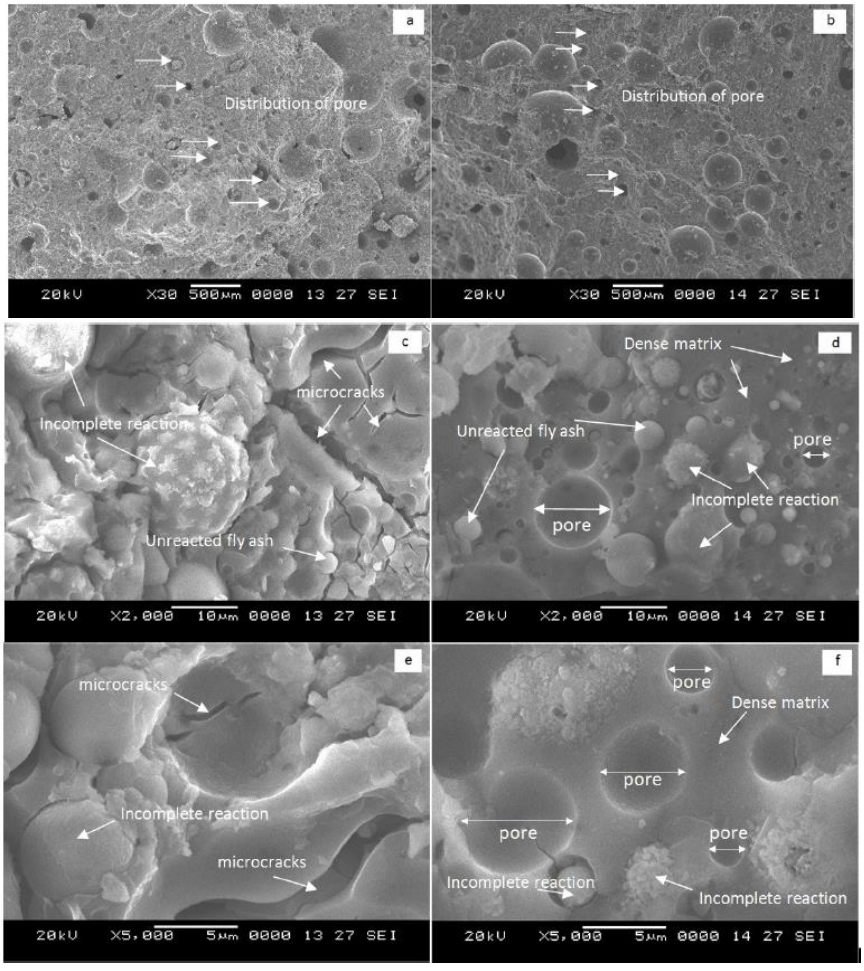

Fig 2.21: Distribution of Pores in LW1 (a), Distribution of pores in LW2 (b), Magnification at 2000X of LW1 (c), Magnification at 2000X of LW2 (d), Magnification at 5000X of LW1 (e), Magnification at 5000X of LW2 (f) *(Abdullah et al. 2012)*

Figure 2.21 (a) and 2.21 (b) depicts the size of pores from 4µm to 37µm. in foam geopolymer concrete, pores distribution is uniform. This attribute the formation of lightweight concrete. Whereas at 2000X and 5000X magnification, microcracks were observed in LW1. Whereas figure 2.21 (f) LW2 shows a denser matrix. This is due to heat curing, which results in the complete reaction between alkaline activator and fly ash. Unreacted fly ash was also present in both LW1, and LW2. in the figure depicts the incomplete dissolution of fly ash particle which results in the less dense matrix which causes high water absorption and porosity in LW1.

CHAPTER 3

EXPERIMENTAL PROGRAM

3.1 General

The present study is intended to study the influence of sillimanite sand replacement with natural sand on mechanical, durability, and microstructural property of geopolymer concrete. To prepare the geopolymer concrete, various test of ingredients has been performed. Also, the design methodology is prepared to develop the sillimanite contained geopolymer concrete. The various test such as compressive strength, split tensile strength, sorptivity, rapid chloride permeability, density & void tests, microstructural analysis is adapted to analyze the properties of geopolymer concrete and detail of tests are presented in the subsequent section.

3.2 Material used in the Present Study

3.2.1 Fly ash: fly ash is a by-product of pulverized coal obtained from coal-burning power plants. It is fine, gray in color, spherical in shape, particle size range from 1 micron to 150 microns. According to ASTM C618-05, categories fly ash into three categories:

Class N— Raw or calcinated natural pozzolans like diatomaceous soil, opaline shales, volcanic tufts or pumicites, uncalcined or calcined clay, and shales fall into this category.

Class F — Fly ash usually made of anthracite or bituminous coal. This class of fly ash does have pozzolanic qualities, but it does not harden itself.

Class C — Fly ash generated from sub-bituminous or lignite coal. This fly ash class has both pozzolanic and cemented characteristics.

Fig 3.1: Fly ash

Generally, low calcium (class F) fly ash is preferred in manufacturing of geopolymer concrete rather than high calcium (class C) fly ash because high calcium class C fly ash may alter the performance by changing the microstructure by the polymerization process.

Fly ash used in the present dissertation was obtained from Larsen & Turbo super thermal power plant in Patiala district of Punjab, which is of class F category. SEM and EDS analysis were also performed to observe microstructural characteristics and composition of particles. The detailed analysis is shown below:

Table 3.1: Physical Property of Fly ash

Characteristics	**Value/Observation**
Particle size	8-14 um
Specific gravity	2.35
Blain fineness	265 m^2/kg
Color	Gray
Shape	Spherical

Table 3.2: Chemical Property of Fly ash

Compound	**Value (%) Provided by the Supplier**	**Require as per ASTM C618-05**
$SiO_2+Al_2O_3+ Fe_2O_3$, min	92	70
SO_3, max	0.2	5
Moisture content, max	-	3
Loss on ignition, max	0.5	6

Further to observe the microstructure of fly ash particle SEM & EDS analysis has also been carried out, from EDS analysis of fly ash particle lies in the category of class F. The detailed procedure of microstructure test is discussed in the later section.

Table 3.3: Fly ash Composition from EDS Analysis

Oxides	**Fly ash (%)**
SiO_2	56.87
Al_2O_3	37.55
Fe_2O_3	2.29
CaO	0.83
MgO	0.27
SO_3	0.3
Na_2O	0.2
K_2O	0.87
TiO_2	0.97

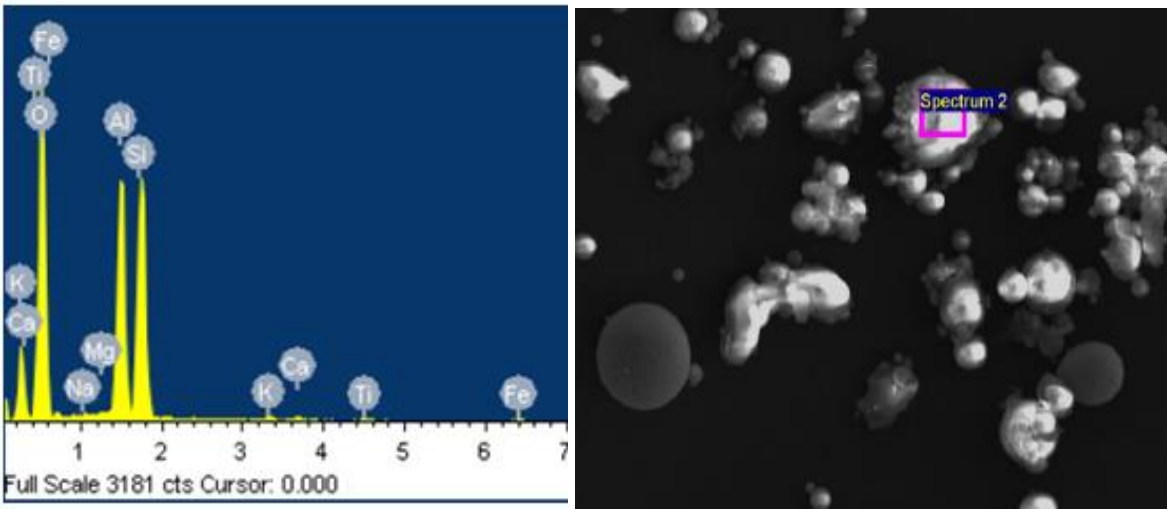

Fig 3.2: EDS and SEM Analysis of Fly ash - Spectrum 2

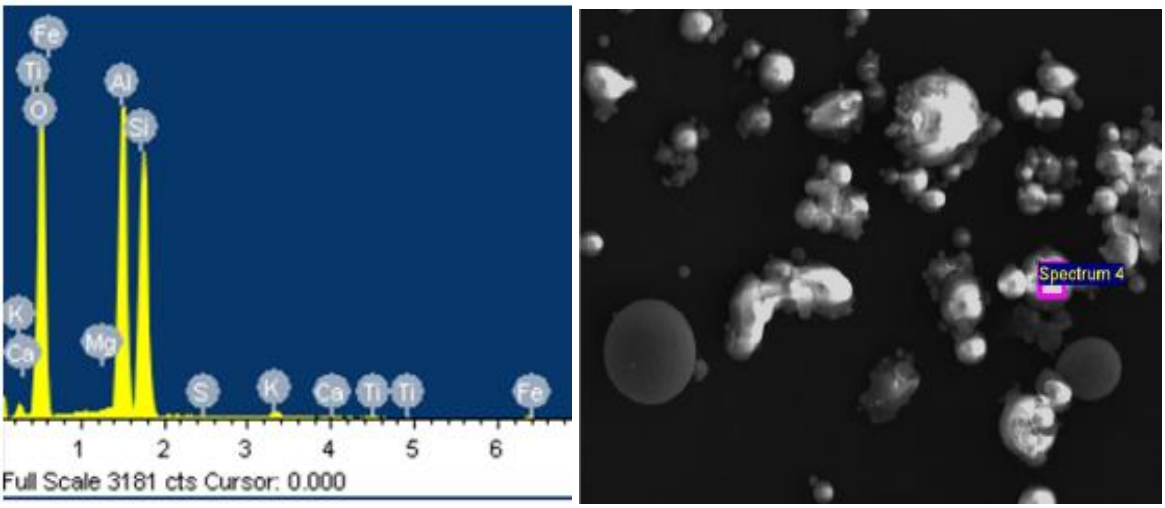

Fig 3.3: EDS and SEM Analysis of Fly ash - Spectrum 4

3.2.2 Sillimanite Sand: Sillimanite, which is Al_2SiO_5 occurred in nature in rock form. However, the rock formations of sillimanite have been exhausted in many parts of the world. Now only available in coastal areas as beach sand composite. This composite is rich in alumina – silicate compound, presence of alumina-silica in sillimanite sand, Increase the sand's thermomechanical characteristics and enhance the strength and toughness of the mixture by the presence of Zircon.

When sillimanite is heated above 1545^0C it converts Sillimanite into mullite and tridymite

$$3Al_2SiO_5 \longrightarrow Al_6Si_2O_{13} + SiO_2 \quad (3.1)$$

Sillimanite (100%) Mullite (88%) Tridymite (12%)

The mineral shows negligible expansion while changing over to mullite and can be used without calcination. It is used as a refractory material due to its high melting point.

Fig 3.4: Sillimanite Sand

Uses of Sillimanite sand

1. Sillimanite sand is extensively used in the manufacturing of high alumina refractories which are used in iron and steel, cement, zinc, electrical and petrochemical industries due to its very low thermal expansion coefficient, spalling resistance, slag and abrasion resistance.
2. Mullite which is produced at high temperature from Sillimanite is used in the lining of furnaces and manufacturing of high-temperature containers used in metal, glass and ceramic industries due to its high resistance to spalling, chemical attack of soda and corrosive action of molten glass.
3. Raw Sillimanite of calcined form is also used in the manufacturing of different shapes of molds, joint-free, and self-supporting monolithic refractory linings.
4. Raw and calcinated Sillimanite is also used in ceramic tile body components, electrical ceramic, ceramic honeycombs, spinnable mullite fibers, high-temperature insulation, extrusion dies and grinding media.
5. Other uses of Sillimanite sand include foundry-molds facings, burner bodies, pyrometer tubes, and welding rod coatings. Also used to produce Si-Al alloys, silicon & aluminum oxides, and metallic fibers (Wu 1990).

Generally, there are two types of Sillimanite found in India ‘Q’ Grade and ‘OR’ Grade. ‘Q’ Grade is produced at Chavara, Kerala ‘OR’ grade is produced at OSCOM, Chatarpur, Orissa by India Rare Earth Limited.

In the present work, the Sillimanite sand which is using is of 'OR' Grade and obtained from OSCOM, Chatarpur, Orissa as per the information provide by the supplier physical and chemical parameters of sillimanite sand 'OR' grade is given below:

Table 3.4: Physical Properties of Sillimanite Sand

Characteristics	**Values/Observation**
Color	Golden Yellow
Hardness (Moh's Scales)	6-7
Bulk Density	1950-2050 kg/m^3
Crystal System	Orthorhombic
Specific Gravity	3.20-3.25

Table 3.5: Chemical Properties of Sillimanite Sand

Compound	**Value % Provided by the Supplier**
Al2O3	57.0
SiO2	38.0
Fe2O3	0.4
TiO2	0.3
ZrO2	2.0

Table 3.6: Fineness analyses of Sillimanite Sand

Mesh Size (Tyler Screen)	**Sieve Opening in Micron**	**Cumulative Weight Percent Retained**
35	425	Nil
48	300	0.1
6	212	9.0
100	150	54.9
150	106	93.2
200	75	99.6

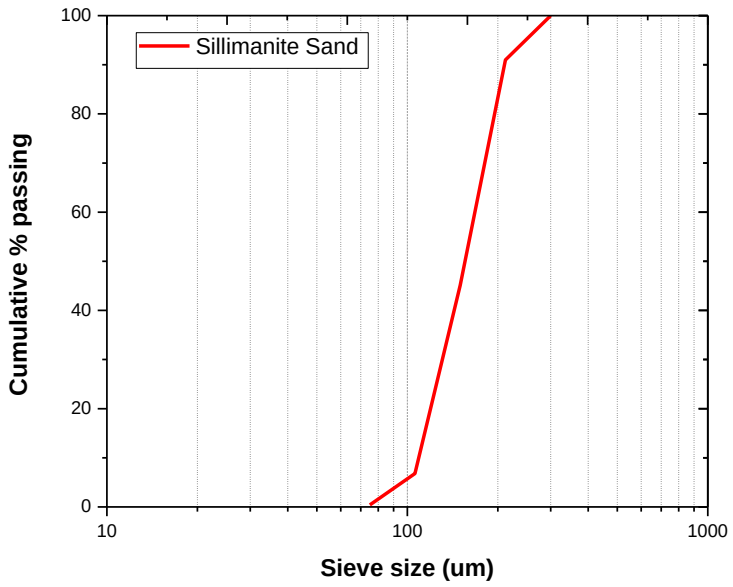

Fig 3.5: Cumulative Size Distribution Curve of Sillimanite Sand Particle

Table 3.7: Sillimanite Sand Composition from EDS Analysis

Oxides	**Sillimanite Sand (%)**
SiO_2	39.55
Al_2O_3	58.7
Fe_2O_3	1.24
CaO	0.4
MgO	-
SO_3	-
Na_2O	0.18
K_2O	-
TiO_2	0.43
ZrO_2	0.16

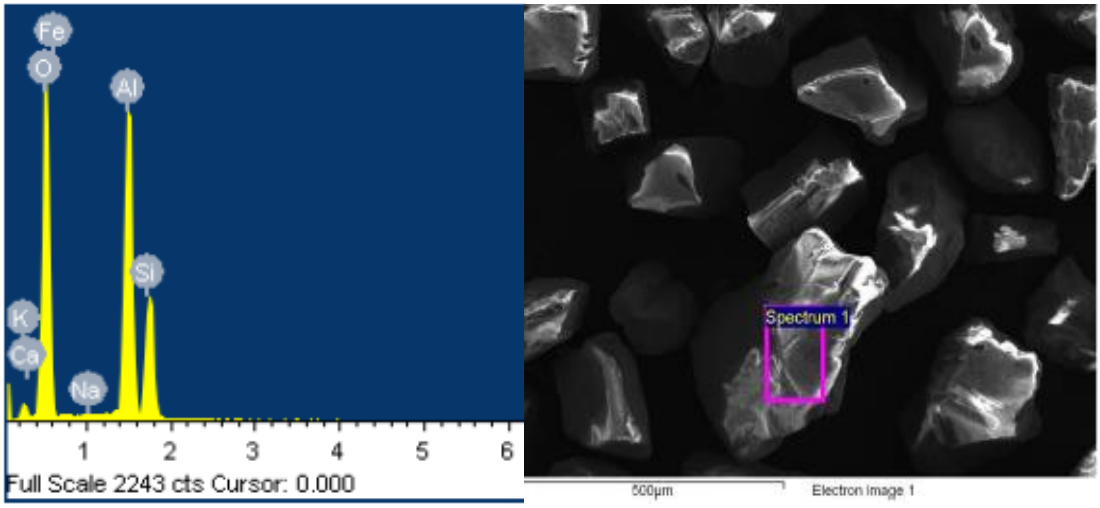

Fig 3.6: EDS and SEM Analysis of Sillimanite Sand - Spectrum 1

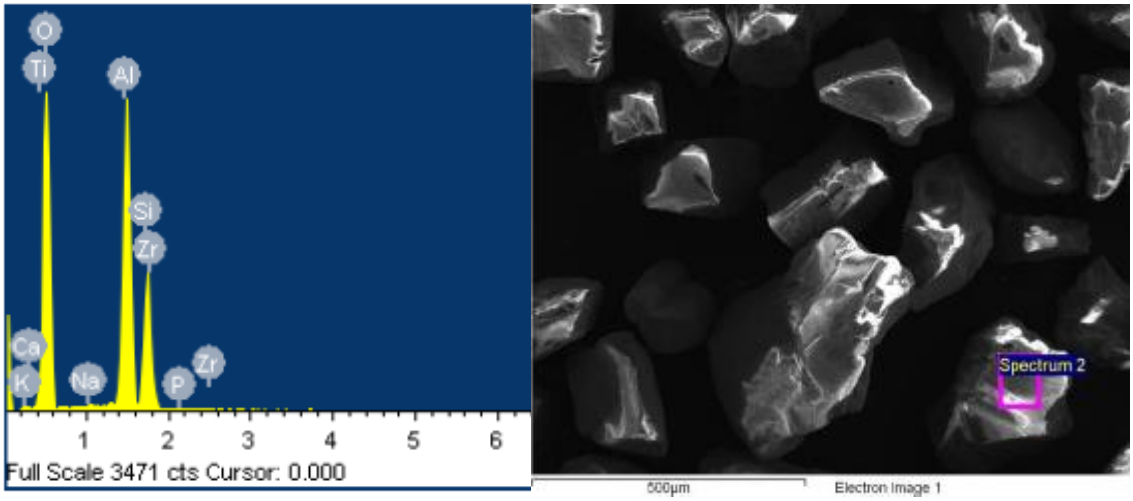

Fig 3.7: EDS and SEM Analysis of Sillimanite Sand - Spectrum 2

3.2.3 Coarse Aggregate: The aggregate that stood at 4.75 mm dia. Sieve is called a coarse aggregate. It is acquired from natural rock, crushed gravel or stone disintegration. It is a necessary ingredient of concrete it can be characterized as smooth, rounded, or angular. It takes up a substantial quantity of concrete and decreases the mixture costs. Further concrete strength is varied by aggregate size, shape, grading, texture, and mineralogy. It provides abrasion resistance and makes the concrete hard, whereas coarse aggregate occupies a significant volume of concrete.

Coarse aggregates with a nominal size of 20 and 10 mm were used in the present work. These aggregates are adequately washed to make it dust free and used in the dry surface condition. The result of various tests such as specific gravity, water absorption, and Sieve analysis was calculated as follows:

Table 3.8: Physical Properties of 10 mm Size Coarse Aggregate

Characteristics	**Value/Observation**
Type	Crushed
Shape	Angular
Fineness Modulus	6.44
Total Water Absorption	0.4
Specific Gravity	2.67

Table 3.9: Sieve Analysis of 10 mm Size Coarse Aggregate

Sr No.	Sieve Size	Mass Retained (gm)	The Percentage Retained	The Cumulative Percentage Retained	Percent Passing
1.	20 mm	136.5	4.55	4.55	95.45
2.	10 mm	1172	39.06	43.61	56.37
3.	4.75 mm	1593.5	53.11	96.72	3.28
4.	PAN	97	3.23	100	0

Table 3.10: Physical Properties of 20 mm Size Coarse Aggregate

Characteristics	Value/Observation
Type	Crushed
Shape	Angular
Fineness Modulus	6.83
Total Water Absorption	0.5
Specific Gravity	2.72

Table 3.11: Sieve Analysis of 20 mm Size Coarse Aggregate

Sr No.	Sieve Size	Mass Retained (gm)	The Percentage Retained	The Cumulative Percentage Retained	Percent Passing
1.	20 mm	267	8.9	8.9	91.1
2.	10 mm	2029	67.65	76.55	23.45
3.	4.75 mm	634.5	21.15	97.7	2.3
4.	PAN	69	2.3	100	0

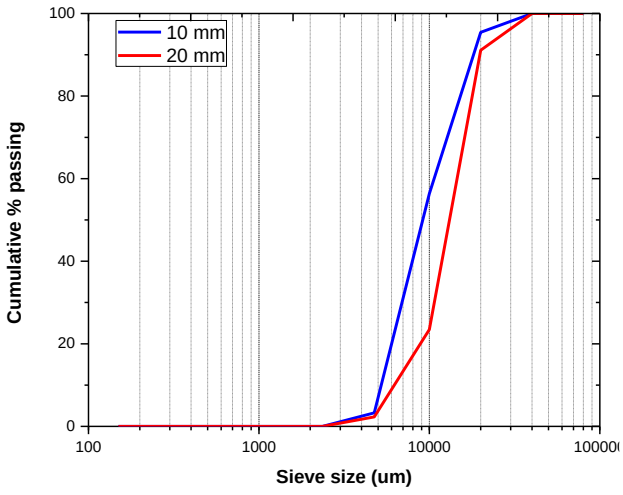

Fig 3.8: Cumulative Size Distribution Curve of Coarse Aggregate Particle

3.2.4 Fine Aggregate: The aggregate that passes through the sieve of 4.75 mm is termed as fine aggregate. It is obtained from natural disintegration of rocks, crushing of hard stone, crushing of natural gravels classified as natural sand, crushed stone, crushed gravel respectively. It provides uniformity by filling voids and act as workability agent. It reduces shrinkage cracking and provides plasticity to the mixture.

The aggregate was sieved to obtain sieve analysis. From sieve analysis aggregate were conforming to zone II and The results of tests such as Specific Gravity, Water Absorption, Sieve Analysis were calculated as follows:

Table 3.12: Physical Properties of Fine Aggregate

Characteristics	**Value/Observation**
Type	River Sand
Grading	Zone II
Fineness Modulus	2.59
Total Water Absorption	1.1
Specific Gravity	2.65

Table 3.13: Sieve Analysis of Fine Aggregate

Sr no.	**Sieve size**	**Mass Retained (gm)**	**The Percentage Retained**	**The Cumulative Percentage Retained**	**Percent Passing**
1.	4.75 mm	4	0.4	0.4	99.6
2.	2.36 mm	62	6.2	6.6	93.4
3.	1.18 mm	145	14.5	21.1	78.9
4.	600 um	224	22.4	43.5	56.5
5.	300 um	458	45.8	89.3	10.7
6.	150 um	89	8.9	98.2	1.8
7.	PAN	18	1.8	100	0

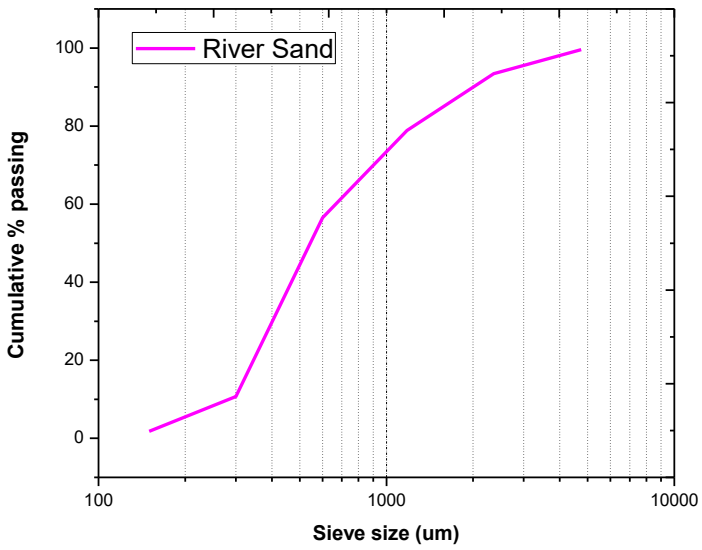

Fig 3.9: Cumulative Particle Size Distribution Curve of River Sand

3.2.5 Alkaline Liquid: Alkaline liquid is used to activate the geopolymer source material such as fly ash containing silica-alumina so that it can undergo polymerization. Instead of potassium hydroxide (KOH) and potassium silicate (K_2SiO_3), sodium hydroxide(NaOH) and sodium silicate(Na_2SiO_3) combinations are used. Due to the high cost of potassium hydroxide and potassium silicate, and its lowest extent of dissolution than sodium hydroxide, sodium hydroxide solution is preferable (Xu and Van Deventer 2000).

In the present work, the sodium hydroxide and sodium silicate solution were mixed, at least one day before use, because it releases high heat due to exothermic reactions between sodium hydroxide flakes.

3.2.5.1 ***Sodium Hydroxide Solution:*** NaOH solution of different concentration was prepared by mixing NaOH flakes in varying amounts. It must dissolve in water to make a solution with the required concentration. Concentration is expressed in terms of molarity in the range 8M to 16M.

To make 8M concentration solution, generally, 320 gm (8 x 40 =320 gm) (40 molecular weight) of NaOH flakes were added and made up to one liter. However, the mass of solid NaOH was taken as 255 gm in one kilogram for 8M and 444.6 gm in one kilogram for a 16M solution. In solution, the significant portion contains only water.

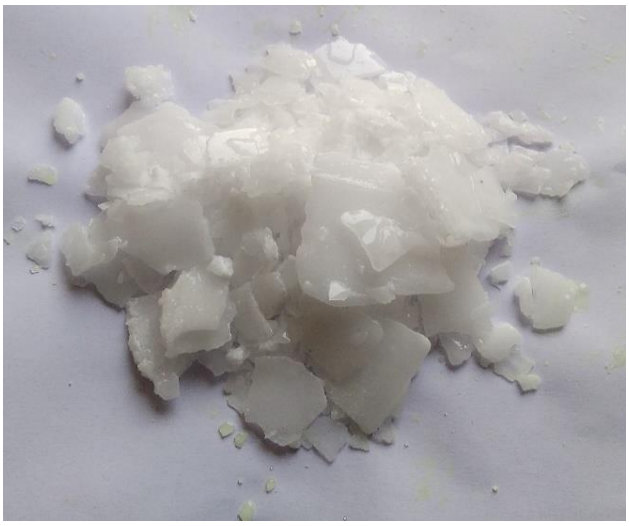

Fig 3.10: Sodium Hydroxide Flakes

Sodium hydroxide is also referred to as caustic soda. It is an ebullient product, so skin contact should be avoided. Globus and mask should be used during handling.

Table 3.14: Physical Properties of Sodium Hydroxide Flakes

Characteristics	**Value/Observation**
Nature	Hygroscopic
Shape	Semi-spherical
Color	White
Specific 8M	1.29
Gravity 16M	1.47
Molecular Weight	40
Density (g/ml)	2.13
PH	14

3.2.5.2 *Sodium Silicate*: It is accessible in a compact liquid form, also referred to as water or liquid glass. Sodium silicate has various industrial and commercial applications, commonly used in soap and detergent industries.

Table 3.15: Physical Properties of Sodium Silicate

Characteristics	**Value/ Observation**
Specific Gravity	1.52
Viscosity at 20^0C	400 cP

Table 3.16: Chemical Properties of Sodium Silicate

Sr No.	Constituents	Percentage Composition
1.	Na_2O	13.7
2.	SiO_2	29.4
3.	Water	55.9

Fig 3.11: Sodium Silicate Solution

3.3 Mix Design

In the present study, mix design was formulated on many natural sand substitutes at distinct Molarities, and separate tests are performed at 28 days to evaluate GPC's mechanical and durability characteristics. Various test data parameters, sample scheme, mix ratio adopted for mix design are shown here

3.3.1 Parameter and Mix Proportion

The different trials are done to develop the optimum mix proportion for the casting of geopolymer concrete. Different trials of alkaline liquid to fly ash ratio of 0.4, 0.45,0.5 and 0.55 are performed and based on strength achieved on these trials Alkaline liquid to fly ash ratio by mass is determined to be 0.5. Sodium silicate to sodium hydroxide ratio is chosen to be 2.5 based on the past literature (Hardjito 2005; Lloyd and Rangan 2010). Water to Geopolymer solid ratio is found out to be 0.251 and 0.224 for 8M and 16M geopolymer mix respectively.

Table 3.17: Mix Proportion of Geopolymer Concrete containing Sillimanite Sand

Mixes	Aggregate (kg/m^3)				Fly Ash (Kg/m^3)	NaOH Solution		Na_2SiO_3 Solution (kg/m^3)	Curing Conditions
	River Sand	Sillimanite Sand	Coarse Aggregate (20 mm)	Corse Aggregate (10 mm)		Mass (kg/m^3)	Molarity (M)		
GP08000ST	628	0	661	433	440	62	8	154	SC
GP08000	628	0	661	433	440	62	8	154	AC
GP08025	471	157	661	433	440	62	8	154	AC
GP08050	314	314	661	433	440	62	8	154	AC
GP08075	157	471	661	433	440	62	8	154	AC
GP08100	0	628	661	433	440	62	8	154	AC
GP16000ST	634	0	668	437	440	62	16	154	SC
GP16000	634	0	668	437	440	62	16	154	AC
GP16025	475.5	158.5	668	437	440	62	16	154	AC
GP16050	317	317	668	437	440	62	16	154	AC
GP16075	158.5	475.5	668	437	440	62	16	154	AC
GP16100	0	634	668	437	440	62	16	154	AC

SC: Steam curing of the specimen after demolding for 24 hours subsequently subjected to ambient curing for the age of 28 days
AC: Ambient curing of the specimen after demolding for the age of 28 days

The quantity of coarse aggregate and fine aggregate are found out using specific gravity of different material by using the absolute volume method. The coarse aggregates have approximately 63% by mass of total aggregate. Whereas as in coarse aggregate 40% of the particle was 10 mm nominal size and 60% of particles was 20 mm nominal size. The ratio of fly ash, fine aggregate, and coarse aggregate are found out to be 1:1.42:2.48 for 8M and 1:1.44:2.51 for 16M geopolymer mix respectively due to different Specific Gravity of 8M and 16M sodium hydroxide solution.

Different batches of mix proportion are prepared for the replacement natural sand with sillimanite sand at 25, 50, 75 and 100. Two batches of control mix without replacement are also prepared. Each specimen was prepared for two different molarity at 8M and 16M. The designation of the mix is given based on molarity and percentage replacement. GP08000 to GP08100 designation is for 8M molarity, and GP16000 to GP16100 designation is for 16M molarity according to replacement of Sillimanite sand.

3.3.2 Casting and Curing Procedure

The weighted quantities of sand, coarse aggregate, fly ash were dry mixed in a mechanical mixer for about 5 minutes until the uniform color was obtained without any cluster. The alkaline solution was prepared 24 hours before its use by mixing sodium silicate and sodium hydroxide solution, as explained earlier. The solution was added into the mixer at 4-5-minute time interval so that homogenous mixture was obtained.

Fig 3.12: Cast Molds containing Geopolymer Concrete

All the molds were appropriately oiled before pouring the mixture into it. The pouring was done in three layers, and after each layer, a vibrator was used for proper compaction of the mix. The finishing of the molds was done using a trowel and left at room temperature. After demolding of the specimen, the specimens were left for 28 days at ambient curing. One batch of control mixes was steam cured for 24 hours and subsequently left for 28 days at ambient curing. All the specimens were covered with sheets to minimize the moisture loss from them.

Table 3.18: Scheme of Sample Preparation of Geopolymer Concrete

Tests	Mechanical Tests		Durability Tests		
Designation	C. S. T.	S. T. S. T.	R.C.P.T.	S. T.	D. A. V. T.
GP08000ST	3	3	-	-	-
GP08000	3	3	3	3	3
GP08025	3	3	3	3	3
GP08050	3	3	3	3	3
GP08075	3	3	3	3	3
GP08100	3	3	3	3	3
GP16000ST	3	3	-	-	-
GP16000	3	3	3	3	3
GP16025	3	3	3	3	3
GP16050	3	3	3	3	3
GP16075	3	3	3	3	3
GP16100	3	3	3	3	3
Total	36	36	30	30	30

Total Sample prepared = 162

C.S.T.:Compressive Strength Test: (150x150x150) mm Cube
S.T.S.T.: Split Tensile Strength Test: (150 D X 300 H) mm Cylinder
R.C.P.T.: Rapid Chloride Permeability Test:(100 D X 50 H) mm Cylinder
S.T.: Sorptivity Test: (100 D X 50 H) mm Cylinder
D.A.V.T.: Density, Absorption & Void Test: (100 D X 50 H) mm Cylinder

3.4 Test Methods for Evaluation of Properties:

3.4.1 Compressive Strength Test:

By applying uniaxial loading, compressive strength of concrete is determined. The load is applied until stress in the material reaches its ultimate stage and fails. To conduct compressive strength test specimen of size 150x150x150mm were cast and de-molded after 24 hours and cured for 28 days at an ambient curing temperature, whereas control specimen were steam cured for 24 hours and subsequently cured for 28 days at an ambient curing temperature. Testing was done in CTM of 5000KN capacity at the rate of a 5KN / second. The maximum load applied to cube was noted. The compressive strength was calculated by the formula given below

$$\sigma = \frac{P}{A} \tag{3.2}$$

Where

σ = compressive stress in (N/mm^2)

The P = Applied load (N)

A= Cross Sectional area of the specimen in mm^2

Fig 3.13: Compressive Strength Test Setup

3.4.2 Split Tensile Strength:

The tensile strength of a concrete is an indirect method. Defined as maximum tension a material can take without tearing apart. In this test, the load is applied to the cylinder specimen of dia. 150mm and height 300mm by CTM of the 5000KN capacity of the cylinder cross its vertical diameter. The surface of the cylinder should be appropriate before applying load. The load is applied until the sample failure takes place. The following formula is used to calculate the split tensile strength:

$$F_{st} = \frac{2P}{\pi dl} \tag{3.3}$$

Where

F_{st} = split tensile stress in (N/mm^2)

P = Applied load (N)

d= dia of the cylindrical specimen in mm

l= length of the cylindrical specimen in mm

Fig 3.14: Split Tensile Strength Test Setup

3.4.3 Sorptivity Test:

Sorptivity is the material property to absorb water when only one surface of the concrete specimen is exposed to water. It is done by determining the rate of absorption of water by measuring the weight of the specimen as per code specified time intervals. Weight of specimen increases with time due to ingression of water from one surface by capillary action. Sample disc of dia. 100mm and height 50mm is used according to ASTM C1585-04. For testing disc was sealed from the top as well as from side by using epoxy. The initial mass of each sample disc was recorded, and the sample disc was placed in a tray and immersed in water up to a depth of 2-5 mm. The mass of each specimen was measured as per code specified time intervals. Sorptivity is found out by using formulas:

$$S = \frac{I}{\sqrt{t}} \tag{3.4}$$

Where

S= rate of Sorptivity in (mm/s)

t= time elapsed in Second

I= absorption

'I' can be found out using the formula

$$I = \frac{m_t}{a \times d} \quad (3.5)$$

Where

m_t = changed sample weight into grams

a = exposed sample weight in mm^2

d = water density into g / mm

Fig 3.15: Sorptivity Test Setup

3.4.4 Density, Absorption, and Void Test:

Density referred to as "how much solidify a material is" or say the Mass of the material divided by its volume. Whereas the percentage of absorption is the percentage of fluids that the material absorbs and the volume of permeable voids is the volume of voids that carry water through it. These characteristics are used in the determination of the matrix and the microstructure of concrete specimens. Density, Percentage absorption, the volume of permeable voids is determined as per guidelines of ASTM C642-06. Discs of size 100x50 mm were used at the age of 28 days. For purposes of conducting tests, the initial mass of each specimen was recorded and dry it in the oven at the temperature of 100^0 C to 110^0C for 24 hours. Cool it in a dry place and determine the mass. If there is a difference of 0.5 percent between two successive mass values, the specimen is returned in the oven. If the mass is less than 0.5% of the lowest value, designate it value "A." Immerse the specimen in the water at 21^0C for 48 hours. If two successive values of the mass of SSD sample at an interval of 24 hours show an increase in the mass of less than 0.5 % of larger value then designate it as "B." Place the specimen for 5 hours in hot water and allow the specimen to cool for a further 14 hours, by natural heat loss, and refer to the specimen mass as "C." Suspend the

specimen with wire to determine the apparent water mass and specify the specimen mass as "D." By using these values, the following calculations are done:

Bulk density, dry = $[A/(C-D)]\rho = g_1$

Apparent density = $[A/(A-D)]\rho = g_2$

Absorption after immersion and boiling (%) = $[(C-A)/A]x100$

Volume of permeable pore space (voids), % = $(g_2-g_1)/g_2 \times 100$

Total void volume, % = $(g_3-g_1)/g_3 x\ 100$

g_1 = bulk density, dry, Mg/m^3

g_2 = apparent density, Mg/m^3

g_3 = absolute density, Mg/m^3

ρ = density of water = 1 Mg/m^3

3.4.5 Rapid Chloride Permeability Test (RCPT):

The permeability of chloride in the structure influences the durability of concrete. Chlorides penetrate through voids in the concrete structure which weakens the bond and deteriorates the steel reinforcement leading to serious concerns. Chloride permeability of the concrete specimen is measured as per the guidelines of the ASTM C1202-97. The value of change of coulombs determines chloride ion permeability through the specimen of size 100x 50mm at the age of 28 days. Samples were placed in desiccator up to 3 hours, and the water was allowed to flow in the desiccator. The specimen was allowed to submerge for another 18 hours in a desiccator before testing. After that specimen was placed between two molds in which one mold was filled with 3 percent of NaCl solution and another mold is filled with 0.3N NaOH solution. The power supply of 60V was maintained throughout 6 hours. Total charge passed over 6 hours was noted.

Fig 3.16: Vacuum Pump & Desiccator

Fig 3.17: RCPT Test Setup

3.4.6. Scanning Electron Microscope (SEM):

SEM uses the high energy focused of an electron to magnify a specific sample region. A particular sample containing an area of interest is placed at the bottom of the SEM column within the vacuum chamber. Electron is produced by cathode column and strike the specimen. The specimen reflects some of the electrons, and some are absorbed. Two types of signals are detected by the electron microscope in which one is the secondary electron (SE), and the second is backscattered (BSE).

Fig 3.18: Scanning Electron Microscope

These signals create grayscale images of the sample of high resolution and magnifications. SEM plays an essential role in analyzing the microstructure of concrete. It characterized the

microstructure of concrete, which consist of aggregate, interfacial transition zone, and particle bonding, and it is used to find the factors which alter the mechanical and durability properties of concrete. SEM effectively magnify a sample region up to 50,000 times.

3.4.7. Energy Dispersive X-Ray Spectroscopy (EDS) & Element Mapping:

EDS is used in conjunction with SEM and analyzes the elemental composition of an area of interest by identifying and observing X- Rays, the detected X-Rays are then segregated into energy channels which form a spectrum of detected energy. EDS quantifies voltage pulses in Kev. Which are generated are identified as chemical elements.

Through EDS Line mapping and area mapping of element composition in the sample region can also be identified. Through line mapping, we can identify each element concentration throughout the line. Whereas in area mapping can also be obtained for each element and use varying colors to show the concentration of the specific element across the area which is inspected. Further, this mapping is used in the sample for screening purposes or failure related issue.

3.4.8. X-Ray Powder Diffraction:

XRD is used to identify the phase of the material's crystallinity. X-ray diffraction is based on the crystalline sample's constructive interference with the monochromatic X Rays. X rays are transmitted by a cathode ray tube, filtered by monochromic radiation and incident upon crystalline solid and diffracted by crystallographer planes in various directions. These scattered phases produce constructive interference. When the waves are in phase or satisfy Bragg's law ($n\lambda=2dSin\omega$) (where n is an integer, λ is wavelength and d is spacing between two planes) produces constructive interference and when the waves are out of phase or not satisfy Bragg's law produces destructive interferences. The sample can be measured using a range from 2ω angle to achieve all diffraction directions in the lattice. d spacing of planes enables to identify the mineral because of the distinctive d-spacing of each mineral, and this is achieved by comparing d-spacing to conventional reference patterns. XRD is used for determination of unknown crystal structure of solid. Rigaku makes X-ray diffractometer (model ultima-IV) at NPL, New Delhi was used to carry out the XRD analysis.

Fig 3.19: X-Ray Powder Diffractometer

CHAPTER 4
RESULTS AND DISCUSSIONS

4.1 General

The discussion and analysis have been made to figure out the influence of various parameters such as the effect of replacing natural sand by sillimanite sand, the effect of molarity of NaOH and curing condition on the geopolymer concrete. The mechanical and durability tests were conducted on the control geopolymer concrete, and sillimanite contained concrete and discussed thoroughly in this section. In addition to it, the SEM, EDS, line mapping, area mapping, and XRD analysis are also performed to analyze the microstructure of geopolymer concrete.

4.2 Compressive Strength Test

The compressive strength result of geopolymer concrete mix category of GP16 and GP08 are shown in Table 4.1. It is observed that steam cured sample shows the highest compressive strength among all sample for both GP16 and GP08 mix. The compressive strength of mixtures cured at only ambient curing temperature shows lesser strength compared to the steam-cured sample.

Table 4.1: Compressive Strength Result of GP 16 and GP 08 Category Geopolymer Concrete

Designation	**Compressive Strength (MPa)**	**Standard Error (±MPa)**	**Designation**	**Compressive Strength (MPa)**	**Standard Error (±MPa)**
GP16000ST	**38.46**	3.49158	GP08000ST	**29.26**	1.24544
GP16000	24.67	0.35277	GP08000	21.6	1.21655
GP16025	33.53	0.98206	GP08025	**27.8**	1.90088
GP16050	**35**	1.31149	GP08050	24.6	1.02632
GP16075	26.33	1.00885	GP08075	23.8	0.98658
GP16100	25.6	0.23094	GP08100	23.1	0.72111

However, from observation, it was clear that the overall strength of the GP16 mix is higher than that of the GP08 category mix. It has been observed that the strength is increased up to 50% replacement of natural sand with sillimanite sand and then starts decreasing in GP16 mix. The gain of strength at 50% replacement of sillimanite sand (GP16050) is highest

(41.87%) compared to the control sample (GP16000). Whereas gain of strength of specimen GP16025, GP16075 and GP16100 are 35.91%, 6.73%, and 3.77% compared to control sample (GP16000). Whereas specimen GP16050 shows only a 9% decline in strength compared to steam cured sample (GP16000ST).

The similar trend is also observed for the GP08 mix, which shows the maximum strength is obtained at 25% replacement level. The compressive strength of GP08025 is 27.8MPa, and it is 32.38% higher than the control sample (GP16000). However, strength is 4.98% lower than steam cured sample (GP08000ST) whereas the strength was increasing at the rate of 17.14%, 13.33% and 10% for GP08050, GP08075, and GP08100 sample as compared with the control sample (GP16000).

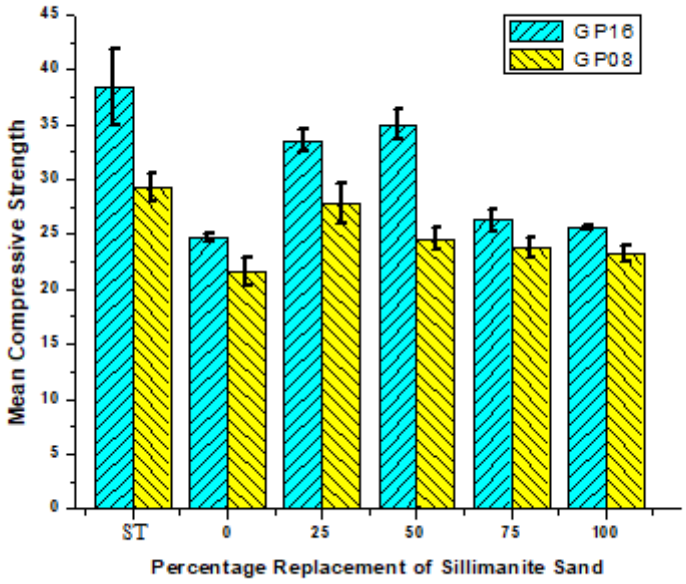

Fig 4.1: Compressive Strength Results of GP 16 and GP 08 Category Geopolymer Concrete

A higher strength of GP16 mix in comparison to GP08 mix is due to higher NaOH concentration, which leads to more dissolution of Si and Al elements which are present in fly ash. Also, this action leads to form more NASH gel, which connects more substantial material, and solid content increases, this leads to the denser matrix which improves compressive strength (Malkawi et al. 2016; Reddy et al. 2010; Shadnia and Zhang 2017).

In all batches, the steam-cured sample shows the highest strength this was since steam curing enhances the polymerization process by liberating its heat energy to the molecules of polymerizing material. The rapid reaction between binder gel leads to an increase in strength in a short time. The trends are similar to observed in previous studies (Adam and Horianto 2014; Al Bakria et al. 2011; İlkentapar et al. 2017).

It can be seen that the maximum strength is observed for GP16050 and GP08025 mixes. The increase in strength of GP16 category mix up to 50% replacement of natural sand with sillimanite sand is due to the conversion of Al-Si fly ash by structure-forming alkaline metal (Na^+) present in the alkaline solution which dissolves it into amorphous alumina silicate gel. This gel acts as a binder and dispersed across partially dissolve flyash and sillimanite sand particle. Also, this formed geopolymer is a mixture of undissolved crystalline aluminosilicate Flyash particle and semi-crystalline to the amorphous aluminosilicate gel phase. In this polymer, Si, and Al ion is tetrahedrally arranged and crosslinked together (Davidovits 1991; Xu and Van Deventer 2002). The sillimanite sand particle which is already orthorhombic crystal formed the substantial crystalline structure by combining with semicrystalline polymers. The higher molarity may also cause the dissolution of sillimanite crystal structure, making a robust O-Si-O-Al gel which can make concrete denser and can enhance strength. However, river sand also plays a vital role in particle packaging due to its good gradient in comparison to sillimanite sand (Cai 2017). Also, the coarser structure of river sand helps in making active interfacial transition zone, which leads to an increase in strength (Muttashar et al. 2018).

When sillimanite sand is increased beyond 50%, this leads to the formation of the more crystalline product but also increases the risk of instantaneous cracks. The finer particle more than 50% act in a two way; some amount of sand actively participate in the formation of the crystalline product whereas some amount act as a filler material. Also, sillimanite sand particles which are act as a filler material (unreacted or does not participate in crystallinity of matrix) introduce slippage due to its smooth surface texture. One of the reasons for decreasing the strength more than 50% replacement is that finer material has a larger specific area which leads to the reduction in alumina silicate gel as finer material consume more gel on its outer circumference (Nguyen et al. 2018; Singh and Siddique 2012). However, mix GP08 shows higher strength at 25% replacement, which also attribute to less molarity of the solution and which participate in less sillimanite content. Addition of more sillimanite does not contribute to an increase in strength and strength starts to decrease.

4.3 Split Tensile Strength Test

Table 4.2 shows the split tensile strength results of control mix and natural sand replaced with sillimanite contained geopolymer concrete. The steam cured sample GP16000ST and GP08000ST shows the peak strength among all specimen. Whereas overall strength of GP16

mix is higher in comparison to GP08 mix. The reason for that is already explained in compressive strength section.

The results show a similar inclination as of compressive strength. The variation of strength among all specimen is low, but strength is exceptionally high. in GP16 mix gain of strength of sample GP16025, GP16050, GP16075, and GP16100 is 13.20%, 15.09%, 2.83%, and 5.66% compared to control sample. Sample GP16050 shows the highest strength among all specimen cured at ambient curing, whereas its strength is 15.56% lower than steam cured sample (GP16000ST). However, exception observed in case of sample GP16100 which show an increase in strength in comparison to GP16075.

Table 4.2: Split Tensile Strength Results of GP16 and GP08 Category Geopolymer Concrete

Designation	**Split Tensile Strength (MPa)**	**Standard Error (±MPa)**	**Designation**	**Standard Error (±MPa)**	**Split Tensile Strength (MPa)**
GP16000ST	**14.13**	0.40552	GP08000ST	0.13333	**10.93**
GP16000	10.6	0.5696	GP08000	0.30551	7
GP16025	11.93	0.17638	GP08025	0.48074	**9.26**
GP16050	**12**	0.70238	GP08050	0.17638	7.93
GP16075	11	0.80829	GP08075	0.46667	7.46
GP16100	11.4	0.72111	GP08100	0.23094	6

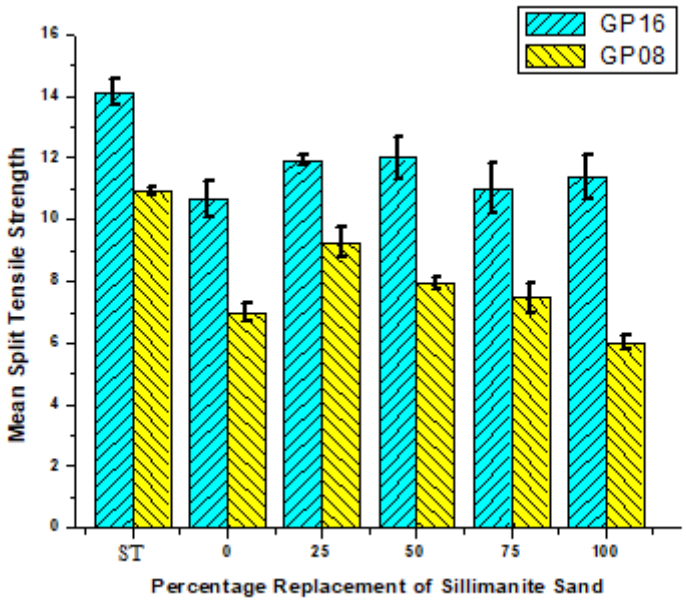

Fig 4.2: Split Tensile Strength of GP 16 and GP 08 Category Geopolymer Concrete

Whereas in GP08 mix split tensile strength of samples are compared with control samples, and it shows a gain in strength of about 32.28%, 13.28%, 6.57% of samples GP08025, GP08050, GP08075 respectively. Whereas a decrease in strength was observed at the rate of 14.28% for sample GP08100. Sample GP08025 shows highest split tensile strength among specimen cured at ambient temperature; however, strength was lower (15.28%) than the steam-cured sample (GP16000ST).

In GP16 mix, 50% replacement shows maximum strength due to higher crystallinity by the contribution of both amorphous to the semi-crystalline structure of geopolymer and sillimanite crystal. However, when the load is applied strength is distributed among its all crystal and When specimen reached its maximum limit, a series of smaller microcracks leads to the formation of bigger crack and specimen breaks. The decrease in strength above 50% replacement is also attributed to increase in specific surface area due to a finer particle which decreases the binder gel content by spreading around the particle and also increase in slippage due to the smooth surface texture of sillimanite particle leads to increase the risk of sudden crack and strength decreases. Whereas in the GP08 mix, 25% replacement shows higher strength due to less alkalinity of material result in a low polymerization rate. Addition of more sillimanite sand leads to an increase in the content of undissolved and unreacted sand particle due to the less dissolving rate of 8M molarity, which leads to decrease the strength.

4.4 Sorptivity Test

Figure 4.3 shows the Sorptivity result of mix GP08 and GP16 category specimen. Where GP16 mix shows less Sorptivity in comparison to GP08 mix. The values of the GP16 mix show more considerable variation among replacement in comparison to GP08 mix where result shows an almost similar result. The graph is showing the result of mix GP16 and GP08.

Table 4.3: Initial Sorptivity Results of GP 16 and GP 08 Category Geopolymer Concrete

Designation	**Initial Sorptivity ($mm/s^{1/2}$)**	**Standard Error ($\pm mm/s^{1/2}$)**	**Designation**	**Initial Sorptivity ($mm/s^{1/2}$)**	**Standard Error ($\pm mm/s^{1/2}$)**
GP08000	0.4687	0.05862	GP16000	0.18266	0.01568
GP08025	0.39328	0.0263	GP16025	0.08115	0.01671
GP08050	0.36901	0.02088	GP16050	0.07463	0.00386
GP08075	0.429	0.02055	GP16075	0.13384	0.00562
GP08100	0.44409	0.02211	GP16100	0.10907	0.00126

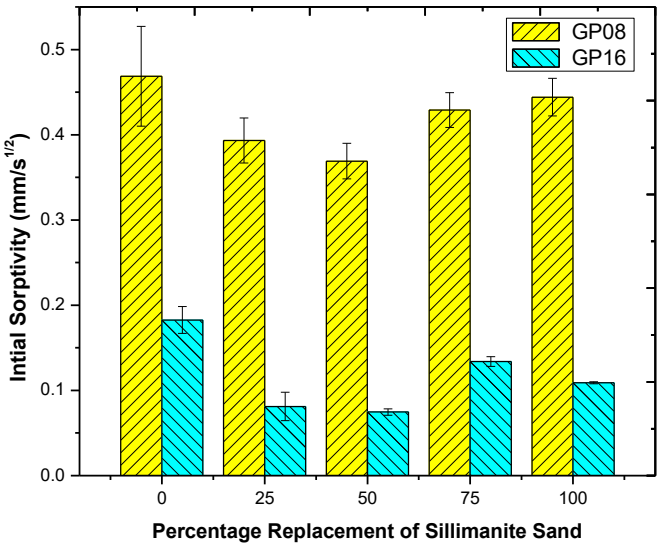

Fig 4.3: Initial Sorptivity Results of GP 16 and GP 08 Category Geopolymer Concrete

In GP16 mix, GP16050 have least value among all other specimen and it is 71.76% lower than control specimen (GP16000) whereas specimen GP16025, GP16075 and GP16100 values are 55.61%, 26.71% and 40.34% lower than control specimen (GP16000).

whereas GP08 mix shows decrease in Sorptivity value at the rate of 16.09%, 21.27%, 8.47% and 5.25% of sample GP08025, GP08050, GP08075 and GP08100 sample compared to control sample. Sample GP08050 shows the least initial Sorptivity value among all other specimens. However, the value of GP08050 is 394.45% higher than GP16050 specimen.

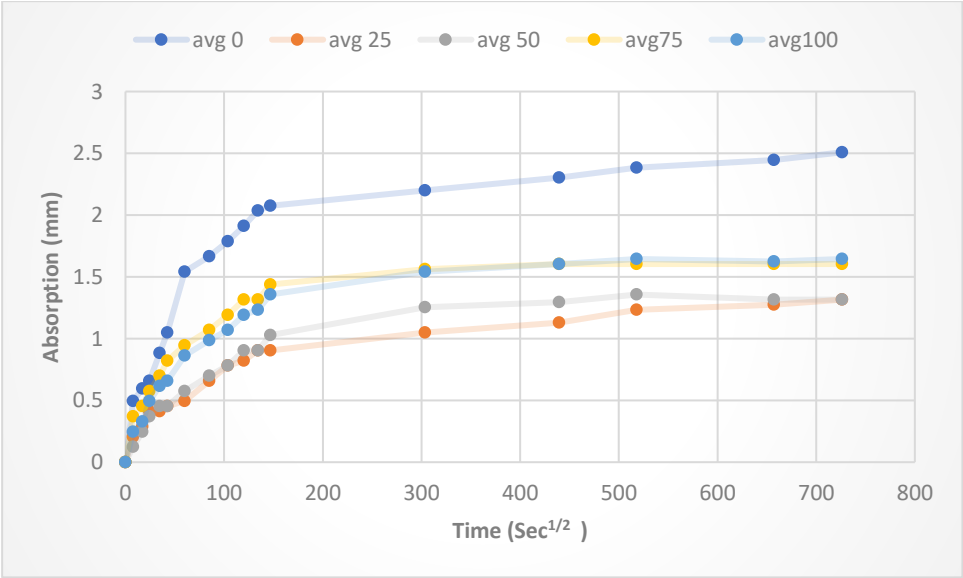

Fig 4.4: Sorptivity Result of GP16 Mix

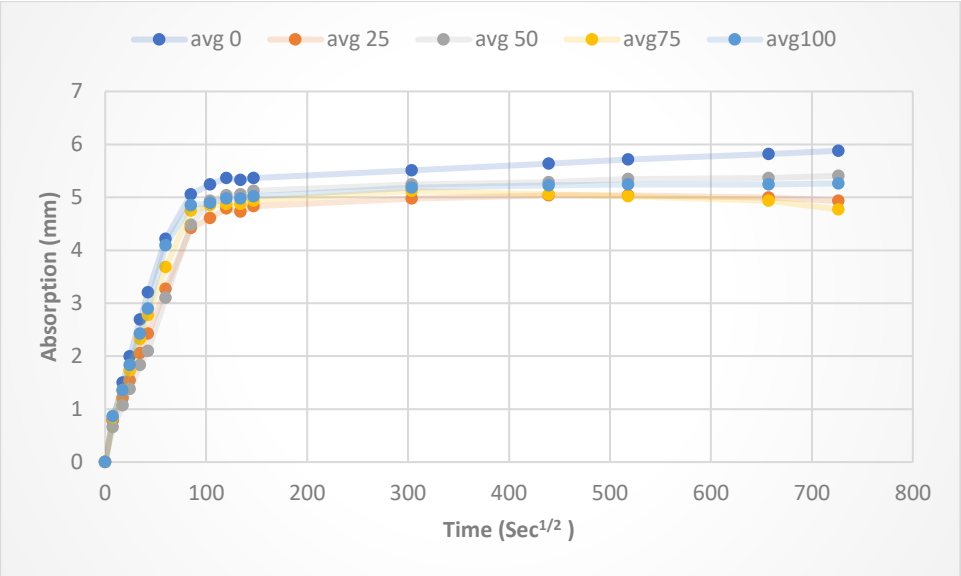

Fig 4.5: Sorptivity Result of GP08 Mix

GP08 mix shows higher Sorptivity due to more voids inside the structure, which is due to less alkalinity of structure result in a faint solid structure. In the GP08 category mix, GP08050 show least Sorptivity, but in GP16 mix sample, GP16025 and GP16050 show least and almost similar Sorptivity. The rapid decrease in Sorptivity value is due to the availability of all size of the particle due to the content of sillimanite sand and river sand, which both are enough to fill up the permeable void inside the structure.

Moreover, particle packaging behavior of the river sand also contributes to filling up the void inside geopolymer concrete, whereas increases in crystallinity due to alumina silicate gel and sillimanite make the structure more impermeable. In specimen GP16000 show high Sorptivity value due to river sand leaves micropores inside the structure, which increase the Sorptivity due to capillary voids inside the structure. The increase in sillimanite content above 50% replacement does not attribute to a decrease in Sorptivity but leaves permeable void due to unreactive sillimanite sand particle. Also, the sparse gradient of sillimanite sand does not contribute to filling permeable voids inside the structure. However, values are not much diverse by increasing sillimanite content.

4.5 Rapid Chloride Permeability Test

Figure 4.6 and Table 4.3 shows the values of charged passed of the rapid chloride permeability test. Initially, the test shows overflow, which is not a good representation of the test. For that purpose, modified geopolymer concrete is used by pretreating it using oven curing for one day before place in the incubation chamber (Thomas and Peethamparan 2017). The overflow appears due to the unreacted residual of the alkaline activator solution, which misleads the result.

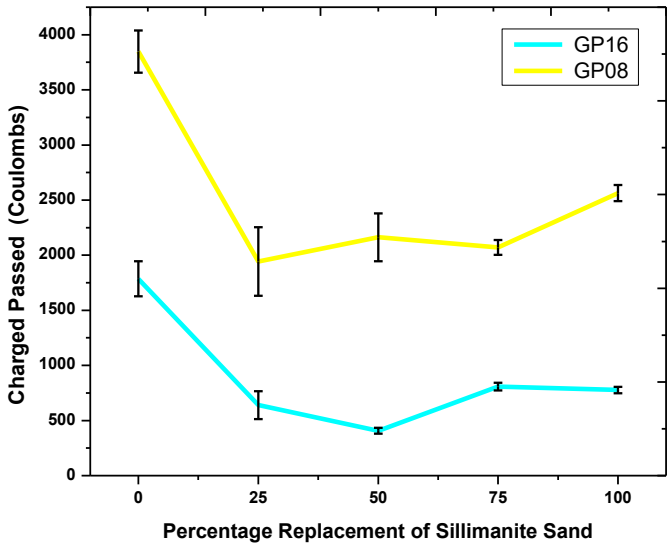

Fig 4.6: Result of Charged Passed in GP08 mix and GP16 Mix Geopolymer Concrete

The mix GP08 shows higher charged passed as compare to GP16 mix. The 50% replacement of natural sand with sillimanite sand (GP16050) shows less charged passed, and its value is 77.24% lower than the control sample (GP16000). Chloride ion permeability of control sample (GP16000) specimen is 'low' whereas, chloride ion permeability of all other specimens of GP16 mix is 'very low.' values of GP16 mix are decreasing at the rate of 64.16%, 54.78% and 56.49% for sample GP16025, GP16075 and GP16100 respectively compared to control sample.

Table 4.4: Chloride ion Permeability Test Results of GP 16 and GP 08 Category Geopolymer Concrete

Designation	**Charged Passed (Coulombs)**	**Standard Error (±Coulombs)**	**Chloride ion Permeability**
GP08000	3847.67	191.7588	Moderate
GP08025	1942.33	310.7091	Low
GP08050	2163	216.7971	Moderate
GP08075	2070	68.15994	Moderate
GP08100	2563.33	72.69648	Moderate
GP16000	1786	158	Low
GP16025	640	127	Very low
GP16050	406.5	26.5	Very low
GP16075	807.67	34.70991	Very low
GP16100	777	28.53653	Very low

In the case of the GP08 category mix, GP08025 shows lowest charged passed. However, the assumption was made up in the case of GP08050 value, which shows higher charged passed as compare to GP08075 but shows almost similar results. Chloride ion permeability of GP08025 specimen is 'low' whereas, chloride ion permeability of all other specimens of GP08 mix is 'Moderate.' Whereas values of GP08 mix are decreasing at the rate of 49.52%, 43.78%, 46.20% and 33.38% for GP08025, GP08050, GP08075, and GP08100 respectively compared to control sample. Furthermore, values of GP08025 and GP08050 are 203.5% and 432.10% higher than GP16025 and GP16050 respectively.

Overall charged passed in GP16 category mix is lower than GP08 mix. This result is due to higher molarity of NaOH solution, which leads to more dissolution of Al and Si ion out of the fly ash, which increases the amount of alumina silicate gel and makes matrix denser. Due to this void decrease and chloride permeability lower itself. In case of GP16 mix, GP16050 show lowest permeability, this was due to sillimanite sand which gives better effect with river sand by filling pores of geopolymer concrete. The less permeability is also achieved due to the denser matrix, which is achieved by crystallinity in geopolymer matrix. Whereas GP16000 shows more permeability, possibly due to micropores inside the structure which is not filled by river sand itself leading to penetration of chloride ion.

4.6 Density, Absorption, and Percentage of Total Voids

Figure 4.7 &4.8 shows the bulk density and apparent density of the GP16 and GP08 category mix. The value of both densities increases linearly with an increase in percentage replacement for GP16 mix and GP08 mix. The bulk density values of GP16025, GP16050, GP16075 and GP16100 are 2.6%, 2.85%, 2.93% and 4.29% higher than control sample. Whereas, values of apparent density are 0.051%, 0.112%, 0.703% and 1.84% higher than control sample for sample GP16025, GP16050, GP16075 and GP16100 respectively.

Table 4.5: Bulk Density, Dry Results of GP 16 and GP 08 Category Geopolymer Concrete

Designation	**Bulk Density, dry (g/cm^3)**	**Standard Error ($\pm g/cm^3$)**	**Designation**	**Bulk Density, Dry (g/cm^3)**	**Standard Error ($\pm g/cm^3$)**
GP08000	2.24589	0.01631	GP16000	2.29504	0.00687
GP08025	2.27171	0.00366	GP16025	2.35479	0.00523
GP08050	2.29882	0.00034	GP16050	2.3605	0.00745
GP08075	2.29789	0.00228	GP16075	2.36233	0.00561
GP08100	2.31984	0.00346	GP16100	2.39352	0.00331

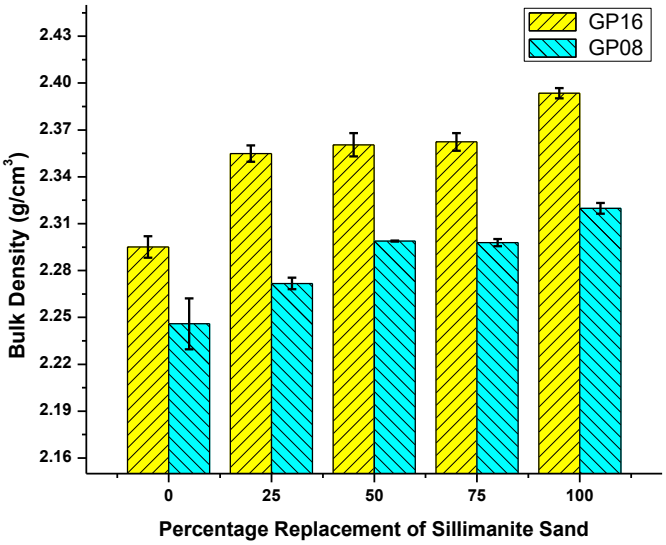

Fig 4.7: Bulk Density- Dry Results of GP 16 and GP 08 Category Geopolymer Concrete

This trend shows that bulk density and apparent density of the GP16 mix is quite similar. GP08 mix shows the linear variation of values among specimens. The bulk density values of GP08025, GP08050, GP08075 and GP08100 are 1.15%, 2.36%, 2.31% and 3.29% higher than control sample. Whereas, values of apparent density are 0.74%, 1.97%, 2.12% and 3.20% higher than control sample for sample GP08025, GP08050, GP08075 and GP08100 respectively.

Increase in bulk density values with increase in percentage replacement was due to the denser structure whereas the density of structure increases with increase in finer content of sillimanite sand, which fills micropores inside the structure, impossible to fill by river sand. Also, less pore space and higher weight in the same volume is the factor for the increase in bulk density. The same reason also stands for apparent density where extra material is occupying space in the same volume due to finer content of sillimanite sand.

Table 4.6: Apparent Density Results of GP 16 and GP 08 Category Geopolymer Concrete

Designation	**Apparent Density (g/cm^3)**	**Standard Error ($\pm g/cm^3$)**	**Designation**	**Apparent Density (g/cm^3)**	**Standard Error ($\pm g/cm^3$)**
GP08000	2.3391	0.02052	GP16000	2.36987	0.01546
GP08025	2.35653	0.00782	GP16025	2.37112	0.00857
GP08050	2.38524	0.00122	GP16050	2.37256	0.00551
GP08075	2.3887	0.00958	GP16075	2.38656	0.00573
GP08100	2.41423	0.00379	GP16100	2.41369	0.006

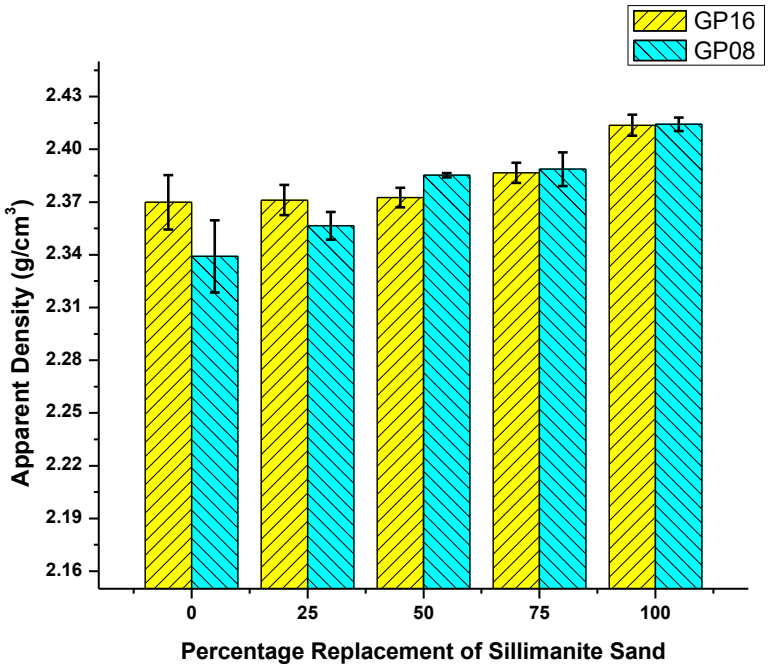

Fig 4.8: Apparent Density Results of GP 16 and GP 08 Category Geopolymer Concrete

The values of percentage absorption and volume of permeable voids values give a similar trend as of Sorptivity values for mixes GP16 mix and GP08 mix, as shown in Figure 4.9 and 4.10. The value of GP16 category mix for GP16025, GP16050, GP16075 and GP16100 of percentage absorption are 78.74%, 84.28%, 68.70%, and 74.56% lower than control sample respectively. Least value is observed for GP16050 sample. For GP08 mix, value of apparent density are 10.56%, 11.07%, 6.72% and 4.90% lower than control sample for sample GP08025, GP08050, GP08075 and GP08100 respectively. Least value was observed in this case were also for GP08050.However, GP08025 gives an almost similar result.

Table 4.7: Absorption after Immersion and Boiling, % Results of GP 16 and GP 08 Mix Geopolymer Concrete

Designation	**Absorption, %**	**Standard Error (± %)**	**Designation**	**Absorption, %**	**Standard Error (±%)**
GP08000	1.77241	0.05213	GP16000	1.37309	0.14951
GP08025	1.58363	0.20787	GP16025	0.29185	0.0729
GP08050	1.5761	0.0206	GP16050	0.21579	0.06252
GP08075	1.65325	0.12468	GP16075	0.42966	0.01159
GP08100	1.68546	0.00363	GP16100	0.34876	0.07739

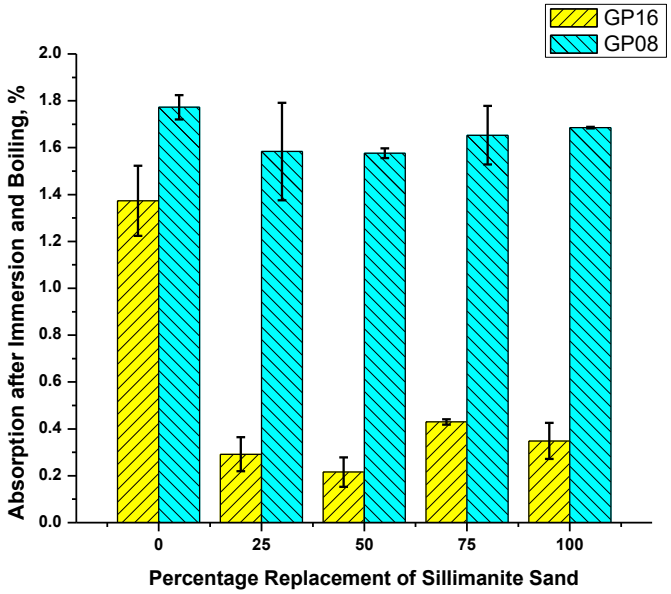

Fig 4.9: Absorption after Immersion and Boiling, % Results of GP 16 and GP 08 Category Geopolymer Concrete

A higher value for GP08000 was attributed to more pore space available due to the less fine particle in river sand which do not participate in filling up pore space. Whereas the least value was observed for 50% replacement in both cases is due to filling up pore space due to a finer particle. Also, the availability of all size of particle in the matrix for 50% replacement. Whereas crystallinity of structure also plays a vital role by making matrix dense and more impermeable.

Table 4.8: Volume of Permeable Pore Space, % Results of GP 16 and GP 08 Category Geopolymer Concrete

Designation	**The Volume of Pore Space, %**	**Standard Error (± %)**	**Designation**	**The volume of Pore Space, %**	**Standard Error (± %)**
GP08000	3.98231	0.14587	GP16000	3.15325	0.35114
GP08025	3.59609	0.4672	GP16025	0.68775	0.17293
GP08050	3.62316	0.04734	GP16050	0.50869	0.14672
GP08075	3.79954	0.29025	GP16075	1.015	0.02741
GP08100	3.90999	0.01098	GP16100	0.83484	0.18541

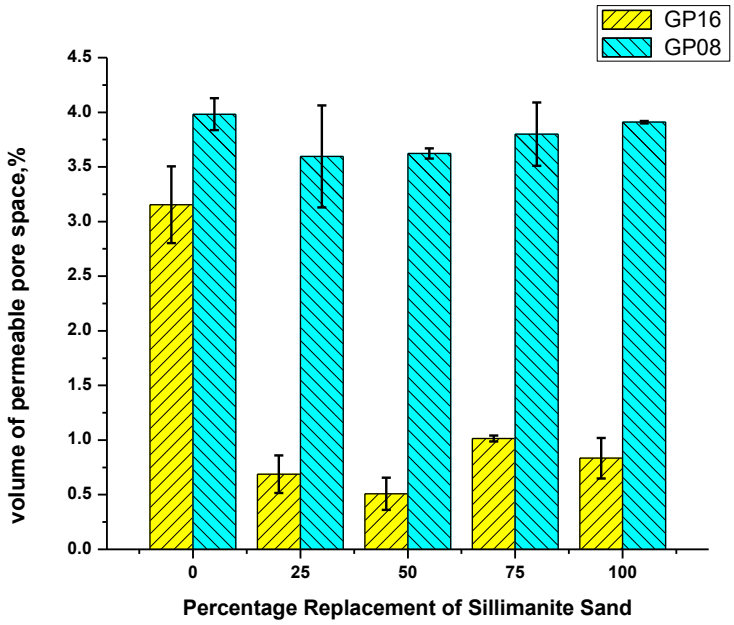

Fig 4.10: Volume of Permeable Pore Space, % Results of GP 16 and GP 08 Category Geopolymer Concrete

The value of volume of permeable voids of GP16 category mix for GP16025, GP16050, GP16075 and GP16100 are 78.19%, 87.22%, 74.51%, and 79.03% lower than control sample respectively. The least and higher value in GP16 category mix is the same as in the case of percentage absorption. However, value of volume of permeable voids in GP08 mix for GP08000, GP08025, GP08050, GP08075 and GP08100 are 9.70%, 9.02%, 4.6% and 1.81% lower than control sample respectively. The least value, in this case, is almost the same for sample GP08025 and GP08050, whereas higher value was observed for sample GP08000. The reason for the highest and lowest value for the volume of permeable voids was similar to as in case of percentage absorption. However overall values of percentage absorption and volume of permeable pore space were greater of GP08 mix due to less dense structure and more permeable space in concrete because of less alkalinity of a solution.

Total void volume percentage is decreasing linearly with increase in the value of percentage replacement, as shown in figure 4.11. The Total void volume value in case of GP08025, GP08050, GP08075, and GP08100 is 15.70%, 32.23%, 31.66%, and 45.04% lower than the control sample. Whereas, values of Total void volume are 51.98%, 56.95%, 58.54% and 85.66% lower than control sample for sample GP16025, GP16050, GP16075 and GP16100 respectively.

The overall value of the total void volume was higher for the GP08 mix. This is due to more permeable pore space in structure due to the less dense structure, which was attributed to less dissolution of fly ash particle by low molarity result in less alumina silicate gel formation.

Whereas value is decreasing with increasing in sillimanite content, decrease in value is attributable to the fineness of sand which fills the micropores inside the structure impossible to fill up by river sand which result in a decrease in the overall void volume.

Table 4.9: Total Void Volume, % of GP 16 and GP 08 Category Geopolymer Concrete

Designation	**Total Void Volume, %**	**Standard Error (± %)**	**Designation**	**Total Void Volume, %**	**Standard Error (± %)**
GP08000	6.80962	0.67681	GP16000	4.77029	0.28503
GP08025	5.73799	0.15178	GP16025	2.29083	0.21685
GP08050	4.61333	0.01424	GP16050	2.05411	0.30932
GP08075	4.65203	0.09476	GP16075	1.97794	0.23283
GP08100	3.74126	0.14355	GP16100	0.68381	0.13716

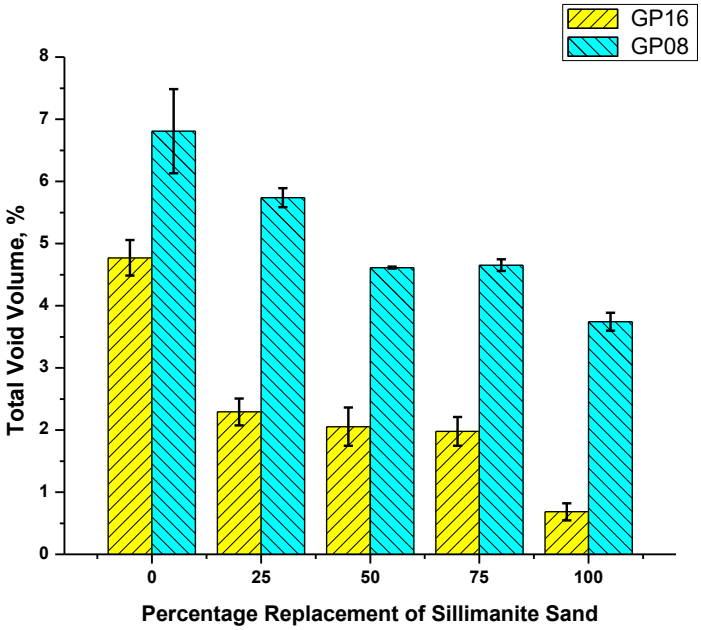

Fig 4.11: Total Void Volume, % of GP 16 and GP 08 Category Geopolymer Concrete

4.7 Microstructural Evaluation

4.7.1 Scanning Electron Microscopy (SEM), Electron Dispersive Spectroscopy (SEM), Line Mapping and Area Mapping

SEM images are used to analyze the microstructural properties of geopolymer concrete using sillimanite sand. Fig 4.12 shows 1500 and 3500 magnification of sample GP08000. From SEM image 4.12 1),2), indicate that particles are bonded with NASH gel, which makes

particles strong to respond to external forces; however, particle voids in the sample is due to the absence of finer material The image 4.12 1) also shows the bundle of the needle of Al-Si gel, which contributes to making geopolymer strong. SEM image 4.12 2) shows the crosslinking between the gel network, which leads to binding up the material. Whereas less alkalinity of the solution resulting in unreacted and partially reacted flyash particle and less dense structure. This indicates the sample's less compressive and tensile strength while the particle's voids indicate the porous structure.

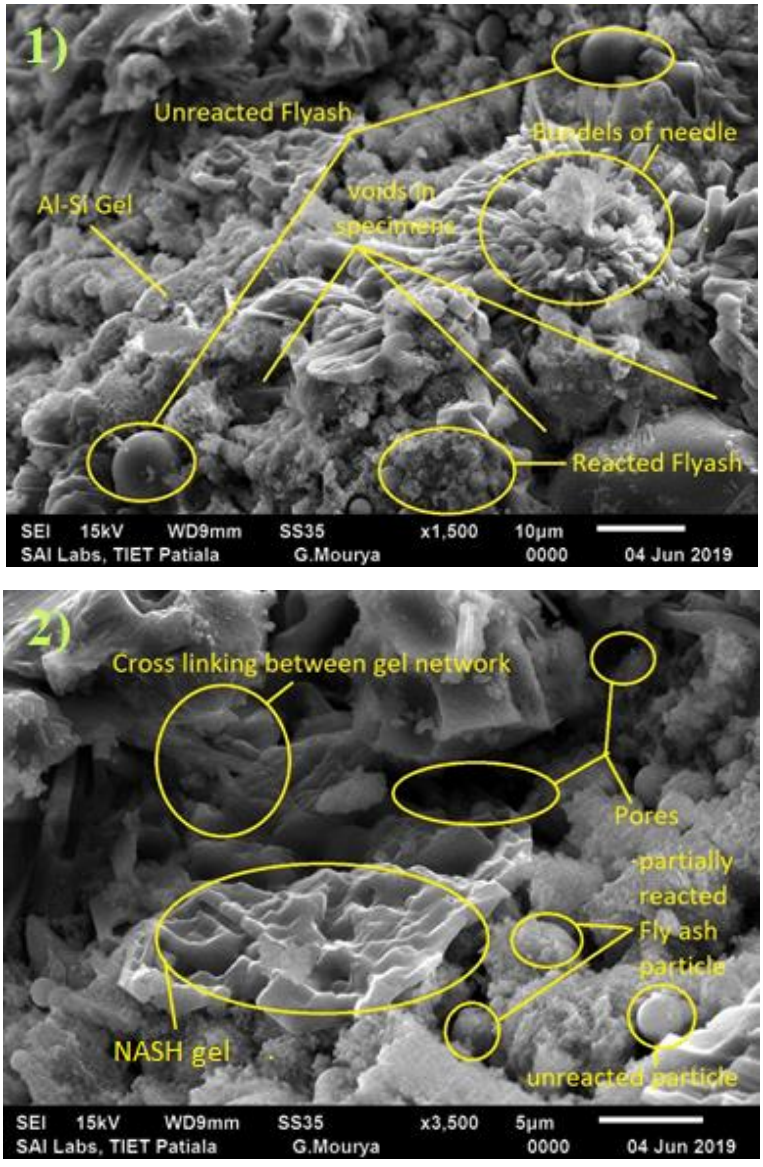

Fig 4.12: SEM Images of Sample GP08000 1) x1500 2) x3500 Magnification

Area mapping in Figure 4.13 shows the proportion of different particle in the mapping. The mapping indicates the uniform distribution of Al, Si, and Na in the sample Na in the structure indicates the development of NASH gel around fly ash particles, whereas Ca present in flyash particles also plays a significant part in CASH gel formation. Whereas Sulphur, zirconium,

ferrous, magnesium are also present in the structure. However, the denseness of ferrous is least.

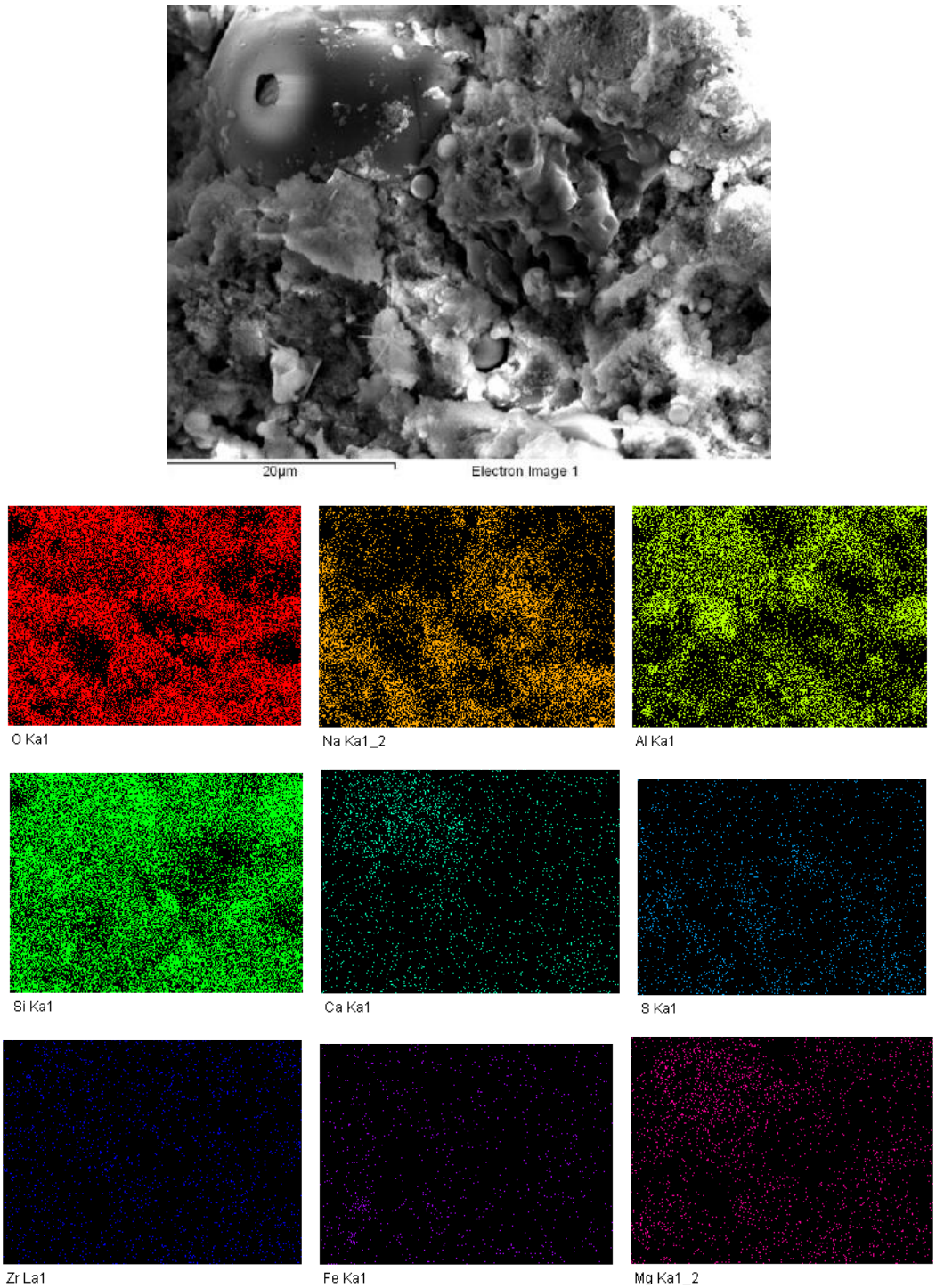

Fig 4.13: Area mapping of GP08000

The line mapping of the GP08000 structure is shown in Fig 4.14, and it is drawn between the zone of fly ash and NASH gel. It is strong evidence that the alkaline solution is contributing to the dissolution of the fly ash particle, making the equilibrium between Al and Si element. The center of the line shows the downturn of the element representing voids. Whereas Al-O-

Si-O bonds are formed on the broader oxide content in the gel region. Unreacted fly ash particles, however, result in lower gel content and lower strength. The elements such as zirconium, sulfur is present in a lower proportion in gel and has minimal impact on geopolymer concrete strength.

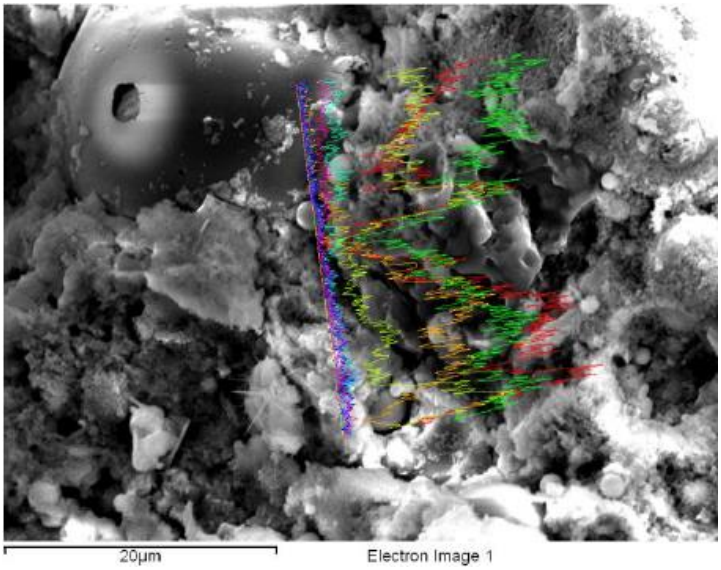

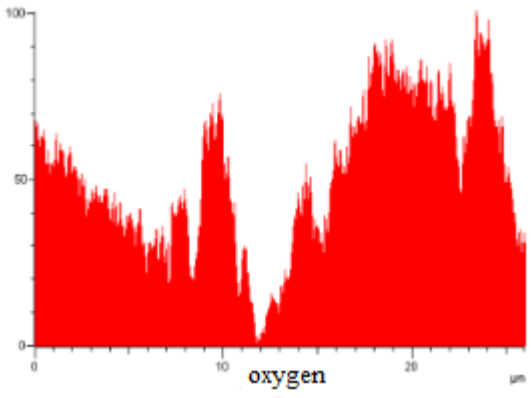

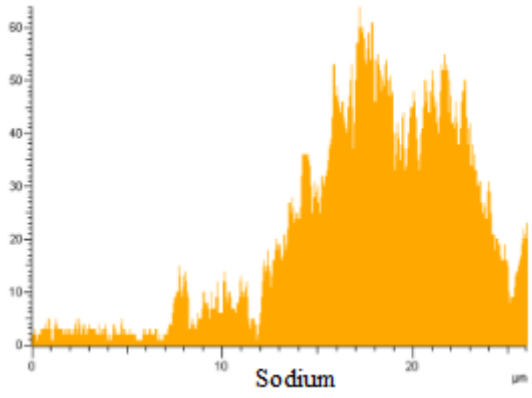

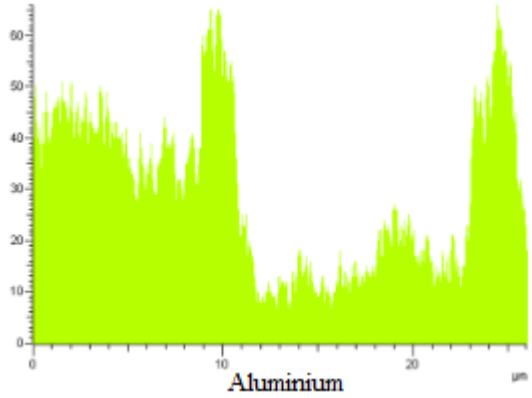

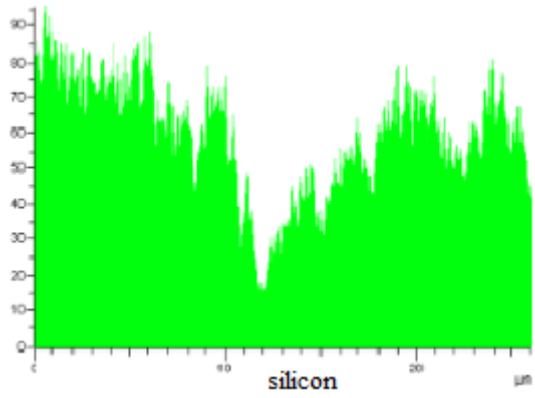

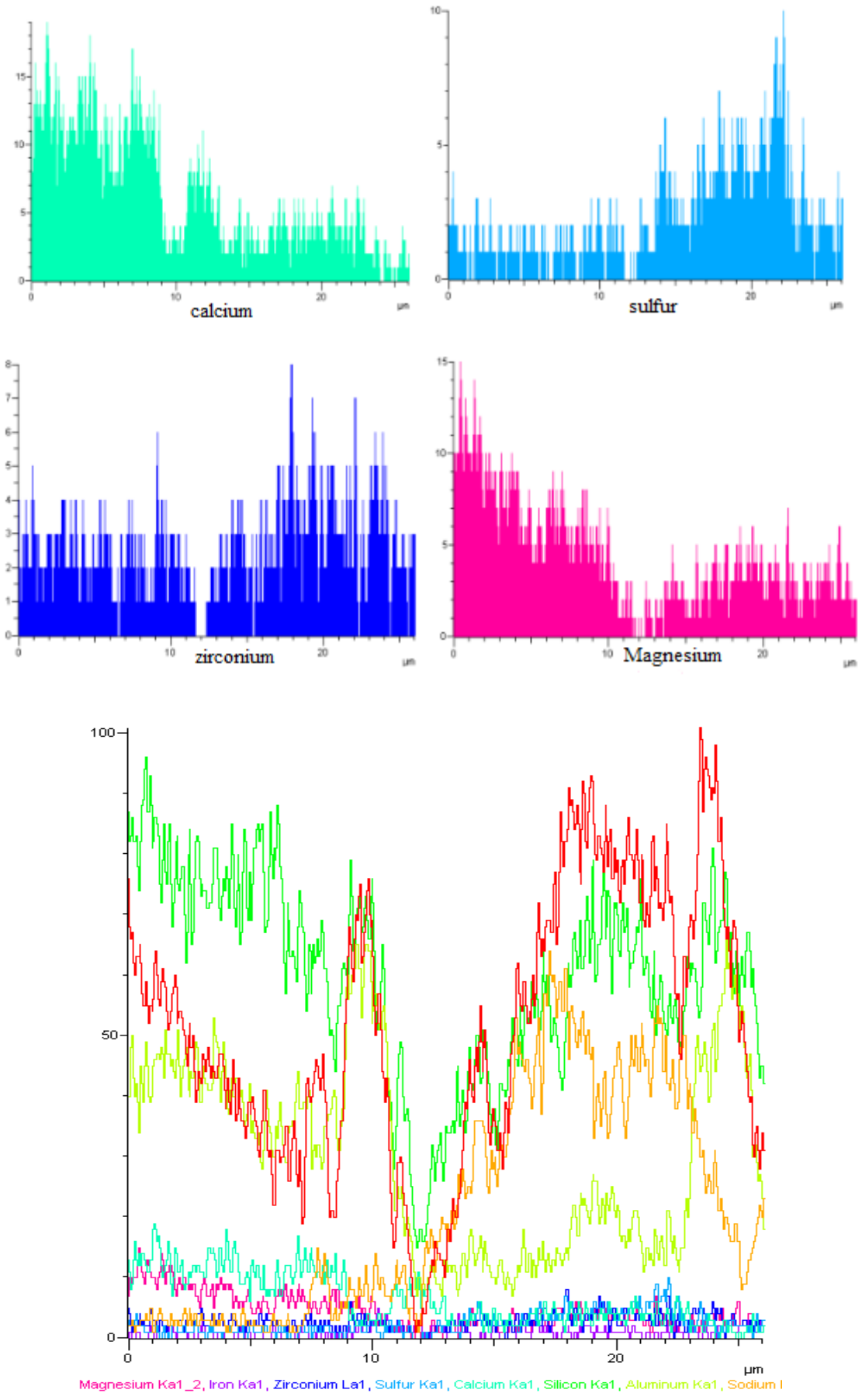

Fig 4.14: Line Mapping of GP08000

In Figure 4.15 showing the EDS spectrum, which shows fully dissolved fly ash particle due to dissolution from the alkaline solution. The particle spreading dissolves gel across its perimeter which functions to bond aggregate however in Figure 4.16 demonstrates the formation of gel with high Na content in which Al and Si are present in lower quantity this contrast represents the unparticipated gel.

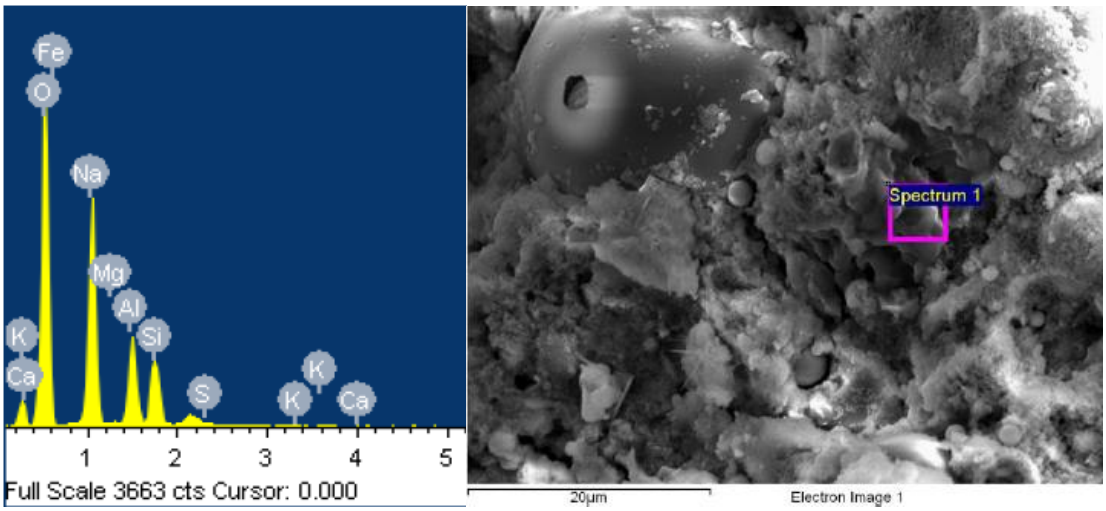

Fig 4.15: EDS and SEM Image of Sample GP08000 Spectrum 1

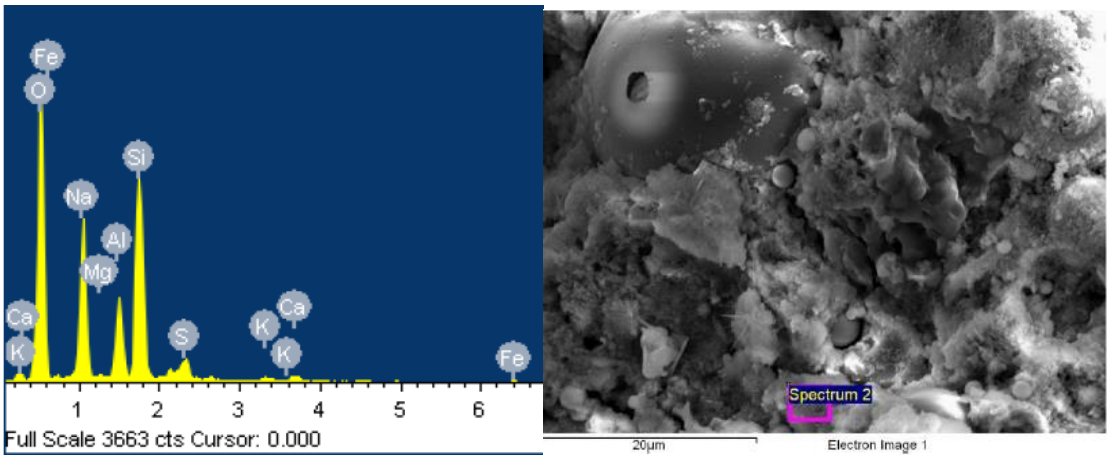

Fig 4.16: EDS and SEM Image of Sample GP08000 Spectrum 2

The SEM image of sample GP08025 is shown in Figure 4.17 1),2). It demonstrates that the pattern of fractures may be due to the compressive strength test after effect. From Figure 4.17 1), It is seen that sand particle, potentially a sillimanite sand particle from EDS analysis, dissolving in alkaline solution. This is strong evidence of formation NASH gel formed by fly ash and sand later converted into an amorphous gel to the semi-crystalline structure. The SEM image 4.17 1) also shows the fully dissolved and partially dissolved particles. The

partially dissolved particle indicates the lesser alkalinity of the solution. Also, pore in the structure indicates less stable content owing to the lesser formation of NASH gel. However, SEM images 4.17 2) demonstrate dissolution of gel between matrix aggregate interface, which enhances the external load carrying capacity by blocking the crack pattern.

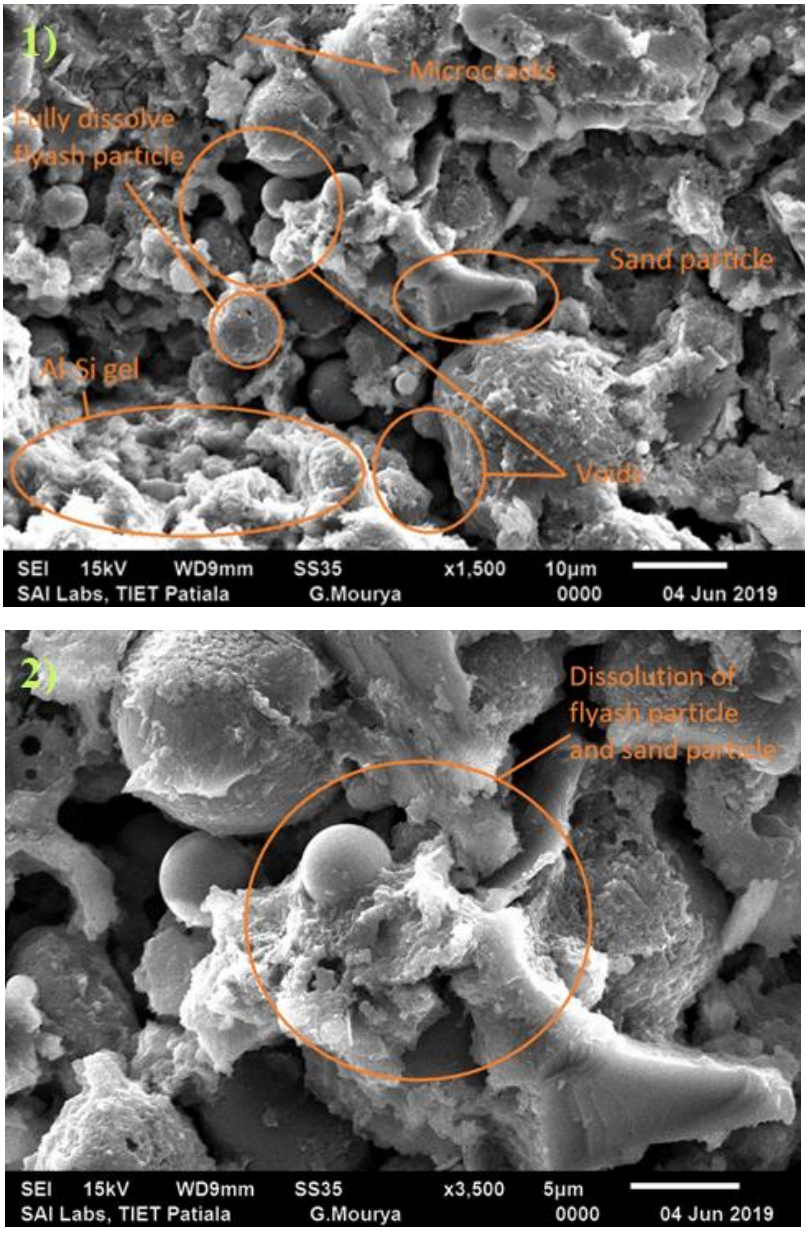

Fig 4.17: SEM Images of Sample GP08025 1) x1500 2) x3500 Magnification

EDS mapping of the area, as shown in Figure 4.18 demonstrates a higher Silica to alumina ratio owing to strong content of Al, Si, and K present on sand particle also seen in EDS figure 4.20 and 4.21. The Higher silica to alumina proportion leads to more polymerization due to more raw material being present. The particle demonstrates the KASH gel due to potassium content concerning Al and Si. While mapping region also demonstrates the influential

interconnection of particles through the gel phase. However, element like Ca and Fe is present in low amount in the sample.

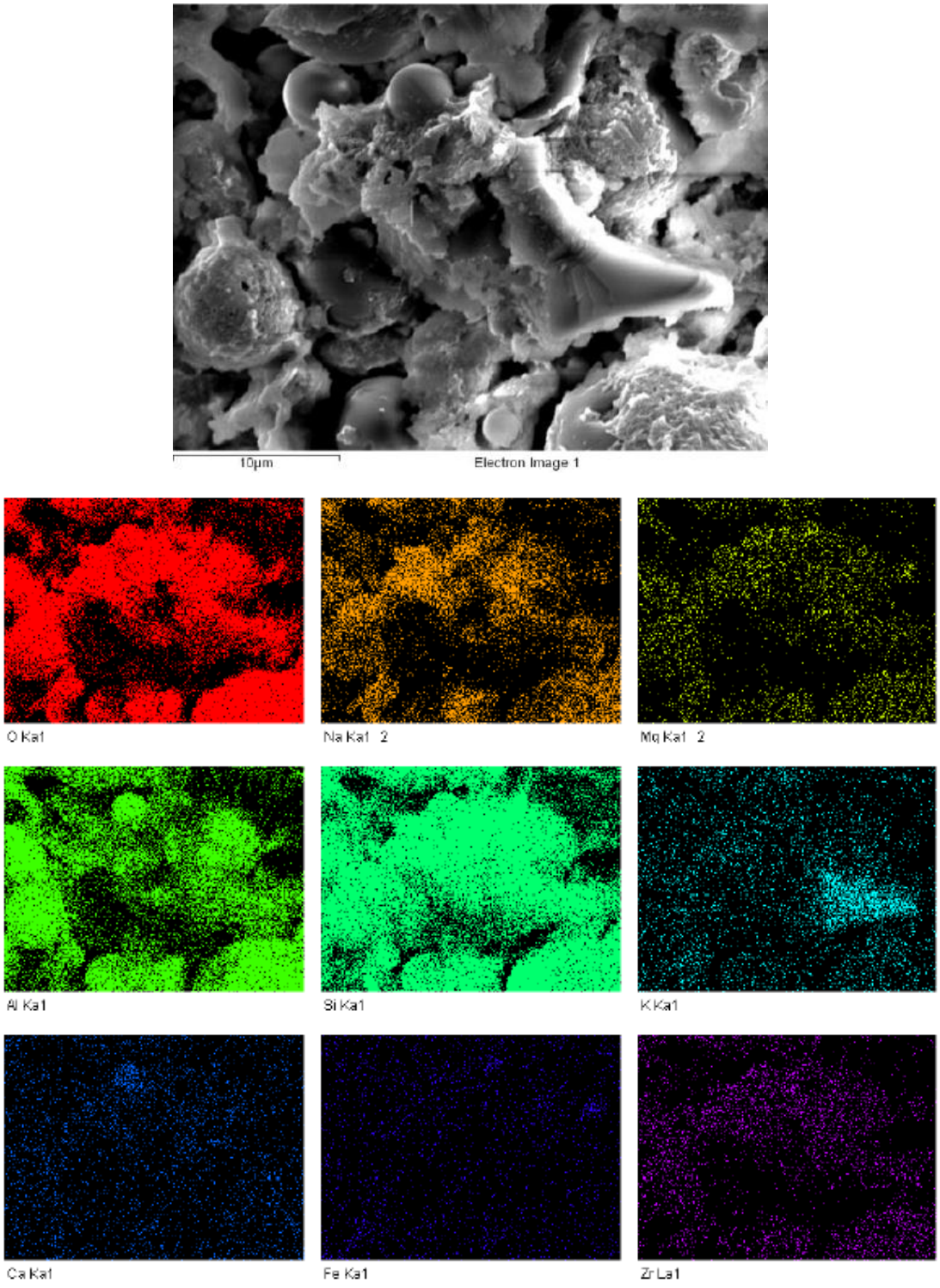

Fig 4.18: Area Mapping of GP08000

Line mapping of the sample, as shown in Figure 4.19, indicate NSH gel between fly ash and sand particle due to high Na and Si content and lesser Al content. After moving forward; it can be seen that the formation of KASH gel also helps to connect the structure. The presence of sillimanite, Alumina, and zirconium element can be seen in triangular shape particle,

which shows possible evidence of sillimanite sand. The calcium present in particles of fly ash also contributes to CASH gel production.

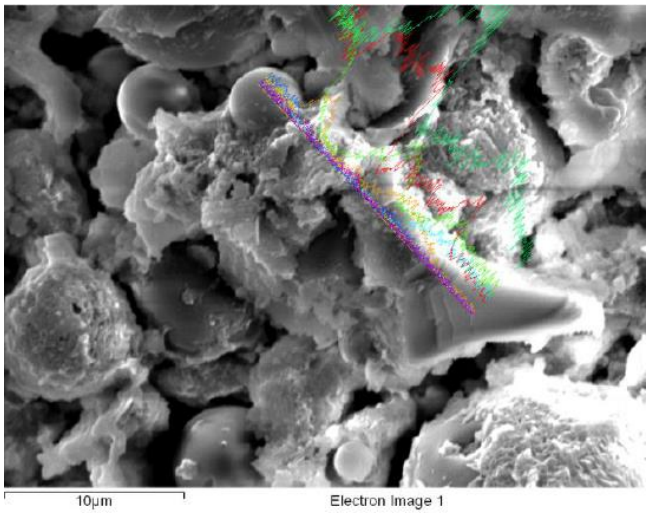

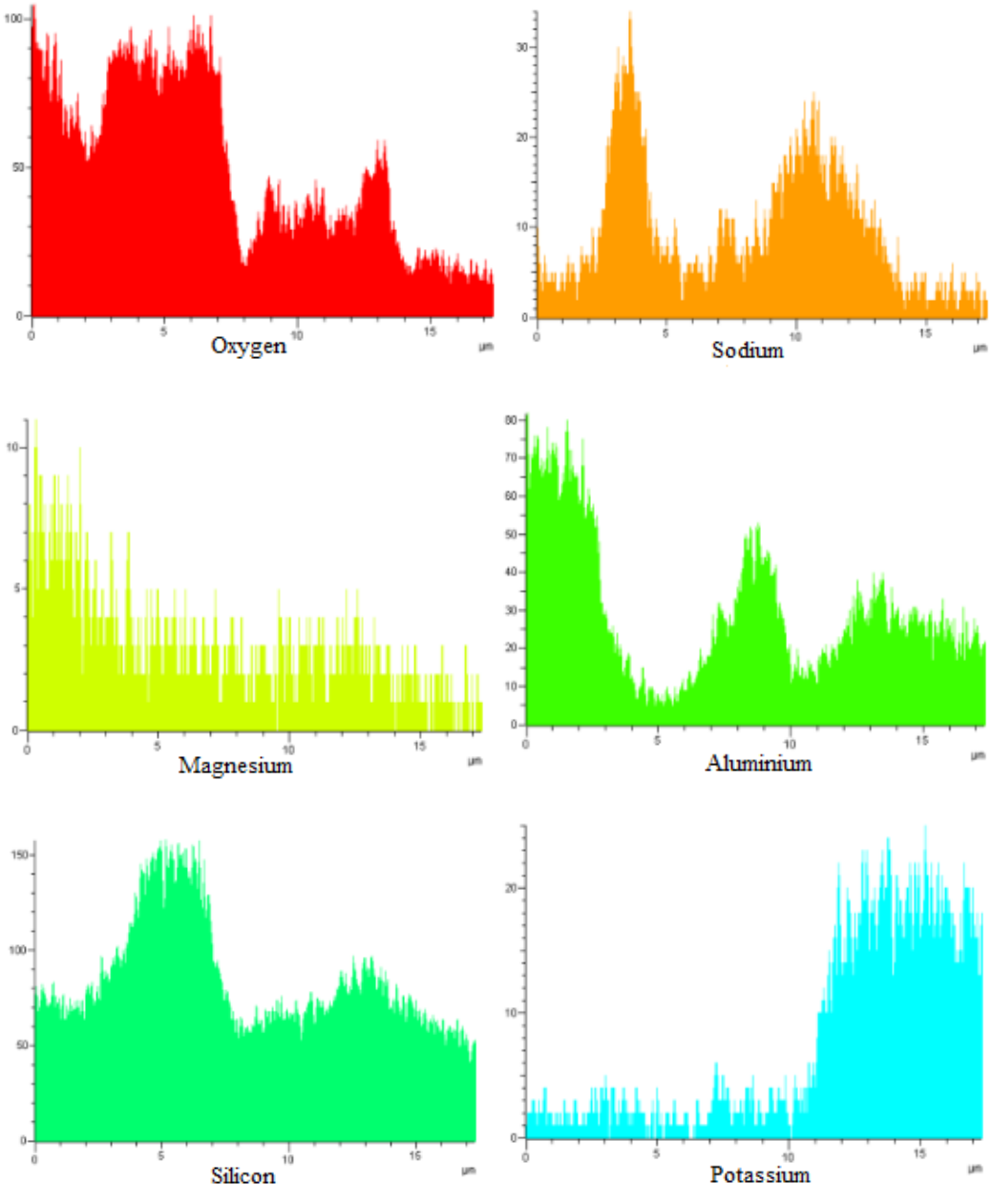

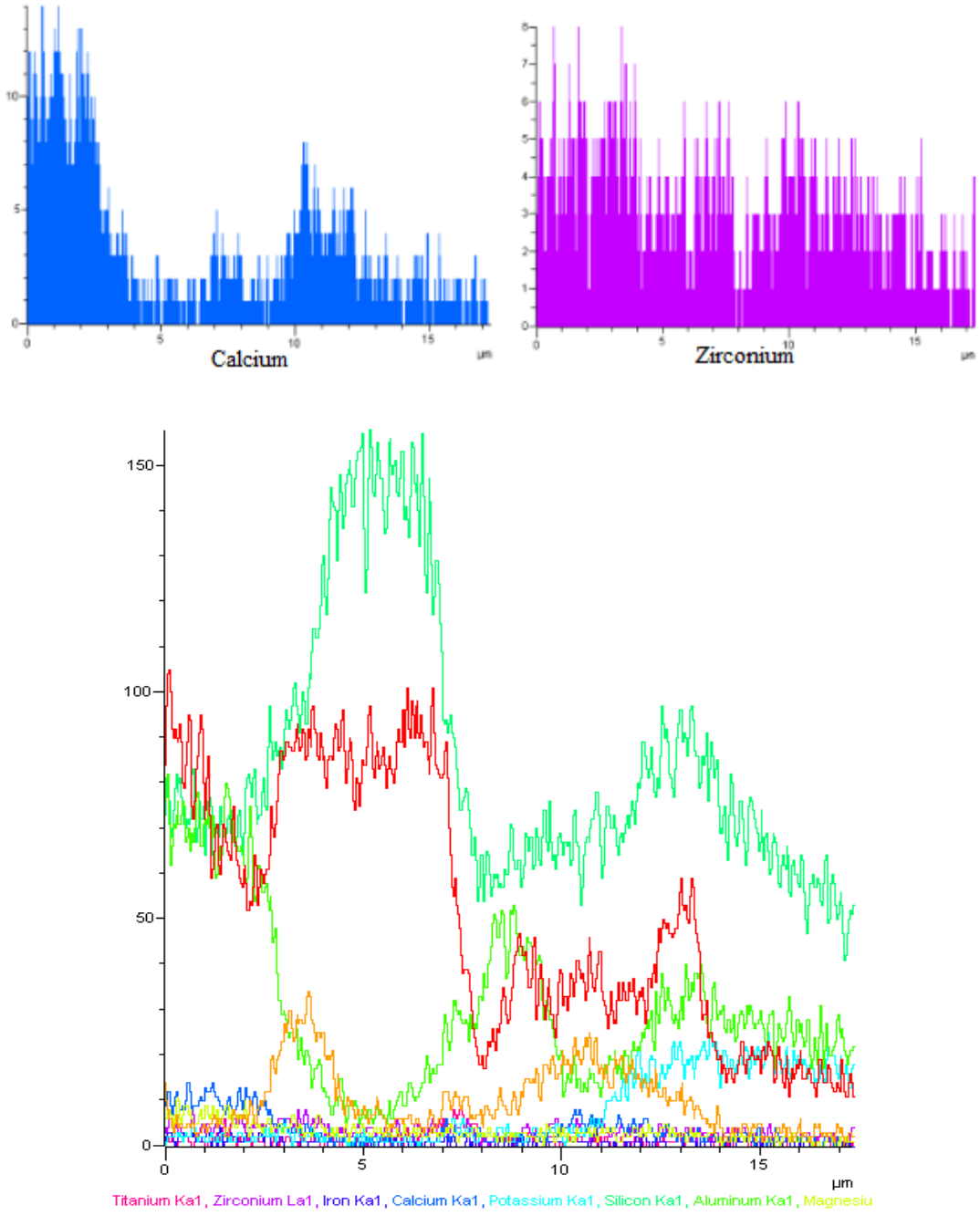

Fig 4.19: Line Mapping of GP08025

The EDS analysis of GP08025 is shown in Figure 4.20. It shows that the high Si content may attribute due to gel formed during polymerization of a sand particle; however, particles also indicates the formation of KASH gel due to potassium content. The different aluminosilicate crystal particles lead to different aluminosilicate gel, and this gel combination leads to difficulties in separating particles from one another and often hard to differentiate particles from each other. Spectrum 2 in Fig. 4.21 indicate interconnected alumina-silicate gel covering particles which result in making matrix denser.

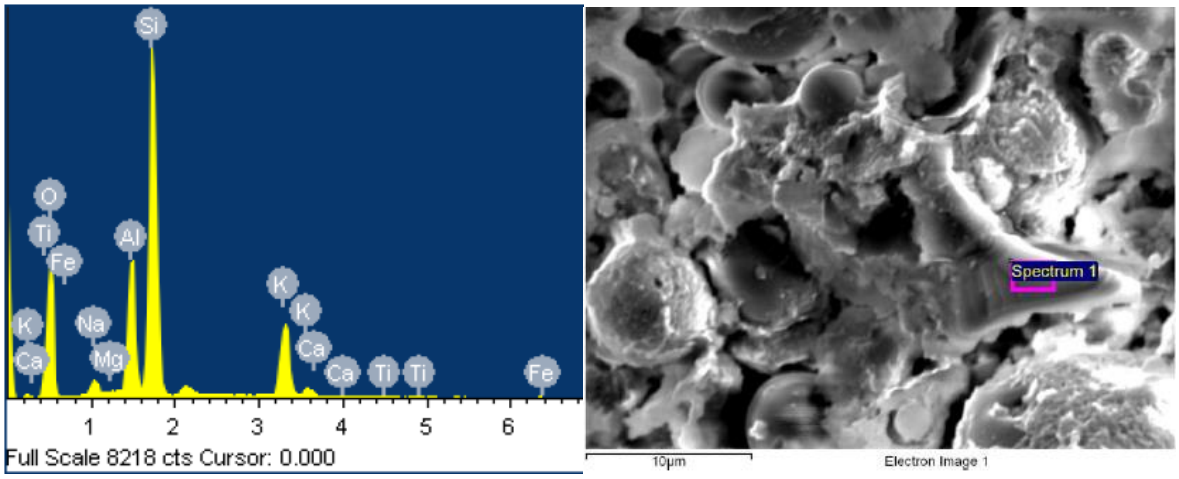

Fig 4.20: EDS and SEM Image of Sample GP08025 Spectrum 1

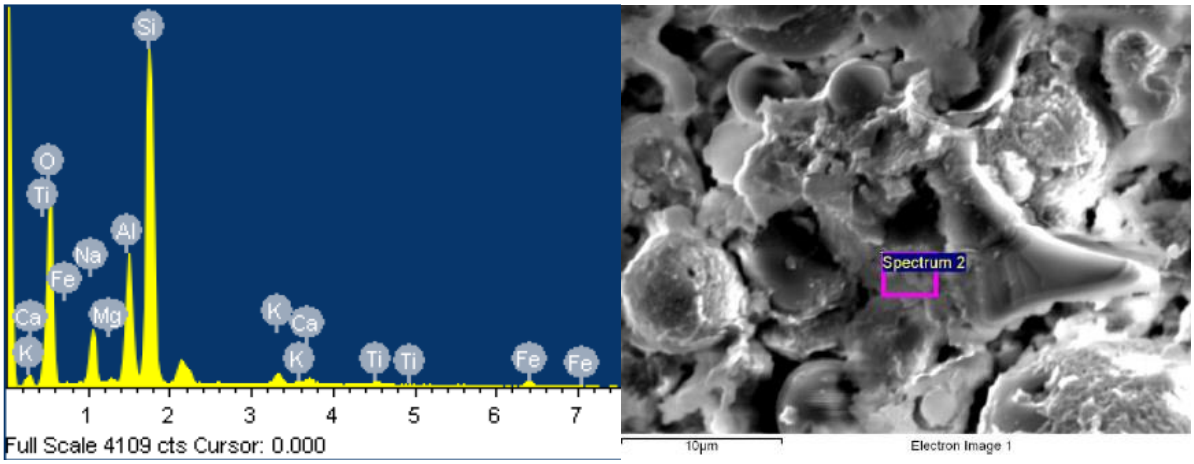

Fig 4.21: EDS and SEM Image of Sample GP08025 Spectrum 2

The SEM figure 4.22 1) of GP16000 indicate a crack pattern in the sample and whereas figure 4.22 2) indicate voids in the structure. The voids may be attributed due to the absence of finer material; however, the Figure shows a denser structure in comparison to the GP08 mix due to more dissolution of Al-Si. This is due to higher NaOH concertation. The denser structure and solid content attribute to the increase in strength. The loosely bonded sand particle in figure 4.22 2) may be due to less crystallinity or gel formation. Figure 4.22 1),2) also show some unreacted or partially reacted fly ash particle but in lesser content, as compared to GP08 mix.

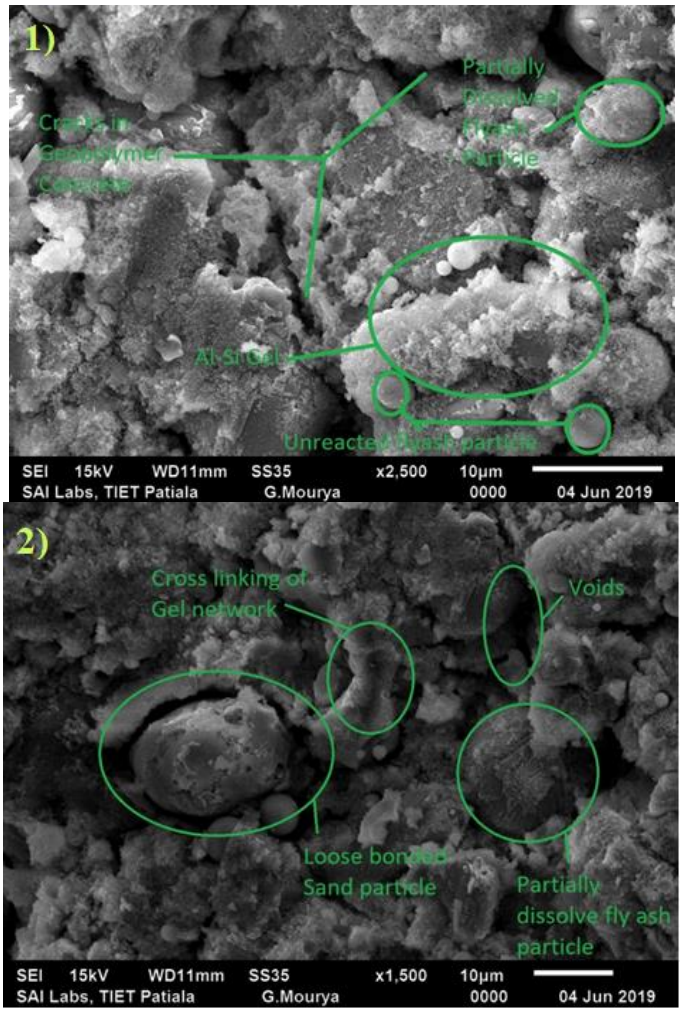

Fig 4.22: SEM Images of Sample GP16000 1) x2500 2) x1500 Magnification

The area mapping, as shown in Figure 4.23, provides substantial evidence of NASH gel spread throughout the specimen, but Al-Si gel is not distributed uniformly. Whereas NASH gel is in more volume on the left side. Mapping also represents a locked connection between aggregate. Whereas the Ca and K content also results in the creation of CASH and NASH gel in lower volumes. The absence of oxide contents represent voids in the specimen.

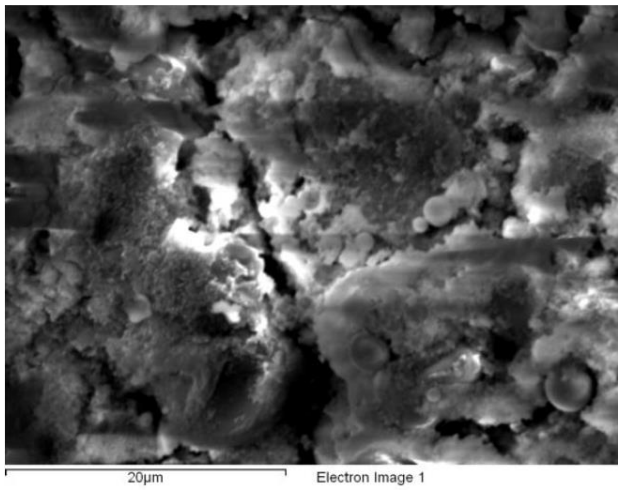

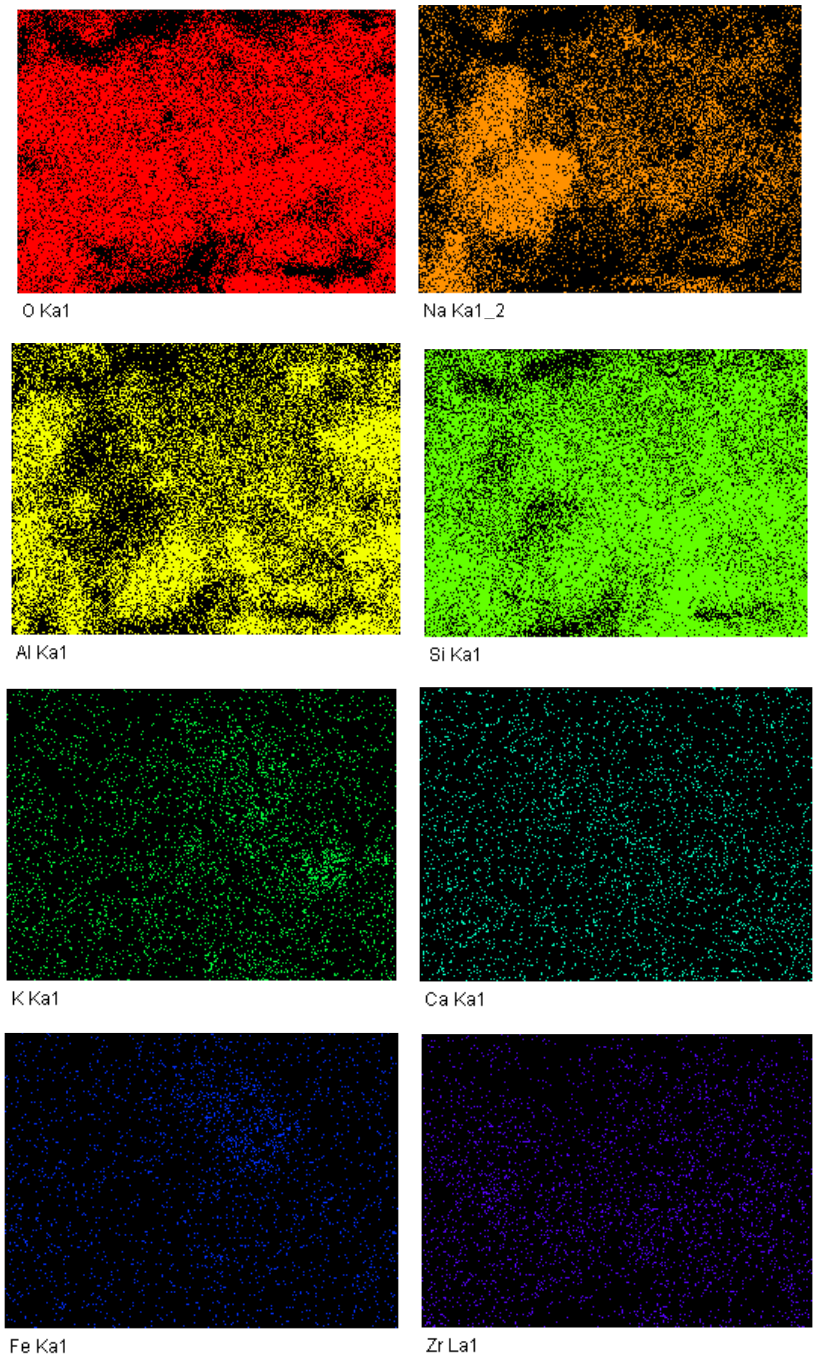

Fig 4.23: Area Mapping of GP16000

The line mapping of aggregate gel interference is shown in Figure 4.24. In mid-line mapping, it is seen that healthy formation of NSH and CSH gel and whereas moving downward formation of NASH gel is seen. The declination after 15 µm indicates loose bonding between fly ash and gel particle. The potassium and calcium content is also found in interference. However GP16 mix demonstrates higher dissolution of the flyash particle, which leads to stronger content of NASH gel, which results in higher strength than GP08 mix.

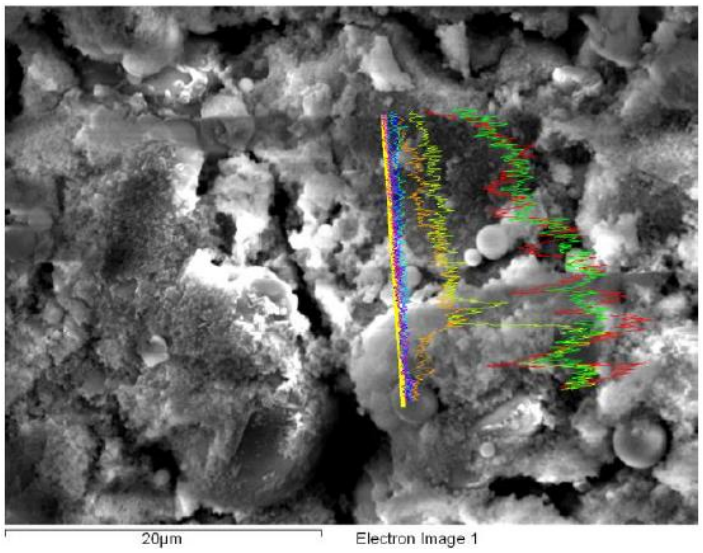
20µm
Electron Image 1

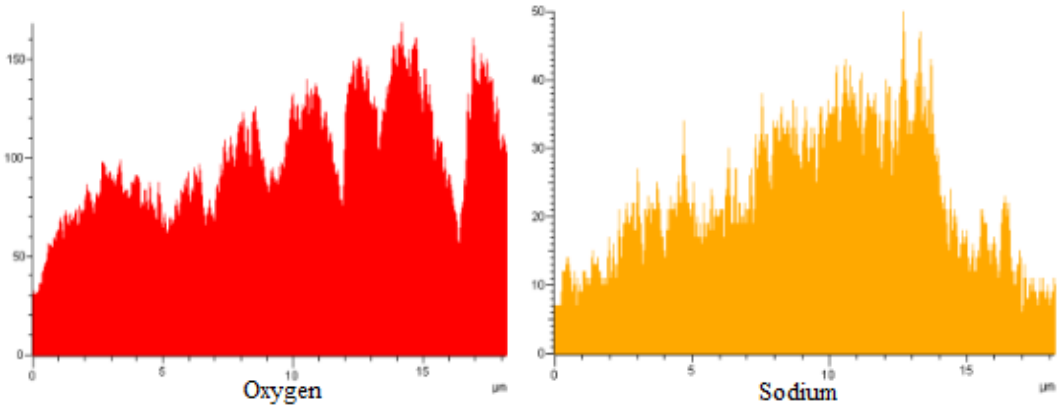
Oxygen
Sodium

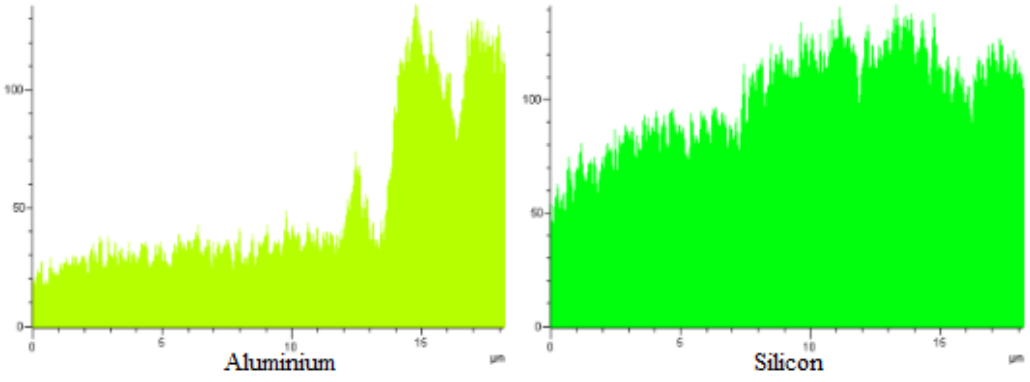
Aluminium
Silicon

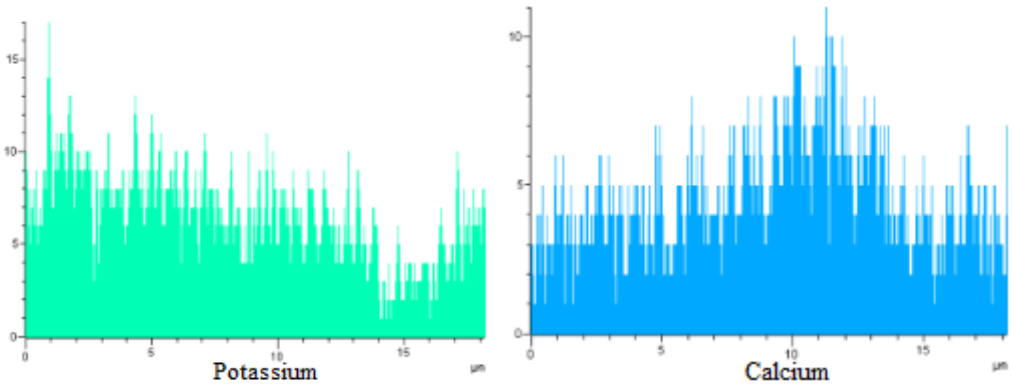
Potassium
Calcium

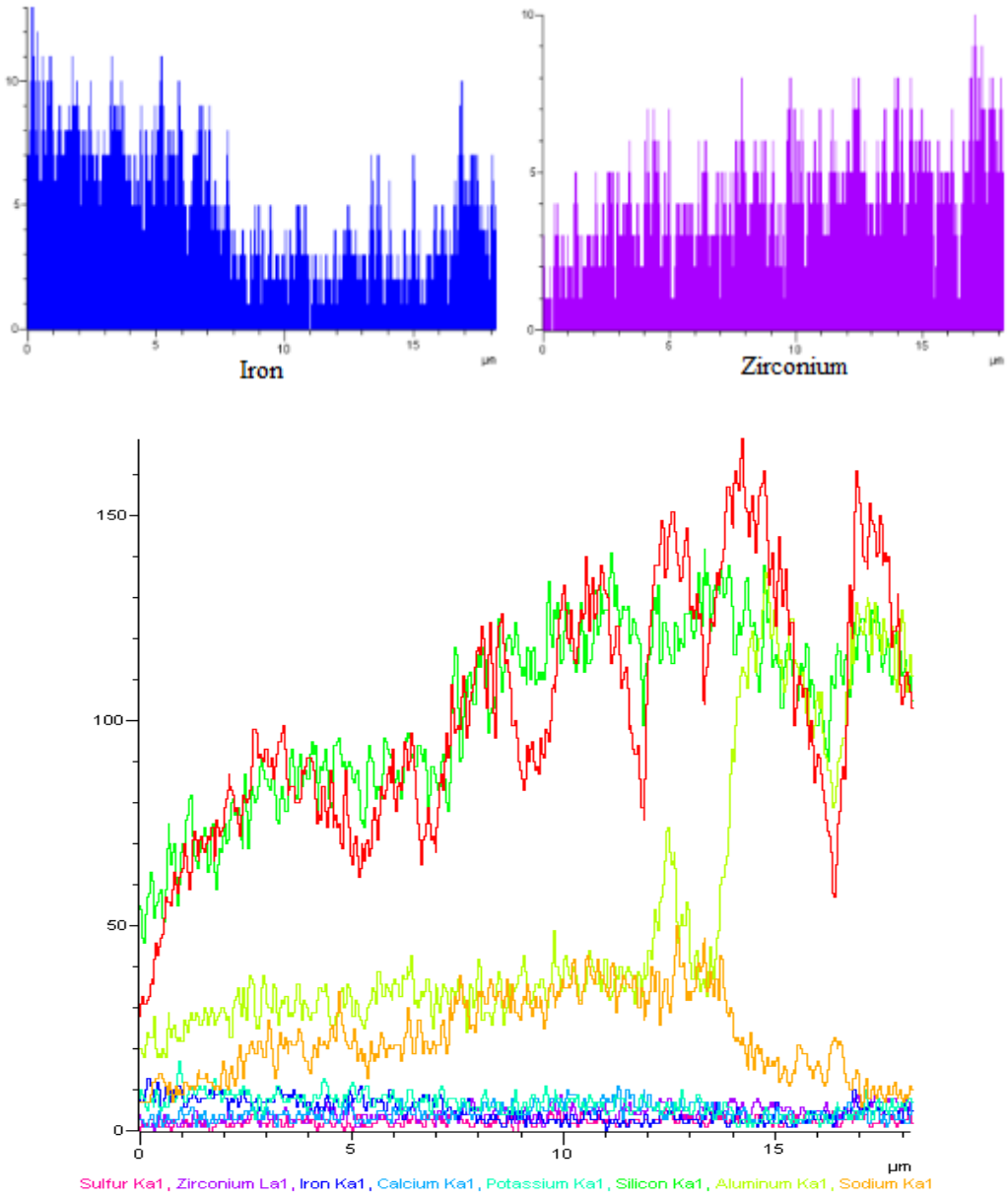

Fig 4.24: Line Mapping of GP16000

EDS analysis of spectrum 1 figure 4.25 show strong Si content however Na and Al content are almost similar to this result in the formation of NASH in the vicinity of aggregate gel interference Whereas the spectrum 3 of Figure 4.26 indicates the aggregate spectrum potentially a sand aggregate spectrum showing Ca, Fe, Si and Al ion in the particle.

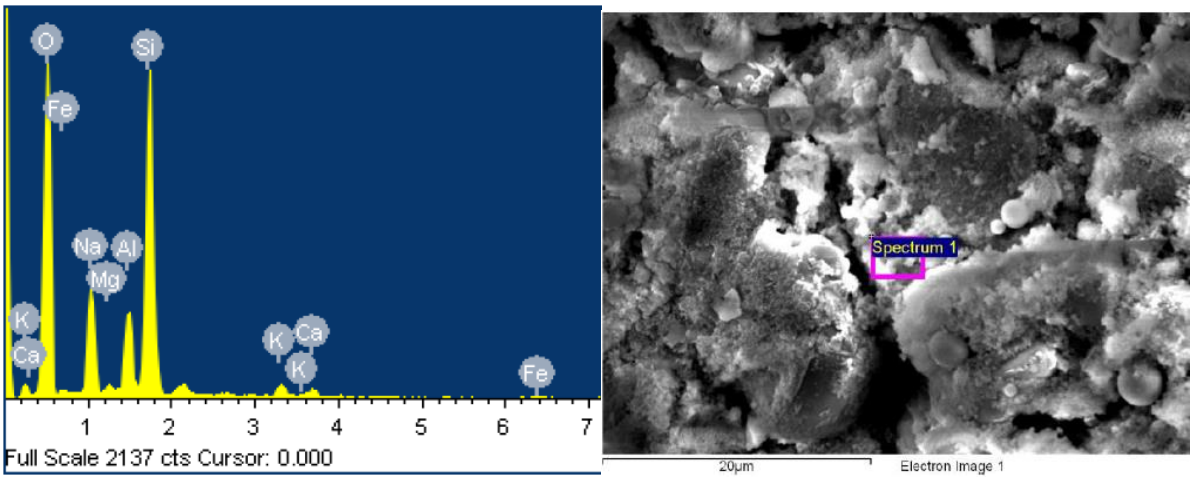

Fig 4.25: EDS and SEM Image of Sample GP16000 Spectrum 1

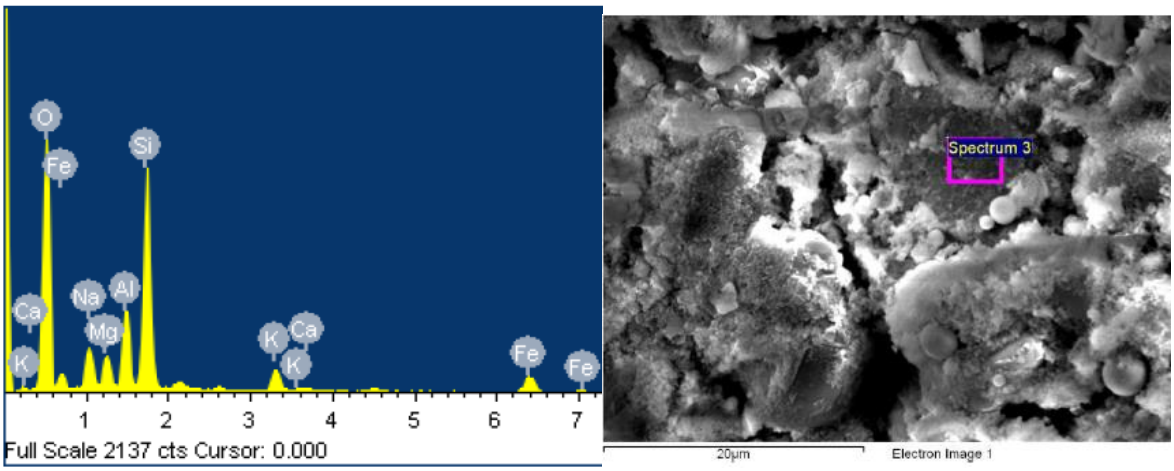

Fig 4.26: EDS and SEM Image of Sample GP16000 Spectrum 3

The SEM Figure 4.27 1-2 shows the dense and non-porous structure with higher solid content. The more NASH gel formation, may be the contribution of both sillimanite sand and fly ash particles. Furthermore, figure 4.27 1) depicts the fly ash particles that is being reacted or dissolved owing to higher solution alkalinity. SEM figure 4.27 2) displays the glassy silicate alumina gel phase. Although sillimanite sand particles are hardly seen in the SEM image 4.27 owing to their uneven form, however, the additional content of Al-Si gel can be used to analyze the contribution of sillimanite sand. This additional content of Al-Si results in stronger geopolymer concrete mechanical and durability properties.

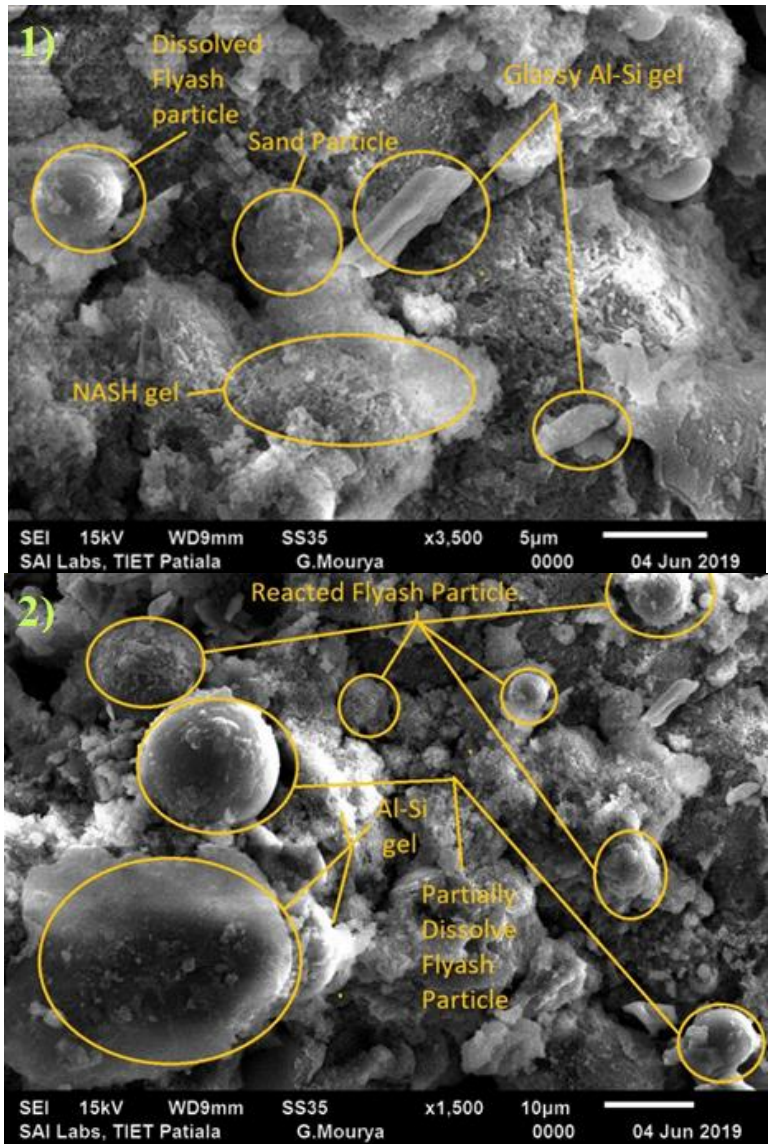

Fig 4.27: SEM Images of Sample GP16050 1) x3500 2) x1500 Magnification

Figure 4.28 shows the area mapping of the specimen. Whereas mapping show distribution of Al-Si gel across the selected area. However, it also evident that structure has fewer pores compares to GP08 specimen. Moreover, crosslinking of gel network also leads to substantial interference between the structure and aggregate whereas Figure also shows Ca and k ion in similar quantity leading to the formation of CASH and KASH gel making the structure more dense and compact.

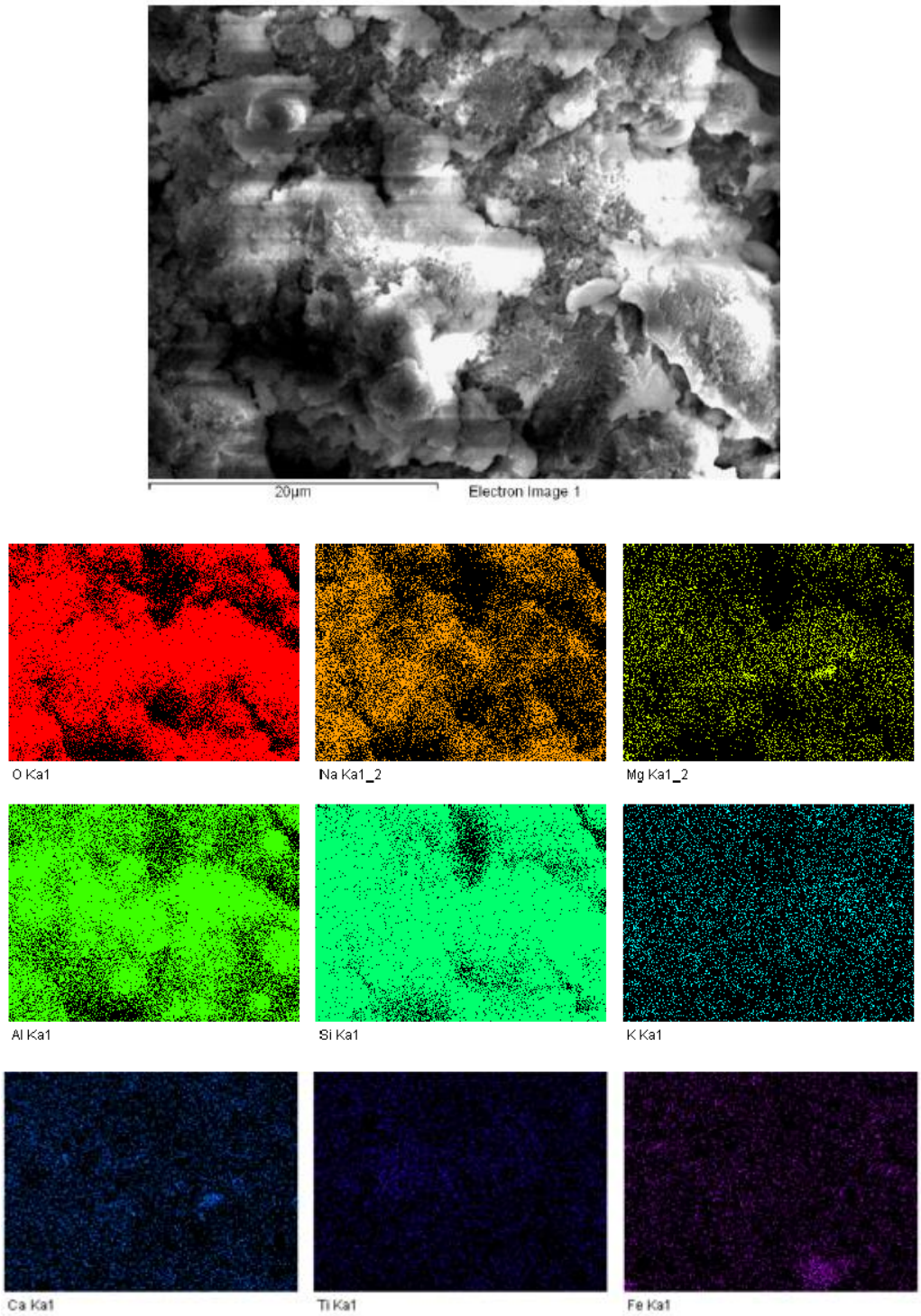

Fig 4.28: Area Mapping of GP16050

Line mapping as shown in Figure 4.29 shows aluminate and silicon oxides, which attribute due to polymerization of Si and Al ion present in material whereas the balance ratio of Si/Al indicate the presence of both sillimanite and fly ash particle. Here the Si / Al percentage is higher than the previous one. This indicates that Al is deposited in the matrix owing to denser matrix polymerization. Other components such as Na, Ca, Fe, Zr, & S were also discovered

in much-reduced amounts in all geopolymeric specimens. This proves that Si-Al-Na-O is the main component of the geopolymer concrete using sillimanite sand.

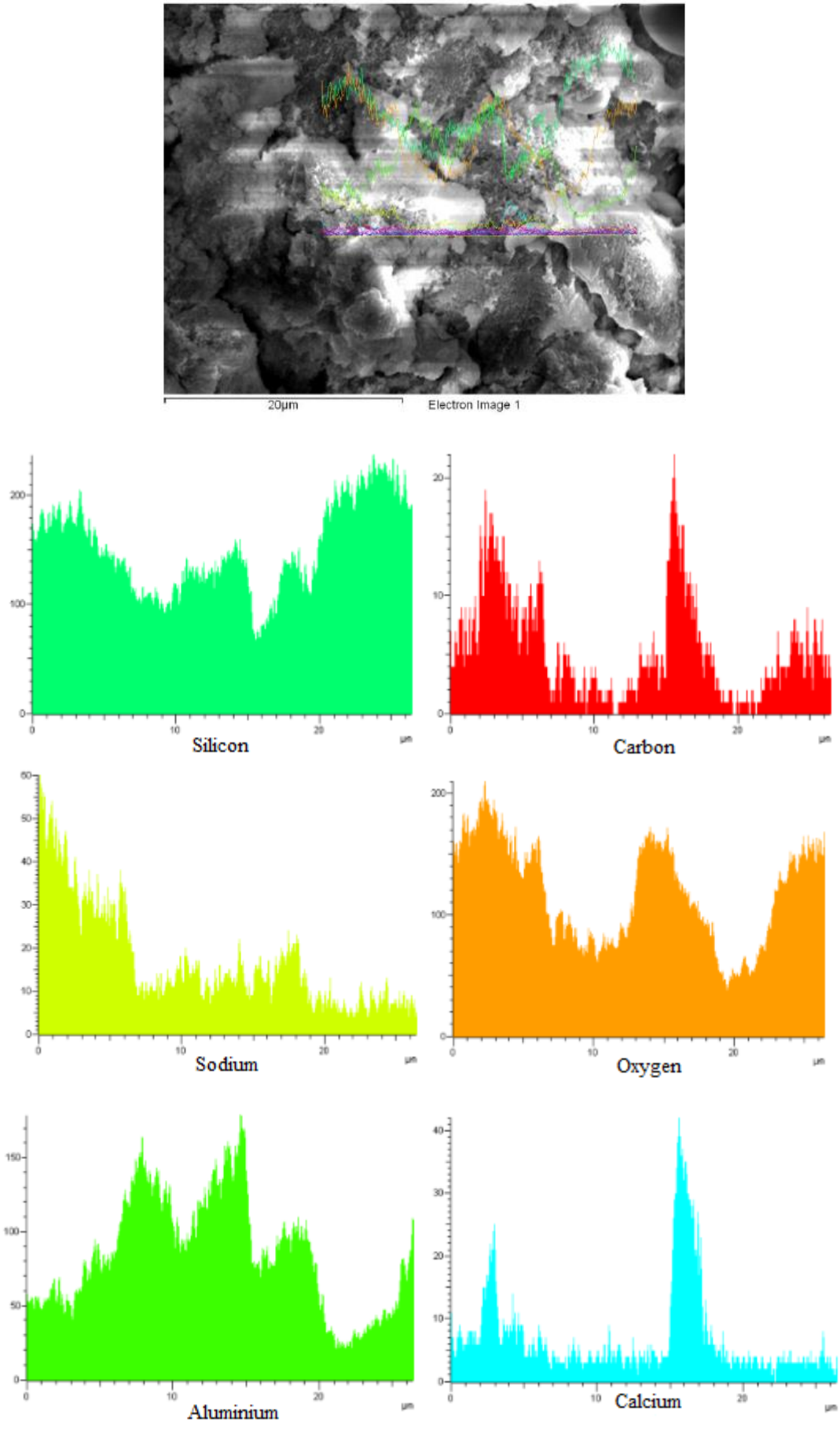

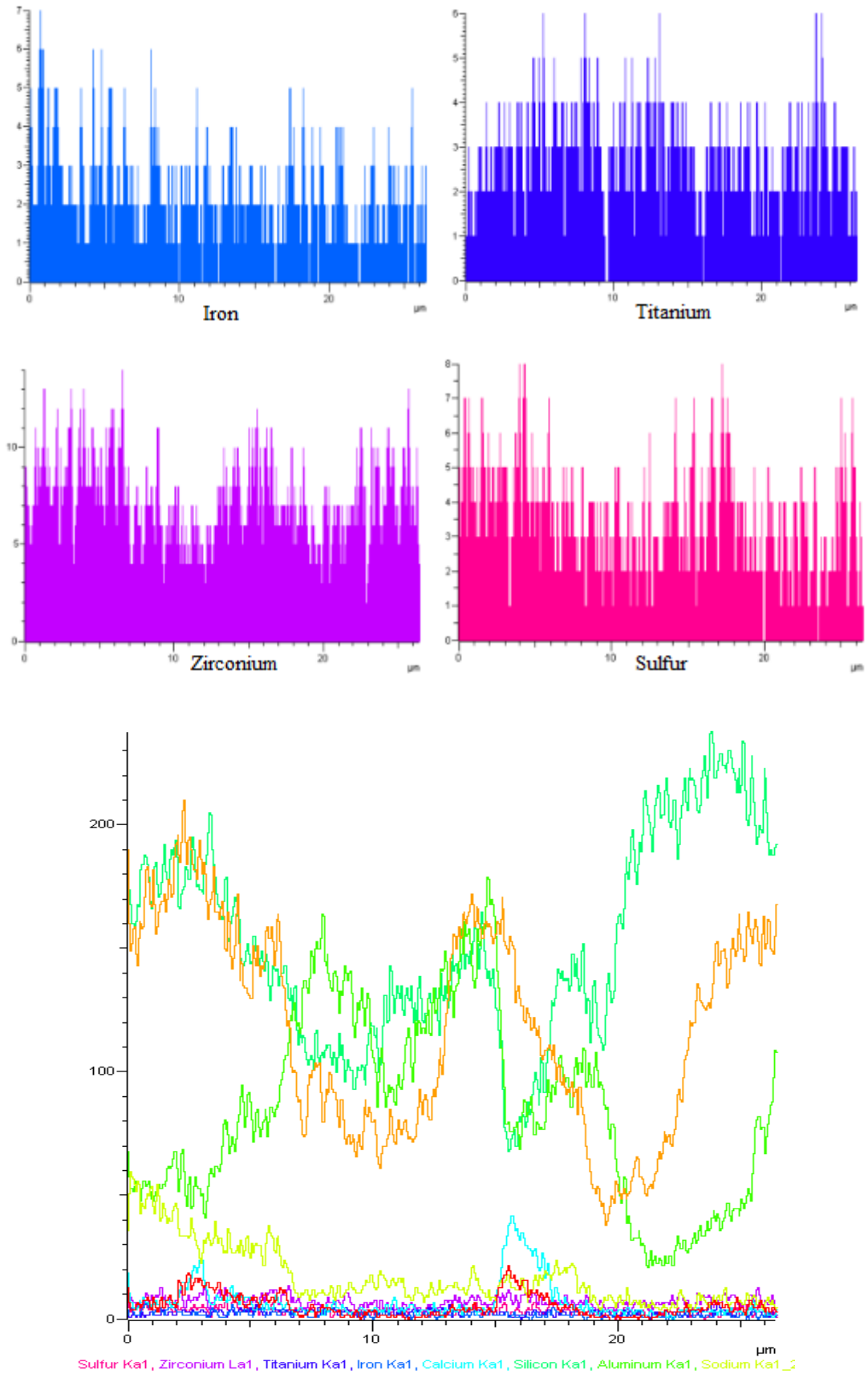

Fig 4.29: Line Mapping of GP16050

Figure 4.30 spectrum 1 EDS shows the geopolymeric, amorphous to the semi-crystalline structure created with Al-Si material with Na in the graph. Due to sillimanite material in the

matrix, condensed Al-Si gel may also be directly related. However, inside the concrete structure particle of sillimanite sand decreases the void in the samples. As a result, the compressive strength of the geopolymer concrete increases. Figure 4.31 spectrum 3 also show the presence of the same content of Al and Si ion result in higher crystallinity due to gel formation. The presence of potassium and calcium ion results in KASH and CASH gel, which also lead to making matrix denser.

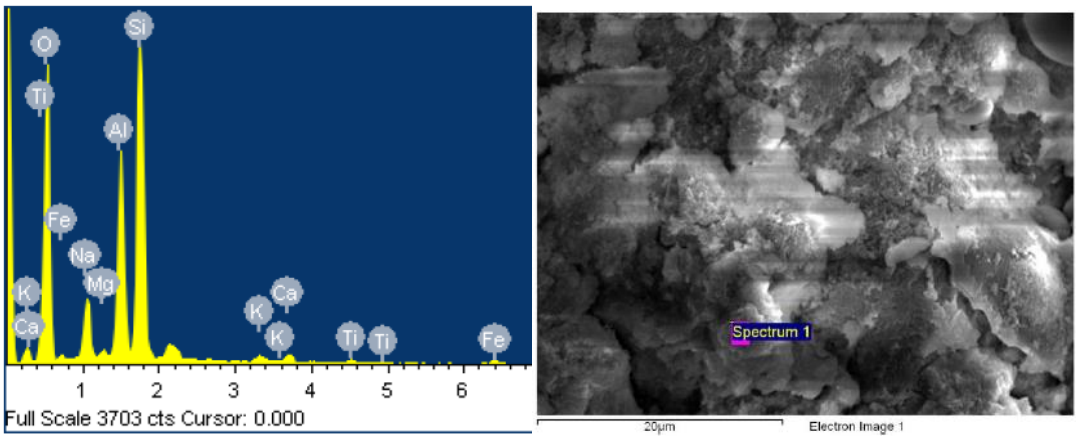

Fig 4.30: EDS and SEM Image of Sample GP16050 Spectrum 1

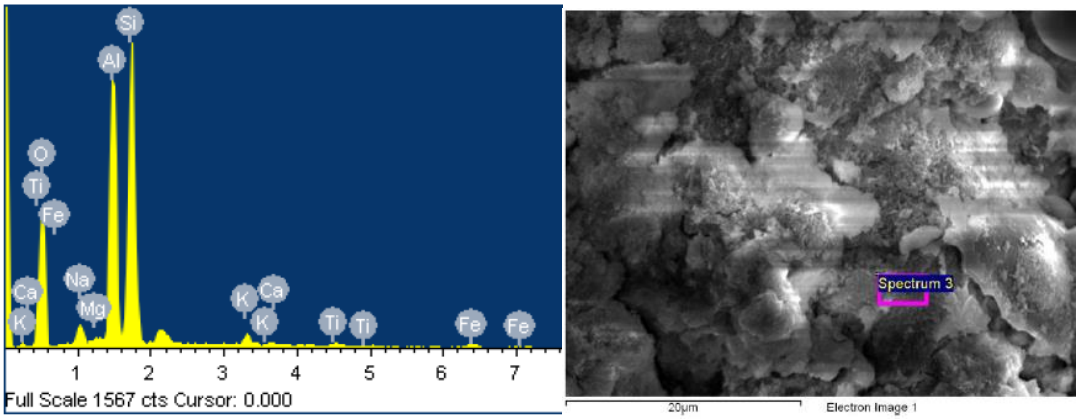

Fig 4.31: EDS and SEM Image of Sample GP16050 Spectrum 3

4.7.2 XRD Analysis

Figure 4.32 shows the XRD analysis of the GP08000, GP08025, GP16000, and GP050 specimens. XRD assessment disclosed the crystallinity of the framework. However, XRD analyzes vary in intensity from sample to sample. From the analysis of XRD pattern, the result shows a sharp peak of the compound like quartz (SiO_2), mullite, nepheline ($NaAlSiO_4$), albite ($NaAlSi_3O_8$), etc. The high quantity of quartz is due to the most of the content inside powder is the source of silica, whereas these high silica quantities in the sample are discovered in the earth's soil and geological environment. Whereas, nepheline in the system indicates the presence of strong Na-Al-Si bonds, which is generated by the polymerization of Al-Si minerals in the system by alkaline solution. The albite also shows the presence of NASH. Previous studies also show the presence of quartz, napthaline, albite in Geopolymer Concrete (Mehta and Siddique 2017). Whereas the presence of mullite indicates the presence of aluminosilicate in the specimen.

In GP08000 shows the presence of quartz, mullite, albite, nepheline, and CASH. The specimen GP08000 also shows the presence of Na-Al-Si crystal structure. Whereas CASH in the system indicates the dissolution of Ca present in fly ash by alkaline solution. Whereas, specimen GP08O25 shows the higher intensity of crystal structure. However, the specimen also indicate the presence of sillimanite, whereas it is difficult to distinguish its presence from albite. However, the increase in intensity indicates the presence of sillimanite.

The XRD analysis of GP16000 shows almost similar graph pattern as GP08000. Whereas in the case of GP16050, a significant hump at 40^0 indicates the presence of strong Na-Al-Si gel, which may indicate the dissolution of sillimanite and fly ash particle in the system. The graph also shows the presence of sillimanite in structure. This evident the sillimanite sand plays a vital role in crystallizing the structure, which ultimately increases the strength of geopolymer concrete. A high hump intensity peak of hematite is also detected in sample GP08025 and GP16050. This high heap may attribute due to ferrous present in both sillimanite and fly ash particle.

Table 4.10: Peaks Compounds and Their Formulas

Peaks	Compound	Formula
Q	Quartz	SiO_2
A	Albite	$NaAlSi_3O_8$
N	Nepheline	$NaAlSiO_4$
M	mullite	$Al_6Si_2O_{13}$
S	Sillimanite	Al_2SiO_5
H	hematite	Fe_2O_3
CASH	Calcium Alumina Silicate Hydrate	

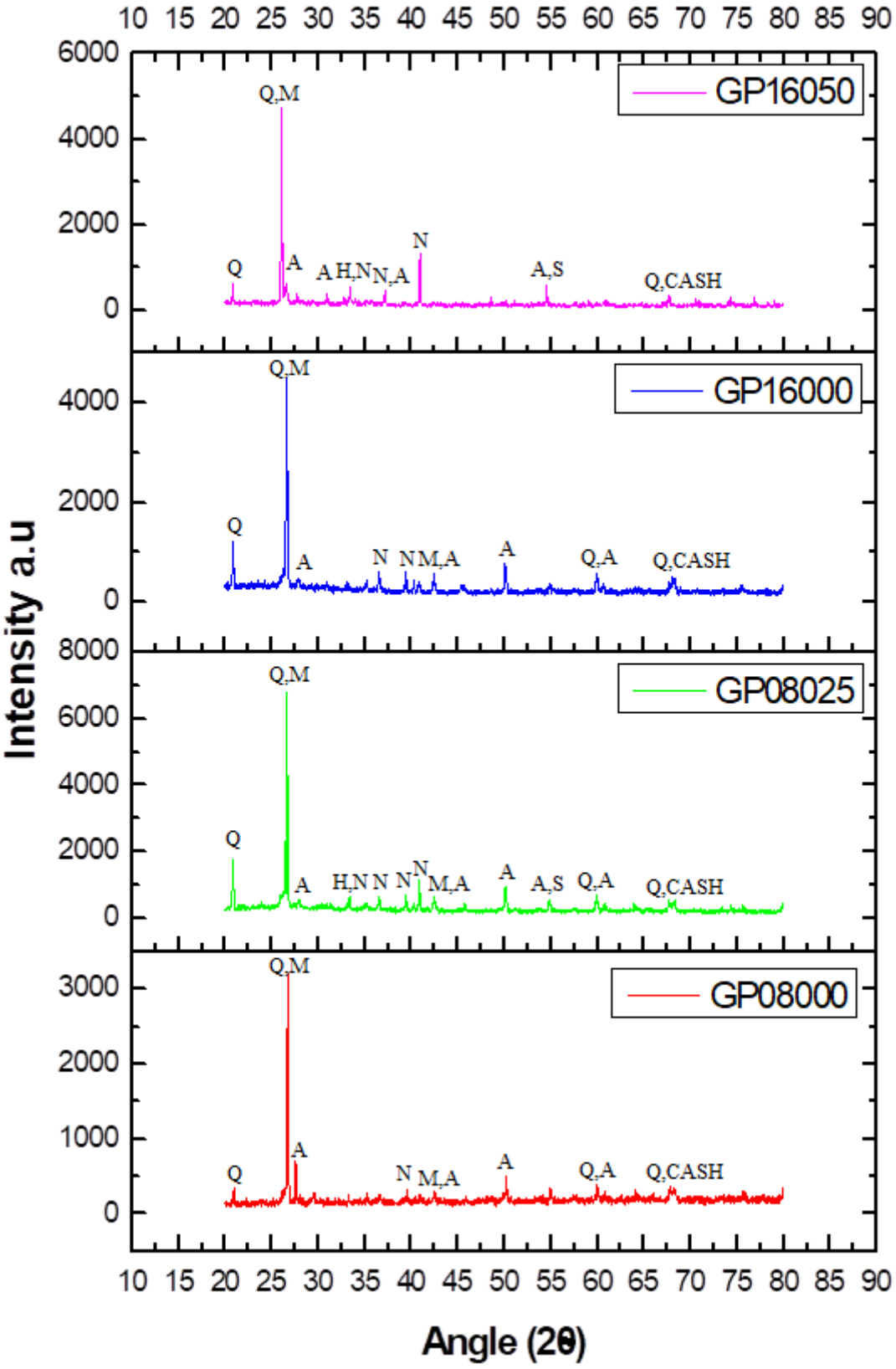

Fig 4.32: XRD of Sample GP08000,GP08025,GP16000 and GP16050

CHAPTER 5
CONCLUSIONS

5.1 General

The present work investigates the effect of replacing river sand at different percentages with sillimanite sand. The result is drawn at different molarities and curing temperatures. Based on the results obtained by various testing such as compressive strength, split tensile strength, sorptivity, rapid chloride permeability, density-absorption, and void test along with SEM, EDS and XRD analysis, conclusions are drawn:

- The compressive strength is found to be higher in sillimanite sand contained geopolymer concrete specimen than the control specimen. The peak strength has been achieved in the GP16 mix of geopolymer concrete with 50 percent sillimanite sand, which is 41.87% higher than control specimen indicating higher crystallinity of geopolymer concrete due to the presence of both Al-Si semi crystal and sillimanite crystal. The replacement of sillimanite sand beyond 50% causes a decrease in strength owing to lower distribution of binder gel due to the higher specific surface area of finer sillimanite sand particles. The maximum strength of the GP08 mix is obtained with a 25% sillimanite sand replacement which due to lower alkalinity of the material. Adding more sillimanite sand results in an increase in the content of undissolved and unreacted sand particles due to the lower dissolving rate of 8 M molarity, resulting in a reduction in strength.
- The GP16 mix's split tensile strength shows a higher strength with a replacement of 50 percent sillimanite sand. The percentage increase in strength is 15.09 % greater than the control sample, whereas the highest strength of the GP08 mixture is shown by 25 percent sillimanite sand. The strength is 32.28 percent greater compared to the control sample.
- The initial sorptivity is lowest for GP16050 specimens in the case of GP16 mix. Moreover, it is increased up to 75% replacement, where it is lower for GP16100 specimen. Control sample indicates 145 % more sorptivity than GP16050 because of the structure's micropores, which are not filled with river sand particles hence increasing the structure's capillary void. Moreover, less structure crystallinity also causes higher sorptivity. The GP08 mixture indicates the parabolic variation of samples with the lowest initial sorptivity in GP08050 specimen.

- Chloride ion permeability of GP16000 is low whereas permeability of all other specimens GP16025, GP16050, GP16075, and GP16100 comes under the very low categorization. The GP16050 shows lowest charged passed among the specimens. This is due to sillimanite sand, which gives better effect with river sand as it occupies the pores of geopolymer concrete, whereas in the case of GP08 mix, chloride ion permeability of GP08025 is low, and chloride ion permeability of all other specimens has moderate permeability.
- The variation of the values of bulk density and apparent density of GP16 mix and GP08 mix is increasing linearly with increase in percentage replacement of sillimanite sand. Bulk density and apparent density of geopolymer concrete increase with the increase in finer content of sillimanite sand, which fills micropores inside the structure. In case of the value of percentage absorption and volume of permeable pore space, GP16050 and GP08050 specimens show the least absorption percentage and the volume of permeable pore space. The higher value of absorption percentage and volume of permeable pore space is shown by GP08000 specimen is due to the lower fine particle content in the river sand which does not participate in filling up pore spaces. This indicates that 25 to 50% replacement level is the optimum percentage replacement level. Whereas, the total void volume (%) result shows a decrease in value with increase in percentage replacement of sillimanite sand in case of GP16 mix and GP08 mix. Moreover, this trend was linear and opposite of bulk density trend.
- The SEM analysis of GP08000 and GP08025 specimen shows the majority of unreacted fly ash particles and voids in the structure. Whereas in the EDS analysis, GP16000 and GP16050 specimen shows dense structure attribution due to alkalinity. Moreover, GP16050 specimen shows spreading of crystallinity over the particle, which is due to sillimanite content in the matrix.
- The XRD analysis of different samples shows the effective napthaline, quartz, and albite content that helps to create a strong matrix network, whereas sillimanite and hematite compounds can be seen in specimen GP08025 and GP16050. A higher napthaline peak in sample GP16050 shows the higher NASH compound that results in increased mechanical and durability properties of geopolymer concrete.

5.2 Scope of Further Work

The conclusions indicate that mechanical and durability properties show the highest strength at 25% to 50% replacement level, making it optimum replacement level. However, further work also needs to be investigated in a few areas which were left during the work. Following are the scope of future work:

- The investigation is needed to be done with percentage replacement of sillimanite sand in area of flexure strength, durability properties such as half-cell potential, carbonation, creep, etc. and microstructural test such as FTIR, TGA, RTA, nanoindentation, etc.
- The work can be extended with the use of other additives such as superplasticizer, fibers, etc. Fibers are needed to be imposed to stop sudden crack effect in case of a mechanical tests.
- Moreover, in the present work, the effect of replacement is only observed at the age of 28 days. The testing has to be done at different ages to study the rate of gain of strength.

REFERENCES

1) Abdullah, M. M. A. B.; Hussin, K.; Bnhussain, M.; Ismail, K. N.; Yahya, Z.; Abdul Razak, R., Fly ash-based geopolymer lightweight concrete using foaming agent. International journal of molecular sciences 2012, 13 (6), 7186-7198.

2) Adam, A. A.; Horianto, X., The effect of temperature and duration of curing on the strength of fly ash based geopolymer mortar. Procedia engineering 2014, 95, 410-414.

3) Ahmed, M. A.; Faisaluddin, M.; Pasha, N.; Ahmed, M. M., Effect of Alkali Activators on Strength Characteristics of GPC. International Journal of Innovative Research in Science, Engineering and Technology 2017, 6 (7), 8.

4) Al Bakria, A. M.; Kamarudin, H.; BinHussain, M.; Nizar, I. K.; Zarina, Y.; Rafiza, A., The effect of curing temperature on physical and chemical properties of geopolymers. Physics Procedia 2011, 22, 286-291.

5) Aldred, J.; Day, J., Is geopolymer concrete a suitable alternative to traditional concrete, 37th Conference on our world in concrete & structures, Singapore, 2012; pp 29-31.

6) Authority, C. E., Report on Fly Ash Generation at Coal/Lignite Based Thermal Power Stations and Its Utilization in the Country for the Year 2014-15. Central Electricity Authority New Delhi, India: 2015.

7) Cai, W. Effect of particle packing on flow property and strength of concrete mortar. Graduate Theses and Dissertations, Iowa State University, 2017.

8) Davidovits, J., Global warming impact on the cement and aggregates industries. World resource review 1994, 6 (2), 263-278.

9) Davidovits, J. Chemistry of geopolymeric systems, terminology, 99th international conference, France 1999; pp 9-39.

10) Davidovits, J. Properties of geopolymer cements, First international conference on alkaline cements and concretes, Scientific Research Institute on Binders and Materials Kiev, Ukraine: 1994; pp 131-149.

11) Davidovits, J. years of successes and failures in geopolymer applications. Market trends and potential breakthroughs, Geopolymer 2002 Conference, Geopolymer Institute Saint-quentin (France), Melbourne (Australia): 2002; p 29.

12) Davidovits, J., Geopolymers: inorganic polymeric new materials. Journal of Thermal Analysis and calorimetry 1991, 37 (8), 1633-1656.

13) Duxson, P.; Fernández-Jiménez, A.; Provis, J. L.; Lukey, G. C.; Palomo, A.; van Deventer, J. S., Geopolymer technology: the current state of the art. Journal of materials science 2007, 42 (9), 2917-2933.

14) Ekaputri, J. J.; Priyanka, N. F. The Effect of Temperature Curing on Geopolymer Concrete, MATEC Web of Conferences, EDP Sciences: 2017; p 01005.

15) Fernández-Jiménez, A.; Palomo, A.; Criado, M., Microstructure development of alkali-activated fly ash cement: a descriptive model. Cement and concrete research 2005, 35 (6), 1204-1209.

16) Ganesan, N.; Abraham, R.; Raj, S. D., Durability characteristics of steel fibre reinforced geopolymer concrete. Construction and Building Materials 2015, 93, 471-476.

17) Girawale, M. S., Effects of Alkaline Solution on Geopolymer Concrete. International Journal of Engineering Research and General Science 2015, 3 (4), 6.

18) Hardjito, D., Studies of fly ash-based geopolymer concrete. Doctoral dissertation, Curtin University, 2005.

19) Hardjito, D.; Rangan, B. V., Development and properties of low-calcium fly ash-based geopolymer concrete. 2005.

20) İlkentapar, S.; Atiş, C.; Karahan, O.; Avşaroğlu, E. G., Influence of duration of heat curing and extra rest period after heat curing on the strength and transport characteristic of alkali activated class F fly ash geopolymer mortar. Construction and Building Materials 2017, 151, 363-369.

21) Jansen, M. S.; Christiansen, M. U. Effect of Water-solids ratio on the compressive strength and morphology of fly ash-waste glass geopolymer mortars, World of Coal Ash (WOCA) Conference, Nasvhille, TN, 2015.

22) Kupwade-Patil, K.; Allouche, E. N., Impact of alkali silica reaction on fly ash-based geopolymer concrete. Journal of materials in Civil Engineering 2012, 25 (1), 131-139.

23) Lloyd, N.; Rangan, B., Geopolymer Concrete with Fly Ash, second international conference on sustainable construction material and technologies. June: 2010.

24) Malkawi, A. B.; Nuruddin, M. F.; Fauzi, A.; Almattarneh, H.; Mohammed, B. S., Effects of alkaline solution on properties of the HCFA geopolymer mortars. Procedia engineering 2016, 148, 710-717.

25) Marín-López, C.; Araiza, J. R.; Manzano-Ramírez, A.; Avalos, J. R.; Perez-Bueno, J.; Muñiz-Villareal, M.; Ventura-Ramos, E.; Vorobiev, Y., Synthesis and characterization of a concrete based on metakaolin geopolymer. Inorganic Materials 2009, 45 (12), 1429.

26) Mccaffrey, R., Climate change and the cement industry. Global cement and lime magazine (environmental special issue) 2002, 15, 19.

27) Mehta, A.; Siddique, R., Strength, permeability and micro-structural characteristics of low-calcium fly ash based geopolymers. Construction and Building Materials 2017, 141, 325-334.

28) Muttashar, H. L.; Ariffin, M. A. M.; Hussein, M. N.; Hussin, M. W.; Ishaq, S. B., Self-compacting geopolymer concrete with spend garnet as sand replacement. Journal of Building Engineering 2018, 15, 85-94.

29) Nguyen, K. T.; Le, T. A.; Lee, K., Evaluation of the mechanical properties of sea sand-based geopolymer concrete and the corrosion of embedded steel bar. Construction and Building Materials 2018, 169, 462-472.

30) Özcan, A.; Karakoç, M. B., The Resistance of Blast Furnace Slag-and Ferrochrome Slag-Based Geopolymer Concrete Against Acid Attack. International Journal of Civil Engineering 2019, 1-13.

31) Phoo-ngernkham, T.; Chindaprasirt, P.; Sata, V.; Pangdaeng, S.; Sinsiri, T., Properties of high calcium fly ash geopolymer pastes with Portland cement as an additive. International Journal of Minerals, Metallurgy, and Materials 2013, 20 (2), 214-220.

32) Reddy, B. S. K.; Varaprasad, J.; Reddy, K. N. K., Strength and workability of low lime fly-ash based geopolymer concrete. Indian Journal of Science and Technology 2010, 3 (12), 1188-1189.

33) Sethi, H.; Bansal, P. P.; Sharma, R., Effect of Addition of GGBS and Glass Powder on the Properties of Geopolymer Concrete. Iranian Journal of Science and Technology, Transactions of Civil Engineering 2016, 1-11.

34) Shadnia, R.; Zhang, L., Experimental study of geopolymer synthesized with Class F fly ash and low-calcium slag. Journal of Materials in Civil Engineering 2017, 29 (10), 04017195.

35) Shaikh, F. U., Effects of alkali solutions on corrosion durability of geopolymer concrete. Advances in concrete construction 2014, 2 (2), 109-123.

36) Singh, G.; Siddique, R., Effect of waste foundry sand (WFS) as partial replacement of sand on the strength, ultrasonic pulse velocity and permeability of concrete. Construction and building materials 2012, 26 (1), 416-422.

37) Thomas, R. J.; Peethamparan, S. Modified test for chloride permeability of alkali-activated concrete, 95th Annual Meeting of the Transportation Research Board., 2017.

38) Van Jaarsveld, J.; Van Deventer, J.; Lorenzen, L., The potential use of geopolymeric materials to immobilise toxic metals: Part I. Theory and applications. Minerals engineering 1997, 10 (7), 659-669.

39) Venkatesan, R. P.; Pazhani, K., Strength and durability properties of geopolymer concrete made with ground granulated blast furnace slag and black rice husk ash. KSCE Journal of Civil Engineering 2016, 20 (6), 2384-2391.

40) Wallah, S., Creep behaviour of fly ash-based geopolymer concrete. Civil Engineering Dimension 2010, 12 (2), 73-78.

41) Wallah, S.; Rangan, B. V., Low-calcium fly ash-based geopolymer concrete: long-term properties. 2006.

42) Wu, G., Chinese resources and processing technology for kyanite minerals. Industrial Minerals 1990, (270), 95-98.

43) Xu, H.; Van Deventer, J., The geopolymerisation of alumino-silicate minerals. International journal of mineral processing 2000, 59 (3), 247-266.

44) Xu, H.; Van Deventer, J. S., Microstructural characterisation of geopolymers synthesised from kaolinite/stilbite mixtures using XRD, MAS-NMR, SEM/EDX, TEM/EDX, and HREM. Cement and Concrete research 2002, 32 (11), 1705-1716.